Ninevah University

College of Electronics

Electronic Department

Wireless Powering of Implantable Medical Devices

Doha Hassan Hussein Mohammed

A Thesis in

Electronic Engineering

Supervised by

Assist. Prof.

Ahmed Mohammad Sabaawi

1444 AH   **2022 AD**

Wireless Powering of Implantable Medical Devices

A Thesis Submitted by

Doha Hassan Hussein Mohammed

To

The Council of the College of Electronics Engineering

Ninevah University

as a Partial Fulfillment of the Requirements

for the Degree of Master of Science

in

Electronic Engineering

Supervised by

Assist. Prof.

Ahmed Mohammad Sabaawi

1444 AH   **2023 AD**

بِسْمِ اللَّهِ الرَّحْمَنِ الرَّحِيمِ

وقُلِ إعملوا فسيرى اللهُ عَمَلَكُم ورَسولهُ والمؤمنون وستُردونَ الى عالمِ الغيبِ والشهادةِ فينبئكُم بما كُنتم تَعملونْ(105)

صَدَقَ اللهُ العَظيم

سورة التوبة

ACKNOWLEDGEMENTS

Thanks the deep of my heart to the light of my eyes, the light of my path, and the joy of my life, whose prayers and words were a shield and a fortress for me (my dear mother).

My thanks also to those who instilled in me all the meanings of loyalty and sincerity and inherited in me all the motives of giving (my brother and sisters especially Sawsan).

A huge thanks to those who are for my heart, my joy, and my life is good, human (my sisters and brothers).

My thanks and gratitude to my classmates who cooperated and joined hands to share knowledge and were the best for me during my hard times.

"I ask God, the All-Knowing, to teach us what benefits us. And to benefit us with what he taught us. May our knowledge benefit others."

Abstract

In recent years, implantable medical devices become popular and gained lots of interest by researchers and healthcare providers. They are now widely used due to the developed healthcare techniques and the high quality of patient's treatment. The recent advancement and newly emerged technologies have made the fabrication and miniaturization of the medical devices feasible and easy. Powering implanted devices is one of the biggest challenges in developing such kind of medical devices. Batteries are the mostly employed power sources. However, they are one of the biggest limitations for the age and size of the implanted medical devices. The promising solution to overcome this problem and address these limitations is to use the wireless power transfer (WPT) technology. Hence, this dissertation is focused on analysing and developing voltage doubler rectifiers as well as antennas that are used as rectennas of WPT .

It is well known that the rectifier circuit is very essential part of WPT. Thus, rectifiers in this dissertation is designed based on voltage doubler technique and simulated by Advanced Design System (ADS) software. The designed rectifiers in this work exhibits an RF to DC conversion efficiency around 60% with an output DC voltage that reached 6 V, which is sufficient to power up the medical device and/or charging the implanted battery. In addition, the rectifier circuits have been miniaturized to a small dimensions and still has relatively high RF to DC conversion efficiency. It is worth mentioning, that two frequency bands are used in this work and the performance of the rectifier circuit at each frequency band is compared and analysed. These frequency bands are 433 MHz and 915 MHz.

Antennas are very essential part of the WPT system. Several meandered line antennas are designed and simulated in this research by using CST

studio software. Two antennas are designed at 433 MHz and another two antennas are designed to operate at 915 MHz. The implantable meandered antennas are designed with a full groundplane at the back side of the antenna and an SMA connecter is attached to the input port of the antenna. This design makes it easy for the designed antennas to be integrated with the rectifiers to form a compact WPT system .

The designed rectennas (rectifier + antenna) are fabricated by using PCB technology. The performance of the fabricated prototypes are tested in the lab. The measured results are compared with the simulated ones and it is found that an excellent agreement were achieved, which makes the rectifier and antenna designs are valid. These experiments are significantly confirmed the utility of the proposed rectennas in this work to produce sufficient amount of power for many implantable medical devices.

Contents

List of tables

List of Figures

Acronyms

AC	Alternative Current
ADS	Advanced Design System
CC	Constant Current
CST	Computer Simulation Technology
FCC	Federal Communications Commission
GPS	Global Positioning System
ICNIRP	International Commission on Non-Ionizing Radiation
IEEE	Institute of Electrical and Electronics Engineers
IMD	Implantable Medical Device
ISM	Industrial Scientific & Medical
WPT	Wireless Power Transfer
UWB	Ultra-Wideband
RF	Radio Frequency
MICS	Medical Implant Communication Service
MedRadio	Medical Device Radiocommunications Service
TX	Transmitter
RX	Receiver
ETSI	European Telecommunications Standards Institute
EIRP	Equivalent Isotropically Radiated Power
WMTS	Wireless Medical Telemetry Service

Symbol	Explanation	Unit
ε_r	Dielectric permittivity	F m^{-1}
G_{TX}	Gain of transmitting antennas	
G_{RX}	Gain of receiving antennas	
L_P	Path loss	[dB]
e_P	The polarization mismatch	
P_{RX}	Power received	[W]
P_{TX}	Power transmitted	[W]
ω	Rotational frequency	[rad/s]
$|E|$	Electric field intensity	[V/m]
dV	Differential volume element	
P_{in}	Input power	[W]
P_{rad}	Radiated power	[W]

CHAPTER ONE

INTRODUCTION AND LITERATURE REVIEW

1.1 Introduction

Our world is evolving very quickly due to the quick advancement of scientific research techniques and equipment. Human requirements in various living styles, including health and leisure, provide the foundation for such change. There is no question that the health comes before the majority of other necessities because it directly affects human life. It has a thriving market and draws a lot of research funding. Therefore, it is of great interest to researchers in both academic and industrial fields to create and develop medical and health tools and systems that are more dependable, safe, and comfortable. Medical devices can be inserted into people's bodies for a variety of reasons, including monitoring, medicine delivery, or targeted stimulation. A pacemaker was successfully placed into the human body for the first time in 1960 [1].

Implantable medical devices (IMDs) make it possible to monitor and manage a variety of illnesses, including diabetes, Parkinson's disease, and cardiac arrhythmia. Pacemakers, Implantable Cardioverter Defibrillators (ICDs), insulin pumps, and neurostimulators are the most popular IMDs. In the United States, there were more than 25 million patients with an IMD as of 2001 [2]. Parkinson's disease affects seven to ten million individuals globally nowadays [3], however, diabetes affects more than 422 million people worldwide [4]. Because of people's bad lifestyles and population aging, the number of persons with chronic diseases who need an IMD will keep increasing.
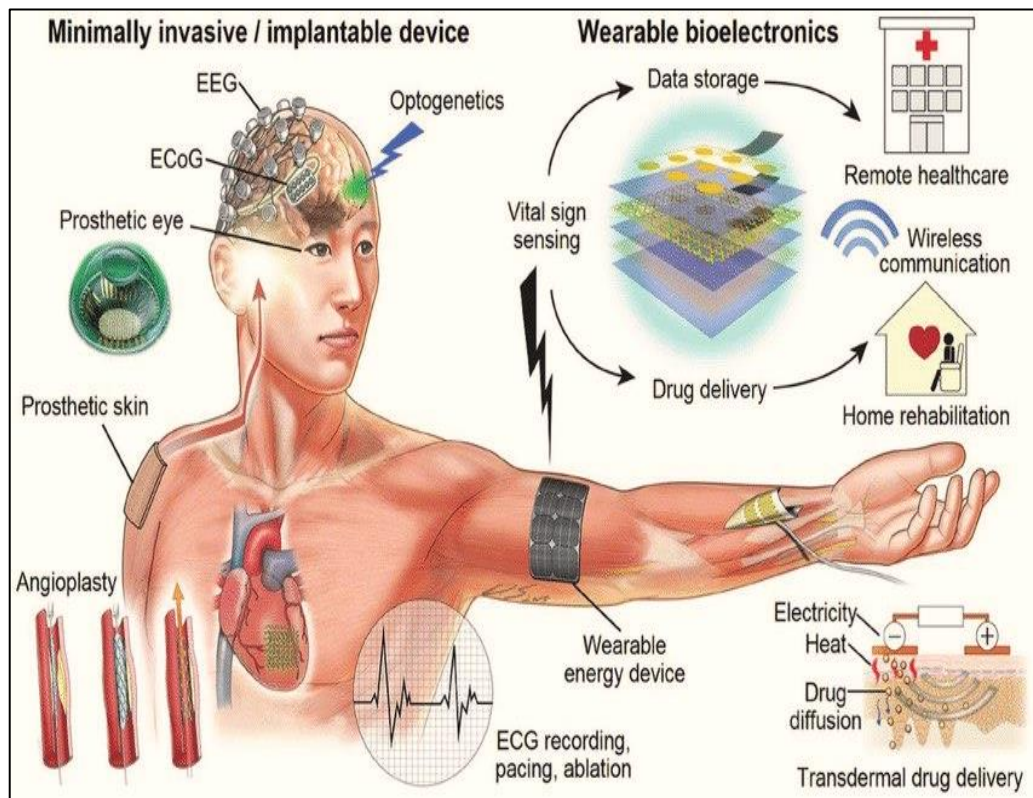
Fig.1.1. Implantable devices.

IMDs with wireless capabilities that can provide patients with complex therapies have been made possible due to recent developments in low-power wireless technologies and energy-efficient hardware platforms. An IMD can only communicate with the outside world once it has been implanted in a patient via its analogue interface (internal sensors) and wireless interface (wireless bidirectional communication connection).

The internal sensors are utilized to continuously monitor the patient's physiological signals, which enables the IMD to recognize abnormal circumstances and respond appropriately. For instance, when the patient's heart is not beating properly, this enables an ICD to shock it electrically.

The IMD can connect with a variety of external devices, including base stations, device programmers, and external sensors, thanks to the wireless interface. The wireless communication path between the IMD and each of these peripherals is the subject of our next discussion.

Doctors can use a device programmer to change the IMD's settings via the wireless interface in addition to gathering telemetry data and patient information from the IMD. Device programmers may occasionally have access to the internet, which enables IMD producers to remotely update their software.

IMDs can often communicate with base stations to keep track of the patient's health when he is at home. In order to gather telemetry data from the IMD while the patient is asleep, base stations are positioned near to the patient's bed. The maker of the IMD frequently maintains a server where this telemetry data is subsequently transferred through phone or the internet. Doctors may access an online portal to evaluate the telemetry data, and in certain situations, patients can do the same. There are several remote monitoring solutions on the market right now.

IMDs now have a larger attack surface and are more vulnerable to failure as a result of all these advances. IMDs are critical-functioning devices, therefore if they malfunction for accidental or deliberate causes, the patient's life might be in danger. Zian Tseng, a doctor who studied cardiac devices at the University of California, asserts that unexpected failures brought on by IMD issues happen more frequently than anticipated [5].

Primary batteries are used to power most implants. Non-rechargeable batteries with a predetermined lifetime, for example,

power deep brain neurostimulators and pacemakers. These batteries have a lifespan of 5 to 7 years, depending on the device's function when the IMD's battery life expires, it must be surgically replaced, which comes at a significant expense and poses a danger of infection to the patient infection rates associated with pacemaker replacements range from (1 – 19) % [6] . Inductive and RF antennas are the two most common methods for establishing communication linkages for biomedical implants. Through inductively connected coils, the operationg frequency bands range from a few kHz to many MHz. Within the near field zone, the effective communication distance between the inductively coupled implanted device and the external reciever is limited to very few centimeters [7, 8].

1.2 Literature Review

1- In (2015), Achraf Ben Amar *et al.* used animal models for medical diagnosis and prognosis, therapeutic applications, and biological science studies, implantable medical devices have been used to treat patients and evaluate in vivo physiological data in humans. Newly developed low-cost and small gadgets now have improved biocompatibility, sensitivity, longevity, and dependability , thanks to advancements in micro- and nanotechnology combined with novel biomaterials. To deliver point-of-care and individualized medicine, closed-loop systems with both sensing and treatment capabilities have been created. However, one of the unresolved issues is how to ensure that there is enough power available continuously to run the entire system. Because implanted devices demand more and more

4

power for wireless transmission and because mobile health is the future of healthcare infrastructure, this problem is becoming more and more important (m-Health) [9].

2- In (2017) , Asimina Kiourti *et al.* reviewed wireless medical gadgets that are inserted into the body to achieve a variety of detecting and/or stimulating functions. Methods: In-body medical devices that are implanted within the body (implantables), taken orally like conventional pills (ingestibles), and injected into the body with needles (needles-injectables) are the subjects of a critical review examination (injectables). Regarding the aforementioned in-body technologies, design concerns, the state of affairs, and potential future developments are explored. Results: A variety of design issues, such as choosing an operating frequency, antenna design, powering, and biocompatibility, are connected to in-body devices. In-body technologies, however, are creating new possibilities for medical diagnosis, prognosis, and therapy that soon exceed the disadvantages. Despite any design issues and/or concerns about their intrusive nature, in-body technologies are rapidly creating new possibilities for medical prevention, prognosis, and therapy. In-body devices are already in use for a variety of medical procedures, including pacemakers, capsule endoscopes, and injectable micro-stimulators. In-body devices are promising a number of novel and as yet undiscovered prospects in healthcare as technology continues to advance. Meaning: It is planned to use inconspicuous in-body devices to gather a wide range of physiological information from each person's early life. With

the use of big data, healthcare may move away from symptom-based treatment and toward preventive care [10].

3- In (2018) , Reem Shadid and Sima Noghanian reviewed and surveyed the inductive coupling-based research on power transmission for biomedical applications. There is interest in wireless power transfer (WPT) for wearable and implantable biomedical equipment, such as implantable electrocardiogram (ECG) recorders or heart pacemakers. In addition to outlining the key design elements found in recent research, this work focused on applications based on near-field power transfer techniques and offers additional details on system modeling and coil tuning[11].

4- Sadeque Reza Khan *et al*. (2020),studied modern multipurpose micro-electronic devices, such as those found in biomedical implants, can now be electrically powered using wireless power transfer (WPT) systems. However, it might be difficult to design and put high power transfer efficiency WPT systems into practice. The size of the WPT system, the distance between the implanted medical device's placement inside the body and the outside environment, the working frequency, and tissue safety owing to power dissipation are important factors to take into account when designing WPT systems. To enhance overall system performance, a wide range of WPT systems have been studied over the past 20 years. This article offers a systematic review of those systems. The many methods used in implantable medical devices to provide wireless power. The various methods used to transfer wireless power to implantable medical devices (IMDs) were examined. These methods include capacitive coupling, inductive coupling, magnetic

resonance coupling, and, more recently, acoustic and optical powering techniques. All of these approaches' advantages and disadvantages are compared, with a focus on the implanted receiver size, the WPT distance, power transfer effectiveness, and tissue safety offered by the resulting systems. According to each IMD, each WPT technique's necessary improvements and trends are also mentioned [12] .

5- Nikolay L Kazanskiy *et al.* (2022) used old-fashioned personal healthcare practices currently a lot of conventional methods, like unwieldy tools and difficult procedures, which in some cases can be time-consuming and inconvenient. Additionally, such antiquated techniques necessitate the use of bulky apparatus, blood samples, and conventional bench-top testing techniques. Patient discomfort and suffering may result from invasive methods of obtaining test samples. On the other hand, wearable sensors can be fitted to a variety of body parts to record various biochemical and physiological data as a growing analytical tool. Health is monitored in many situations using physical, chemical, and biological information that is communicated through the skin.

By analyzing the pulsatile component of the bloodstream, it is possible to estimate important physiological parameters such as pulse inconstancy or variability using photo plethysmo graphy (PPG) and oxygen saturation in arterial blood using pulse oximetry. A new kind of automation called wearable devices with "skin-like" properties is just now starting to leave research labs and enter pre-commercial prototypes. Due to their deformability, lightness, mobility, and flexibility, flexible skin-like sensing devices have achieved a number of

7

capabilities that were previously unattainable for conventional sensing devices. In this work, the authors examined the most recent developments in wearable sensors, including skin-like battery-free sensors and battery-powered wearable sensors based on optical phenomena that have revolutionized wearable sensing automation[13].

6- The scientist Sinéad O' Dwyer et al. Ir J Med Sci. (2021, May) were used textual narrative synthesis, this study intended to identify and summarize the findings of qualitative research that have been published and deal with patients' experiences with dental implant surgery. Relevant qualitative studies up to (January,2020) were discovered by a thorough two-stage electronic and manual literature search. In the included main studies (n = 15), patients' experiences with dental implant therapy were examined using qualitative research techniques including focus groups and interviews. They examined the experience of losing a tooth, the decision-making process, what happens before the implant, what reasons motivate patients to seek treatment, what obstacles stand in the way, and what happens after the implant with the prosthesis. There is a lack of investigation on how conscious sedation affects the patients' intraoperative dental surgery experience [14] .

7- Muayad Kod in September 2016 has worked on multistage voltage doubler rectifiers operating at 433 MHz. He also created in his study a number of different antennas including a meandering loop antenna that is covering the ISM band at 433 MHz, and the MICS band at 403 MHz with strong magnetic flux in the near field. In addition, he designed two broad band

loop antennas operating at 0.4-1 GHz and 2-2.7 GHz. This antenna is made to work with Microsemi's implanted transceiver ZL70323 such that the MICS band, 433 MHz for power, and 2.45 GHz for wake-up signals are all used for communication. A second wearable antenna is also created for by using a meandering loop antenna. Strong fields are produced by this antenna along both axes. The improvement of the magnetic field for improved WPT is this design's contribution. Additionally, two implantable antennas were designed to be integrated to the rectifiers to create a WPT system. The two proposed antennas are flexible so they may be used on flat and curved surfaces and operating at 433 MHz [15].

1.3 Aims of the Dissertation

The study aims to determine the possibility for utilizing voltage doubler rectifiers in wireless implantable devices and whether it is possible to combine the DC output of two or more voltage doubler rectifier. In both situations, this might enhance the amount of energy harvested, whether there is one antenna receiving numerous bands or there are many antennas,and whether they operate within the same or distinct bands. These aims will be achieved by:

1- Studying the output voltage and conversion efficiency of voltage doubler rectifier circuit with varying the input power using Advanced Design System (ADS) software.

2- Comparing single, double and triple stage rectifier circuits for frequencies 433 MHz and 915 MHz through the results of the output voltage efficiency with the goal of obtaining the highest efficiency and choosing the best among them.

3- Designing RF antennas at 915 MHz and 433 MHz to be integrated with the IMD that are placed below the layer of skin. CST Microwave Studio software is empoyed to design and evaluate the performance of the proposed antennas.

4- Manufacturing and fabricating the designed rectennas (rectifier + antenna) and test thier performance in the lab.

5- Comparing the simulated and measured result and draw the main conclusions of this study.

1.4 Thesis Layout

The thesis includes a number of investigations that helped to accomplish the aforementioned goals. The five chapters of this thesis are separated as follows:

- The first chapter discussed the introduction and literature reviwes of implantable medical devices .

- The second chapter includes a review on implantable devices, comparison of different energy sources, discussion on Wireless Power Transfer (WPT), highlight the characteristics of rectifier and demonstrates the design of an implantable antenna equations for typical requirements of Implant Systems.

- The third chapter discusses the simulation methodology of rectifier circuits with single stage rectifier at 433 MHz circuit, double stage rectifier at 433 MHz circuit, single stage rectifier at 915 MHz circuit, and double stage rectifier at 915 MHz circuit. The efficiency and output voltage with varying input power are recorded for all circuits at operating frequency of 433 MHz and 915MHz.

- The fourth chapter focuses on the design of antennas at operating frequency of 433 MHz and 915MHz. The S-parameters, 2D radiation patter and 3D radiaiton pattern of the designed antennas are observed, recorded and discussed with a simple parameteric study is conducted.

- The fifth chapter presentes the conclusion of this work and suggested future works.

CHAPTER TWO

THEORETICAL BACKGROUND

2.1 Introduction

The first electronic device to be placed into a human body was a cardiac pacemaker. The most effective therapeutic devices ever created for preserving human life and enhancing the patient's quality of life are thought to be implantable cardiac pacemakers.

In October 1958, the first implantable cardiac pacemaker was placed. Electrical engineer Dr. Rune Elmqvist of Elema-Schönander created and constructed it .The device was in the size of a hockey puck, ran on rechargeable batteries, and included just one silicon transistor. Mr. Arne Larsson, a patient who had spent months in bed due to severe Gerbezius-Adams-Stokes attacks, had it implanted by Dr. Ake Sen-ning. As the sole "backup" device Elmqvist and Senning had, the initial pacemaker implant only functioned normally for a few hours before it had to be replaced the following day with a second pacemaker of the same type. Fortunately, Mr. Larsson made it through several months of successful use of the second pacemaker. Furthermore, he had more than 25 pacemaker replacements before passing away in 2001. Today, the majority of medical devices that are inserted into people are powered by primary batteries, which has various drawbacks. Despite the use of lithium batteries with a high energy density to lower the size of the batteries, they still take up about 25–60% of the volume of implanted devices. Recently, implanted medical devices have been used for a growing number of

diagnostic and therapeutic tasks [1, 7-8, 17]. These tools must be able to wirelessly interface with other equipment in order to be truly helpful while maintaining patient comfort. In an effort to get beyond the drawbacks of inductive biotelemetry, such as its low data rate, constrained communication range, and sensitivity to inter-coil misalignment, antenna-enabled biotelemetry for implants is receiving a lot of attention [18, 19]. High scientific interest is being shown in implantable antenna design to address the issues of miniaturization, biocompatibility, impedance matching, dependable data sharing, and patient safety.

Due to the rapid progress of technological approaches and instruments, our world is evolving at a breakneck pace. Human requirements in various living styles, such as health and leisure, serve as the foundation for such progress. There is no any doubt that health takes priority over other necessities since it is directly related to life. It has a thriving market and attracts a huge amount of research investment. As a result, industrial and academic researchers are working hard to design and manufacture health instruments and medical gadgets that are more dependable, safer, and convenient. Medical equipment can be planted in the human body for a variety of purposes, including monitoring, medicine delivery, and activation. Inductive and RF antennas are the two most common methods for establishing communication linkages for biomedical implants. Through inductively connected coils, the operating frequency bands range from a few kHz to many MHz. Within the near field zone, the communication distance between the inductively coupled implanted device and the external unit is limited to very short distance [7, 17].

In response to a petition from Medtronic, the US Federal Communications Commission (FCC) awarded the Medical Implant Communication Service (MICS) band of 402–405 MHz in 1999. This will allow implantable devices to communicate via a mobile wireless device. The RF spectrum can be used to enhance the range of a communication link, [8]. The regulation limits the equivalent isotropically radiated power (EIRP) of MICS devices to -16 dBm in order to prevent interference between these devices [18]. The European Telecommunications Standards Institute (ETSI) eventually adopted this frequency in 2002, making it the target spectrum for implantable RF designers [19]. Later, in 2002, the European Telecommunications Standards Institute (ETSI) adopted this band, making it the preferred band for implantable antenna designers [8]. In 2009, the Medical Device Radio Communication (MedRadio) band (401- 406 MHz) was added to the MICS band. The MICS band, on the other hand, remains the heart of the MedRadio system, and it is allocated for implantable device transmission only, with a channel bandwidth of 300 kHz. Medical body-worn devices can utilize the frequency range of 401-402 MHz and 405-406 MHz.

The industrial, scientific, and medical frequency bands (ISM, 433–434 MHz, 902–908 MHz, 2.4–2.48 GHz, 5.715–5.875 GHz), and the wireless medical telemetry service frequency band (WMTS, 1.395–1.4 GHz). In addition, certain foreign locations have approved ultra-wideband frequency bands (UWB, 3.1–10.6 GHz) for high-quality communication [23]. Primary batteries are used to power most implants. Non-rechargeable batteries with a relatively short lifetime, for example, power deep brain neurostimulators and

pacemakers. These batteries have a lifespan of 5 to 7 years, depending on the device's function when the implantable device's battery life expires, it must be surgically replaced, which comes at a significant expense and poses a danger of infection to the patient. Infection rates associated with pacemaker replacements range from 1 percent to 19 percent [19]. Furthermore, several implantable devices that work in direct contact with infected, such as pH and glucose sensors, cannot use batteries due to the risk of poisoning in the event of a leak [6]. Batteries take up more than 50% of the volume of some of the other gadgets. The usage of such batteries as an alternate solution results in a significant reduction in implant size. It also ensures the implant is cost-effective and exhibits a long-term usage. The focus on the power consumption of medical devices is extremely valuable in determining the best power sources. The usual power consumption of an implanted device ranges from 10s to 100s of milliwatts. The pacemaker, for example, requires between 10 μW to 70 μW under typical conditions [6, 20]. The nerve stimulation equipment utilizes 100 μW [9], while the glucose monitoring system uses 48 μW [22].

By continuously monitoring certain illness changes, for instance, implantable devices improve healthcare quality by lowering the likelihood of particular diseases' complications. Additionally, it lowers the cost of healthcare because, for instance, patients can be monitored continually without being admitted to the hospital [6,18-21]. Examples of implanted devices for ongoing monitoring are shown in Figure 2.1.

The primary uses of implanted devices are either diagnostic data collection and transmission or therapeutic applications, such as the treatment of hyperthermia. The importance of continuous monitoring for many diseases, including the heart rate, blood oxygenation levels in patients with chronic obstructive pulmonary disease (COPD), blood sugar levels in patients with diabetes, blood pressure, and patients' daily activities has been demonstrated by medical and biomedical researchers [18-20, 6,23].

In this study, several rectifier circuits will be designed and simulated at frequencies 433MHz and 915MHz, which are considered within the range of frequencies allowed by the World Health Organization. The simulations will be carried out by using ADS program.
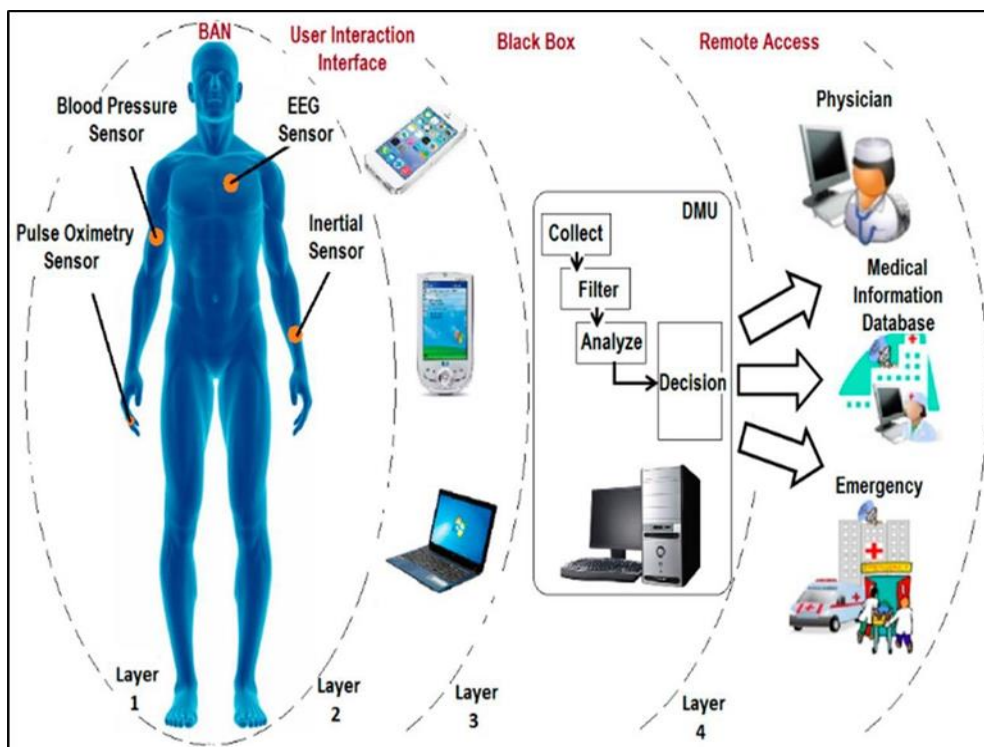
Fig. 2.1. Body sensor network systems [2].

The human body can accommodate a wide variety of implanted devices, as seen in Fig. 2.1. In order to deliver vital bio information, medical implants wirelessly communicate with external readers. Such data are crucial for both therapeutic and diagnostic purposes. Effective antennas are needed in wireless communication to create linkages. Since the antenna is meant to be implanted inside the human body, numerous factors need to be taken into account when designing it. Some of these factors include keeping the size as small as feasible, conforming to the design of the medical device, using radiation in a way that is appropriate for the application. Furthermore, it is most critical to keep the value of the transmitted power lies within the specific absorption rate (SAR) limit for safety reasons.

Implantable device power sources can be categorized into three categories. The primary or rechargeable battery is used as the main supply in the first type. The second type relies on internal body energy sources like thermal, piezoelectric, and biological cell energy to generate power. The third form uses specialized external transmitters and Wireless Power Transfer (WPT) as its foundation. Table 1.1 compares the advantages and disadvantages of several power sources in terms of power density. The most dependable source is the use of as shown in Table 2.1, is the use of primary batteries (nonrechargeable). The batteries must be replaced surgically after a set amount of time because they have a limited lifespan and self-discharging. Because the capacity of such batteries is also constrained, medical gadgets can only perform a limited number of operations in order to prolong battery life [24].

Table 1.1 : Comparing different energy sources

Power source	Power density	Pros	Cons
Batteries	0.09 µW/mm^2/year	Reliable	Limited life span
Piezoelectric	0.2 µW/mm^2	Internal energy	Depending on moving parts
Glucose bio-fuel cell using glucose from blood (5 mM)	2.8 µW/mm2	Internal energy	It is limited by the glucose enzyme density
Thermoelectric, T-5°C	0.6 µW/mm^2	Internal energy	Low efficiency
Electromagnetic power transfer	10 to 1000 µW/mm2	High power density and Controllable	Limited by safety regulations

Additionally, it is the main cause of the big volume that affects the device's size and design. On the other hand, crystalline piezoelectric materials' potential to produce electricity through movement is a possible promising source.

The density of the glucose enzyme, however, places a limit on this method [25]. The thermoelectric is another internal source for energy gathering. Due to its poor efficiency, this power source has limitations [26]. These internal sources are helpful since they are always present, but they have limitations due to factors like poor density, low efficiency, or availability in only certain areas of the body. According to Table 2.1, the WPT system has the maximum power density when compared to other potential sources. This technique can be adjusted and optimized in accordance with the

18

application needs, even though it is constrained by the safety standard for maximum allowable exposures .

Another sort of implanted equipment, known as a capsule endoscopy, which is a process used to study digestive issues, has recently been utilized to diagnosis several additional diseases [27, 28]. Digestion issues manifest as symptoms including persistent abdominal pain, unexplained weight loss, or GI bleeding. Numerous illnesses, including inflammatory bowel disease, Crohn's disease or ulcerative colitis, celiac disease, benign and malignant tumors, or any other digestive problems, may be to blame for these symptoms [27, 28]. For the purpose of identifying sickness or conditions affecting the digestive system, including the stomach and small bowel, capsule endoscopy can be used to obtain photographic pictures. As shown in Figure 2.2, capsule endoscopy comprises of batteries, a light source, camera, transmitter, and antenna in a size comparable to or almost identical to vitamin capsules [27, 28].
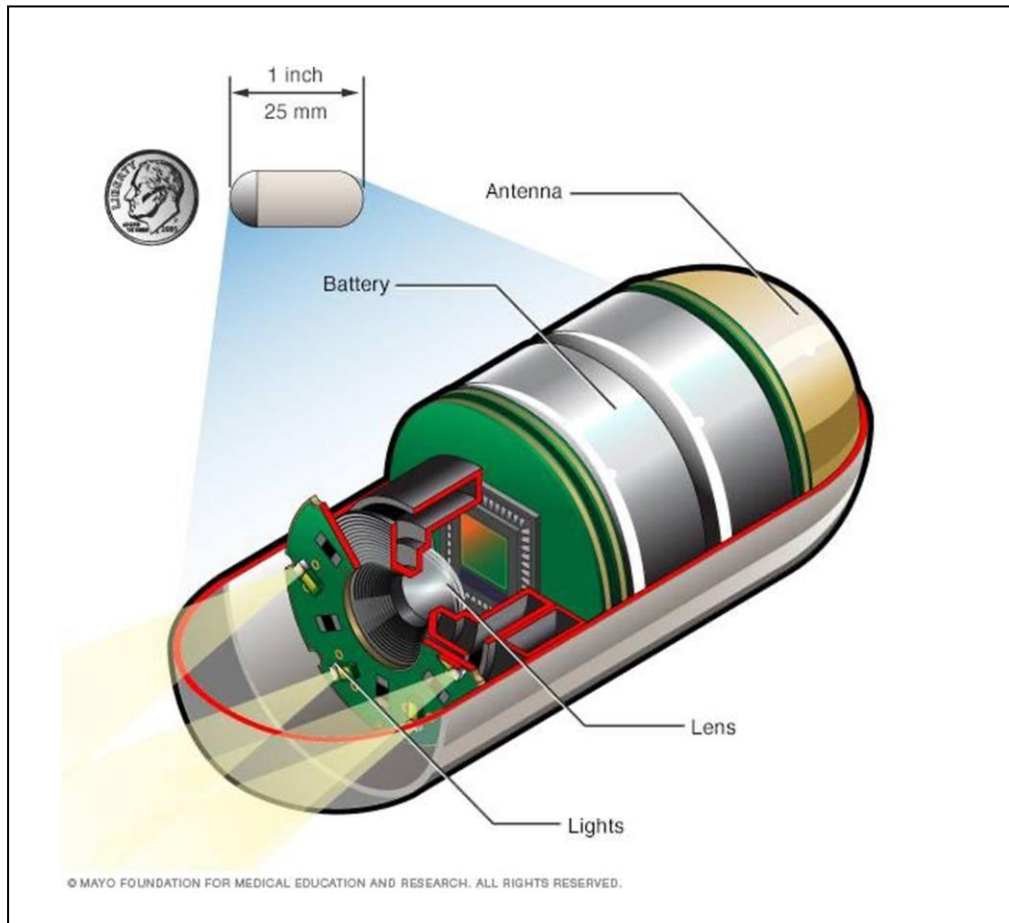
Fig 2.2. Capsule Endoscopy [13].

2.2 Wireless Power Transfer (WPT)

The term "wireless power transfer" (WPT) refers to a method that transmits energy wirelessly over a medium from a power source to an electrical load, without the usage of cables to conduct the energy [29, 30]. This technology is widely employed in a variety of applications, including high-powered electric cars [35–38], high-tech low-power biomedical implants [31-34], and white goods like electric toothbrushes and cell phones. Figure 2.1 includes a taxonomy of WPT approaches along with these significant technological advancements from the 1880s to the present that are pertinent to implanted medical devices (IMDs).

Both electromagnetic (EM) and non-EM energies are used in these methods [39].
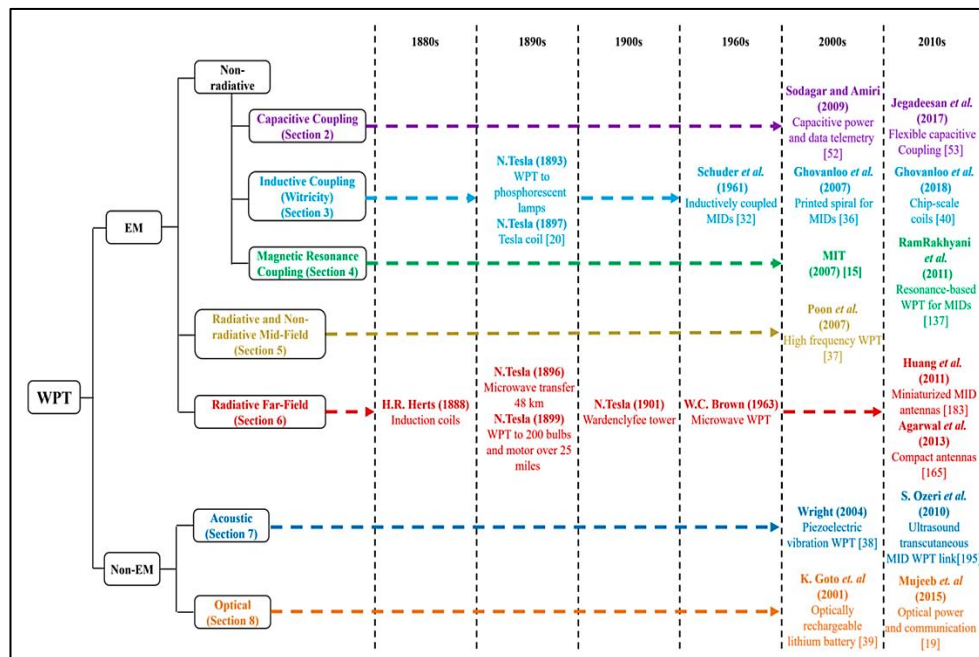
Fig.2.3. Classification and research overview of wireless power transfer (WPT) techniques indicating the key milestones relevant to implantable medical devices [39].

The former consists of electric, magnetic, and optical coupling systems, which may be further divided into radiative transfer and non-radiative transfer systems depending on how close the transmitter and IMD are to one another (less than 100 mm [40]). The midfield WPT, distinguished by a separation of 100 to 500 mm, is located between the radiative and non-radiative zones [41].

Either near-field or far-field electromagnetic (EM) waves can be used to convey wireless power Transfer. Systems for far field wireless power transmission simply transmit using high power antennas, and the radiation is often in the RF or microwave spectrum. But near-field wireless power transfer systems make use of electric and/or magnetic coupling to transmit energy through the near-field, often in a resonant mode.Applications employing far-field EM waves typically have excellent range but are

21

restricted to a direct line of sight between the emitter and receiver and are sensitive to directionality.

In contrast, because non-resonant objects inside the field tend to have a small impact on the power transfer, the near-field wireless system is not constrained to a direct line of sight between emitter and receiver and can be less sensitive to directionality. However, its range is restricted. Furthermore, new study in this area has been sparked by the fact that magnetic coupling-based near-field wireless power transmission devices (such coils) are safer for people than other systems that generate significant electric field energy densities in space [29] .

2.3 Rectifier Characteristics

A rectifier's primary job is to convert AC to DC,where the obtained output DC can be utilized to directly power a particular appliance or to recharge a battery. The voltage doubler rectifier was selected and covered. According to Fig. **2**.4, this circuit is made up of two diodes, a charging capacitor and smoothing capacitor. Figure 2.5 shows a voltage doubler circuit that can provide twice the output voltage when compared to a single diode rectifier [42, 43].
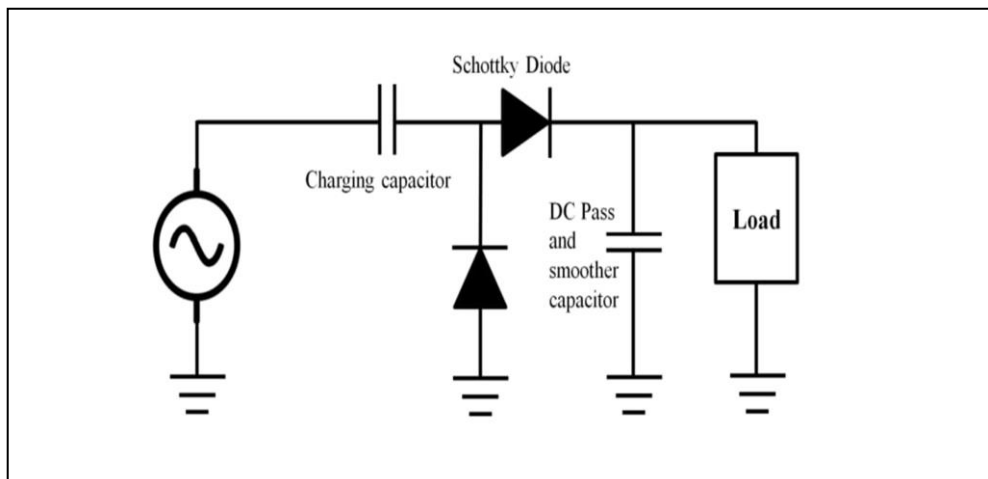

Fig. 2.4: Voltage doubler rectifier circuit diagram [42, 43]
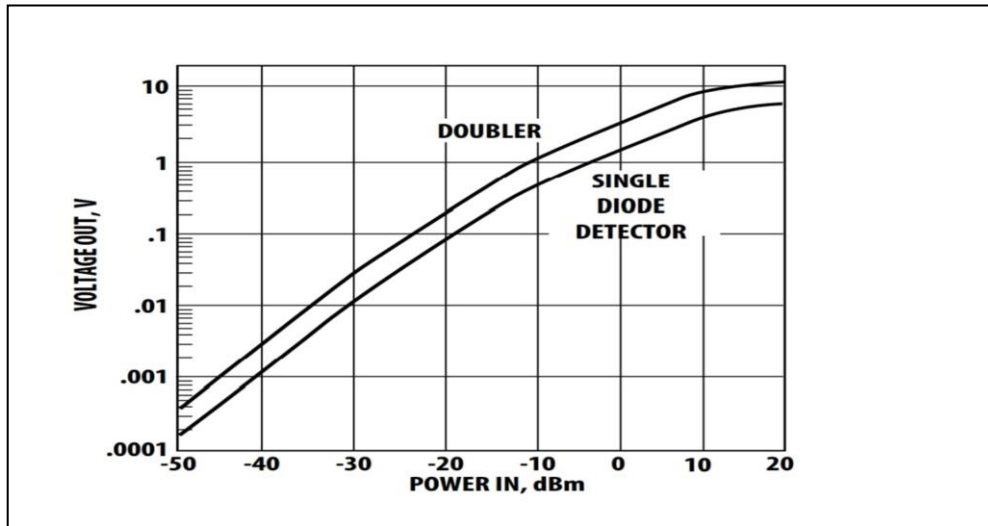
Fig. 2.5 .Voltage doubler output at sweep of input power compared with single diode rectifier [43].

Diodes are selected for a particular application based on a number of distinguishing characteristics. Schottky diodes are frequently utilized in radio frequency applications that expect low power inputs because they have a low forward voltage [44].

Rectifiers are an important component in WPT. As seen in Fig.2.6, it transforms the collected AC signal into DC. The effectiveness of such a rectifier is crucial in determining the WPT system's overall effectiveness. To maximize power transmission, an impedance matching network circuit is typically used between the rectifier and the antenna. Moreover, a smoothing capacitor is further supplied as a shunt to the rectifier's output to provide a constant DC output.

The three major topologies of rectifier circuits are generally recognized. A single diode rectifier is the initial topology [45, 46]. Using this architecture, a half wave rectifier is created. Ideal conversion efficiency for this rectifier is 50%. Diodes require some forward voltage to operate ON, though. Since the HSMS-

23

2852 Schottky diode has a forward threshold voltage of 0.15 V, as illustrated in Figure 2.7, this rectifier has a conversion efficiency of around 40%. The twin diode rectifier is the second kind. This rectifier often functions as a voltage doubler while it is still considered as a half wave rectifier [46].

Compared to single diodes, it may operate with a better conversion efficiency. As illustrated in Fig. 2.8, it typically comprises of two diodes (D1 & D2), a charging capacitor (C1) and a smoothing capacitor (C2) [42, 43].
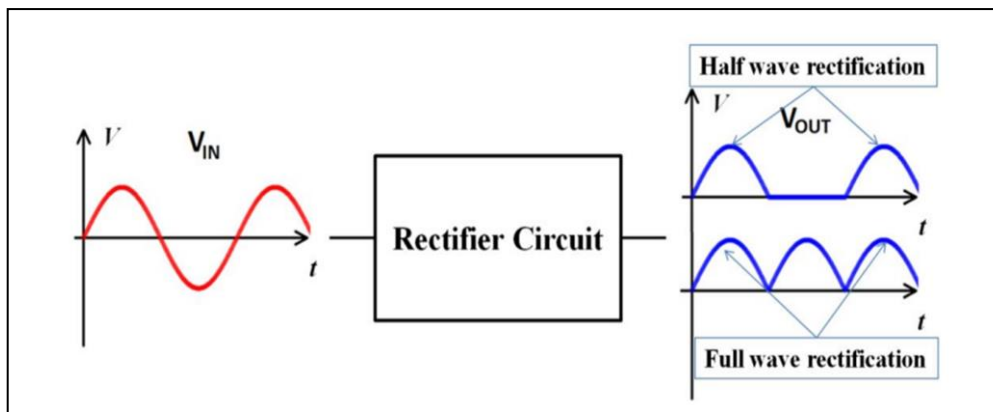

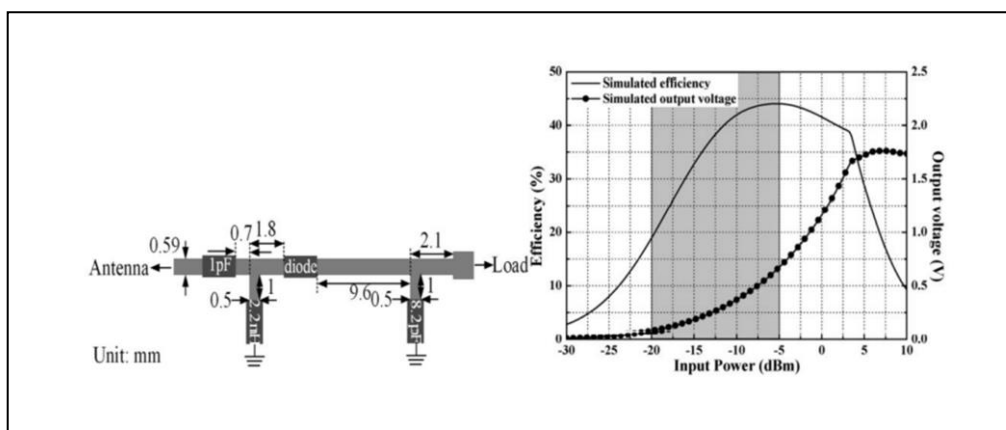**Fig. 2.6. Diagram of the rectification process using half-wave and full-wave rectification [45].**

Fig. 2.7. Diagram of a single diode rectifier showing the results of simulation [46].

24
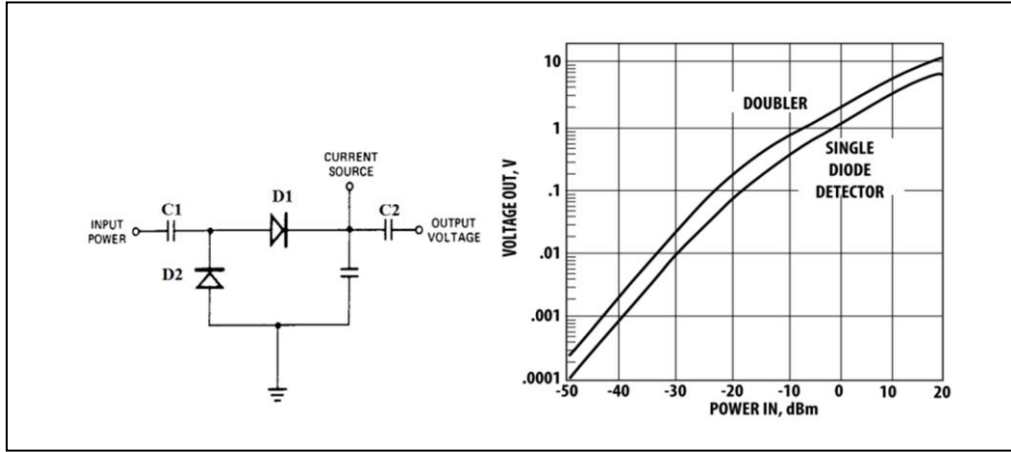
Fig. 2.8.Voltage doubler rectifier with dual diodes [46].

2.4 Implantable Antennas

Antennas for IMDs have been developed for RF applications at megahertz, sub-gigahertz and higher frequencies. In order to create a communication link between the implanted biosensor and distant external units, these antennas are crucial. The performance of the implanted device will be directly impacted by the characteristics of these antennas. Body tissues have an effect on these characteristics. When the body loss is taken into account, the gain of such antennas is extremely low, with values less than 0 dB [47]. Due to the substantial absorption of the emitted signal energy by the tissues, the radiation efficiency is also quite poor. Eq.(2-1) [48] may be used to compute the received power at a certain off-body receiver :

$$P_{RX} = P_{TX} + G_{RX} + G_{TX} - L_P - e_P \quad .... (2\text{-}1)$$

Where G_{RX} and G_{TX} are the gain of receiving and transmitting antennas, respectively, after substracting the antenna impedance mismatch loss, L_P is the path loss, and e_P is the polarization

mismatch. P_{RX} is the power received by the external receiver and P_{TX} is the power supplied to the in-body antenna [49-53].

2.4.1 Difficulties and Requirements for the Design of an Implantable Antenna

The ecology within the human body is extremely complex. The analysis, characterization, realization, and design of implantable antennas are inevitably impacted by their lossy, dispersive, and inhomogeneous nature [54–56]. Different lossy tissues that make up the human body are distinguished by conductivity ([S/m]) and dielectric constant (ε_r). The majority of the antenna radiation is absorbed by these lossy tissues, which lower the radiated power and decrease the antenna radiation efficiency [57, 58]. The formula for the link between radiation efficiency (η) and radiated power is given in Eq. (2-2) [59]:

$$\eta = P_{rad} / P_{in} \quad .... \quad (2\text{-}2)$$

where P_{in} [W] denotes the input power and P_{rad} [W] denotes the radiated power.

In contrast to the situation in free space, the nearby electric field |E| is tightly associated with the tissues of the human body, leading to the power loss via absorption as in Eq. (2-3) [59]:

$$P_{abs} = \omega^2 \iiint \varepsilon_0 \, \varepsilon_r" \, |E|^2 \, dV \quad .... \quad (2\text{-}3)$$

where the rotational frequency is ω [rad/s], the free space permittivity is ε_0 [F/m], $|E|$ [V/m] is the near electric field intensity, dV is the differential volume element over which the integration is taken, and $\varepsilon_r"$ is the imaginary portion of relative permittivity.

The radiated power decreases when a portion of the power is absorbed. [59]:

$$P_{rad} = P_{in} - P_{ref} - P_{abs} \quad \text{.................... (2-4)}$$

2.4.2 Typical Requirements of Implant Systems

There are a number of general parameters that must be taken into consideration while building an implantable electronic system, including small size and weight, low power consumption, high biocompatibility and low toxicity, high data rate, and low data latency. As for any commercial product, consumer expectations and preferences have a significant impact on the design of implantable devices. Smaller and lighter devices are probably less painful and uncomfortable for the host during healing and use, in addition to being less intrusive to the patient's body after implantation.

By exerting pressure on nearby tissues that have already suffered damage as a result of surgery and fueling inflammatory processes in the peri-implant region, the excessive size and weight may be harmful to the healing process. Small and light gadgets allow for greater patient quality of life because they are less limiting of daily activities. While the electric circuitry components have substantially shrunk thanks to breakthroughs in MEMS and nanotechnology, the power supply and encapsulation components continue to be the key contributors to the device's overall weight and size. The implanted module's volume may be further increased by coupling capacitors that are utilized to guarantee charge-balance and effectively reduce current leakage [60,61].

2.4.3 Types of Antenna

1. **Wire Antenna:** This is a length of wire that extends in free space over the PCB and aligns at $\lambda/4$ over a ground plane. Typically, a 50-Ω^4 transmission line supplies this. Because of its size and three-dimensional exposure, the wire antenna performs and has the best RF range. The wire may be looped, helixed, or straight. This construction is three-dimensional (3D), with the antenna sticking out into space at a height of 4-5 mm above the PCB plane depending on the operating frequeny [62] as shown in fig 2.9 .
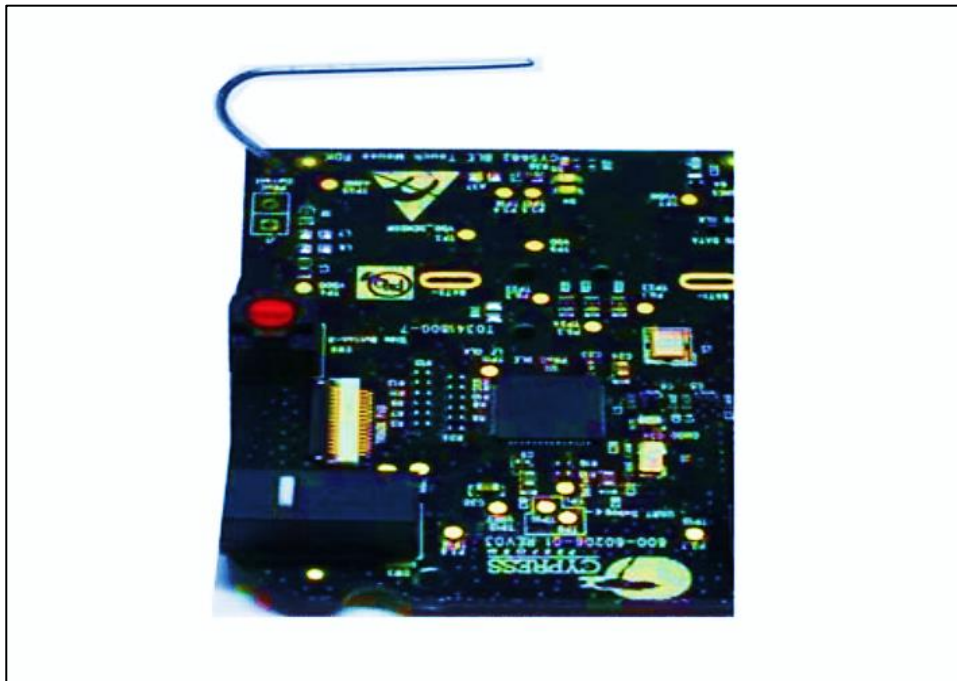

Fig. 2.9. Wire Antenna [62].

2. **PCB Antenna:** is a trace that has been drawn on the PCB. Depending on the antenna type and available space, this can take the form of a straight trace, an inverted F-type trace, a meandering trace, a circular trace, or a curve with wiggles. The

28

antenna in a PCB antenna transforms into a two-dimensional (2D) structure in the same PCB plane; see Figure 2.10. As the 3D antenna exposed in free space is transported to the PCB plane as a 2D PCB trace, there are rules that must be observed. While it is less efficient than a wire antenna and requiring more PCB space, a PCB antenna is nonetheless more affordable. It is simple to manufacture and offers a wireless range that is appropriate for a BLE application [62] .

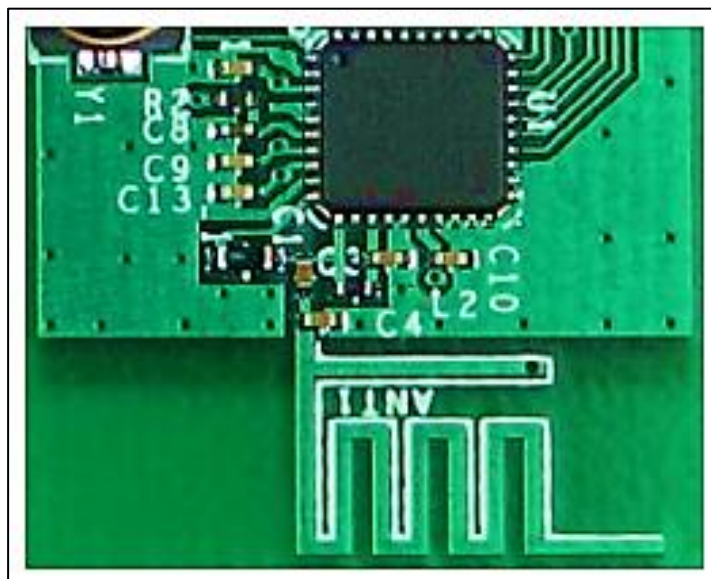**Fig. 2.10. PCB Antenna [62].**

3. **Chip antenna:** An antenna with a conductor packed within is referred to as a "chip antenna" because of its compact form factor. When there isn't enough room to sustain a 3D wire antenna or print a PCB antenna, this is helpful. For a Bluetooth module with a chip antenna, see figure 2.11. This is a comparison of the antenna and module's size to a one-cent coin [62] .

Fig. 2.11. Chip antenna [62]

2.4.4 Antennas Parameters

1- **Return loss:** An antenna's return loss represents its ability to be matched to the transmission line (TL), which is depicted in Figure 2.12 as a signal feed. Typically, the TL characteristic impedance is 50 Ω, however it might be any number. It is most practical to use 50 Ω impedance because it is the industry standard for testing tools and commercial antennas. Return loss measures the amount of incident power that the antenna reflects owing to mismatch . When precisely aligned, an ideal antenna will emit all energy without any reflection [62] .
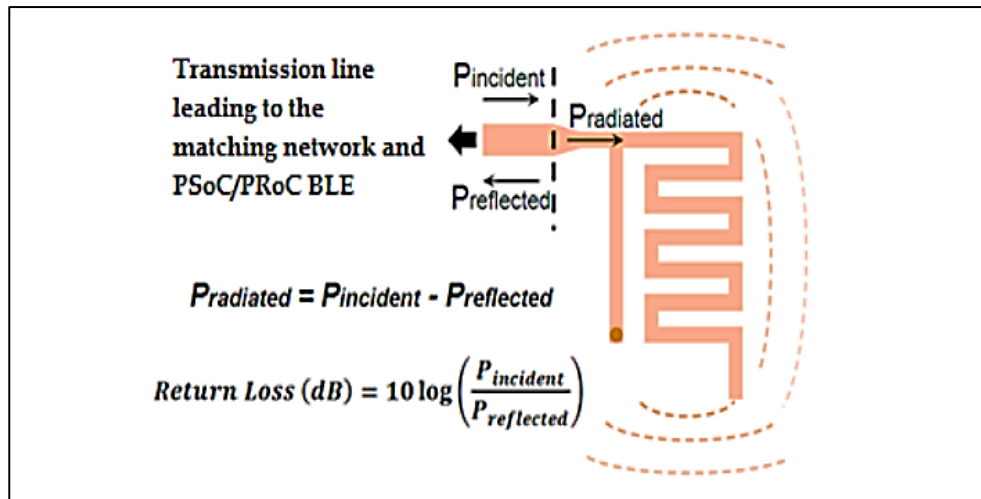
Fig 2.12. Integrating a TL to a meandered antenna to measure the return loss [62] .

2- **Bandwidth:** Bandwidth describes the antenna's frequency response. It represents how well the antenna is matched to the 50 Ω transmission network throughout the entire range of interest [62] .

3- **Radiation efficiency:** Some of the quasi power is lost in the antenna as heat or thermal loss. Dielectric loss in the FR4 substrate and conductor loss in the copper trace are responsible for thermal loss. Radiation efficiency is the term used to describe this information. All non-reflected electricity is radiated to empty space when the radiation efficiency is 100%. The heat loss for a small-form-factor PCB is negligible [62] .

4- **Radiation pattern:** A radiation pattern shows which directions have more and which directions have less radiation, which is a directional attribute of radiation. This knowledge aids in placing the antenna correctly in a given application. When positioned in a plane perpendicular to the antenna axis, an isotropic dipole antenna radiates equally in all directions. The majority of antennas, nonetheless, depart from this ideal

31

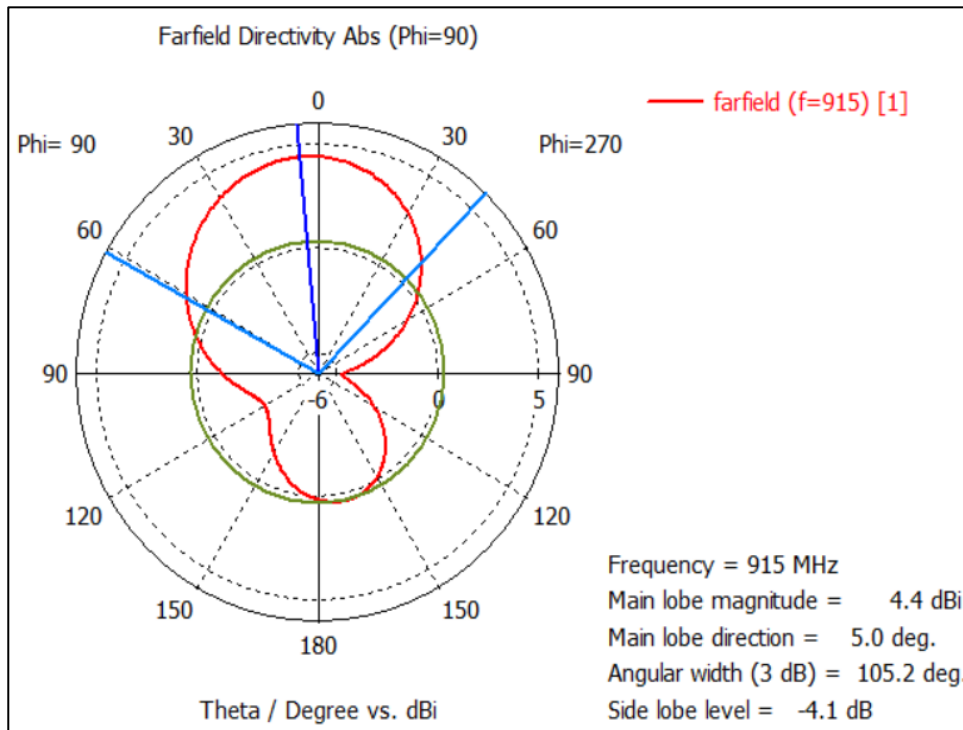conduct. See figure 2.13 for an example of a PCB antenna's radiation pattern [62] .

Farfield Directivity Abs (Phi=90)

Frequency = 915 MHz
Main lobe magnitude =   4.4 dBi
Main lobe direction =   5.0 deg.
Angular width (3 dB) = 105.2 deg.
Side lobe level =   -4.1 dB

Fig 2.13 .Radiation pattern of antenna [62] .

5- **Gain:** As contrast to an isotropic antenna, which radiates evenly in all directions, gain describes the radiation in the direction of interest. The strength of the radiation field relative to an ideal isotropic antenna is measured in decibels (dBi) [62] .

CHAPTER THREE

DESIGN AND SIMULATION OF MULTI-STAGE RECTIFIER CIRCUITS

Using Advanced Design System (ADS) Software, voltage double rectifier and matching circuit design and simulation are performed at 915 MHz and 433 MHz. Without using wires or contacts, Wireless Power Transmission (WPT) is an effective way to transfer power from a source to an end system. Rectennas, which combine an antenna with a rectifier, are used to do this job. The rectifier, which transforms receiving RF power into DC power, is arguably the most significant part of the antenna. In this chapter, several rectifier topologies are designed for rectennas application (RF application). The antenna is employed to receive RF energy and transport it into the matching circuit. Matching circuit will be used to match impedance of the rectifier and antenna while the diode HSMS-2820 is used for rectification (Schottky diode). It is worth mentioning that choosing the right diode is one of the most crucial factors. The simulation results including DC output voltage (Vout), efficiency, and output current with respect to the input power, are recorded and plotted at two frequency bands throughout this chapter. the single-, double- and triple-stage rectifier circuits operating at 433 MHz are already reported in [15]. however, in this work the matching parameters were changed for the aforementioned circuits and were operated at both 433 MHz and 915 MHz for comparison purposes to find out the best performance.

3.1 Single stage rectifier at 433 MHZ

As illustrated in Figure 3.1, a single stage rectifier is developed and simulated using ADS. A power source, which in such systems serves as the antenna component, is included in the circuit. The power source has an internal impedance of 50 Ω and transmits an RF power of 10 dBm at 433 MHz to the circuit. The matching network circuit for the rectifier circuit, which comprises of inductance and is chosen to match the rectifier circuit with the antenna, is also present in the rectifier circuit. Additionally, HSMS2028 diodes were employed, which functions to rectify the coming RF signal and convert it from AC to DC. At the input, the series capacitance acts as voltage doubler. Additionally, the output has a capacitance to smooth the DC output before it is fed to the load as DC power or stored in a battery. It's important to note that the circuit below is intended to be printed on FR-4 substrate with a 4.3 dielectric constant and a 1.57 mm thickness.

Figure 3.2 displays the input voltage waveform that is fed to the single stage rectifier, which is simulated by ADS and was designed for 433MHz.
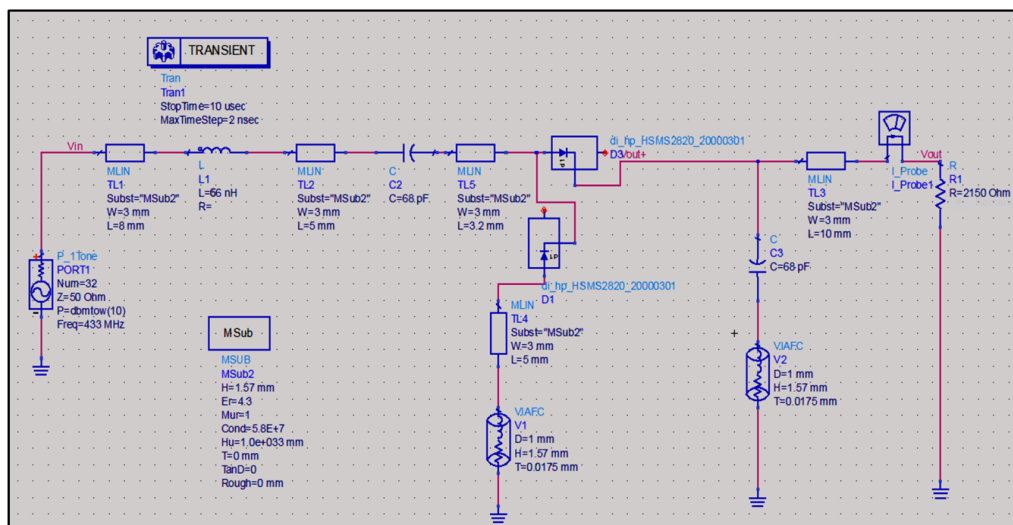

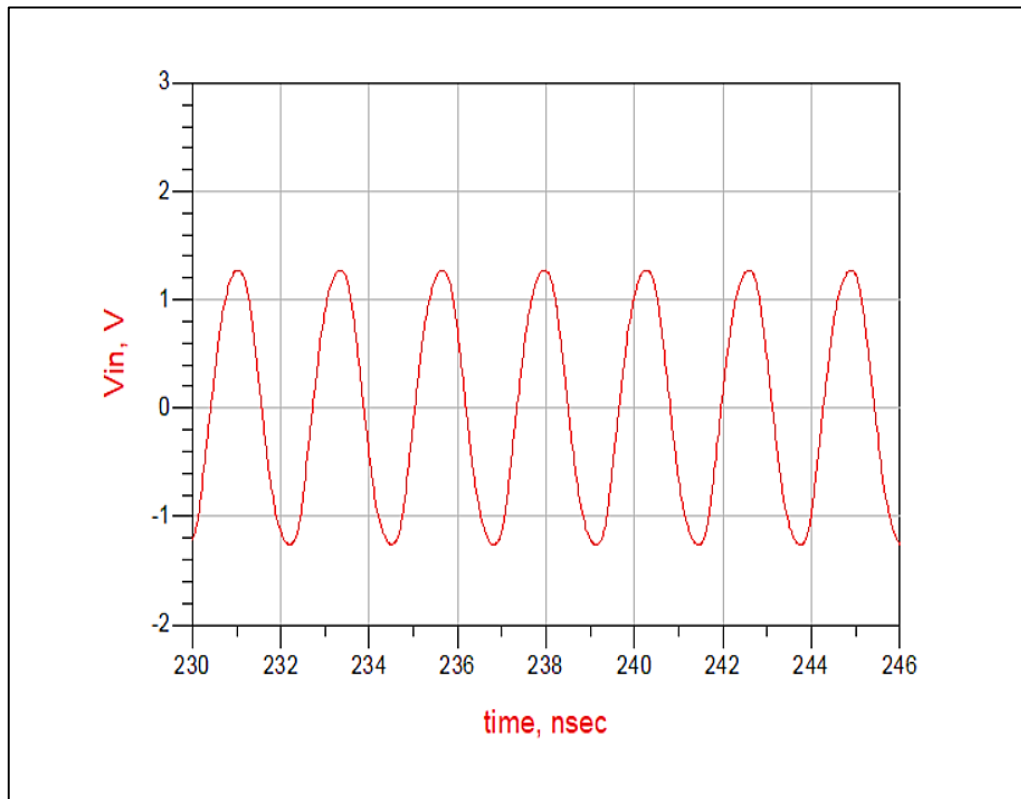**Fig. 3.1. Single stage rectifier operating at 433 MHz.**

Fig. 3.2.Vin (V) of Single stage rectifier operating at 433 MHz.

Figure 3.3 below shows the output voltage waveform of the single stage rectifier at 433MHz. The achieved DC output voltage is around 4 V, as can be seen in Figure 3.3, and there is a noticeable ripple that can be quickly reduced by using a low pass filter or a better smother.
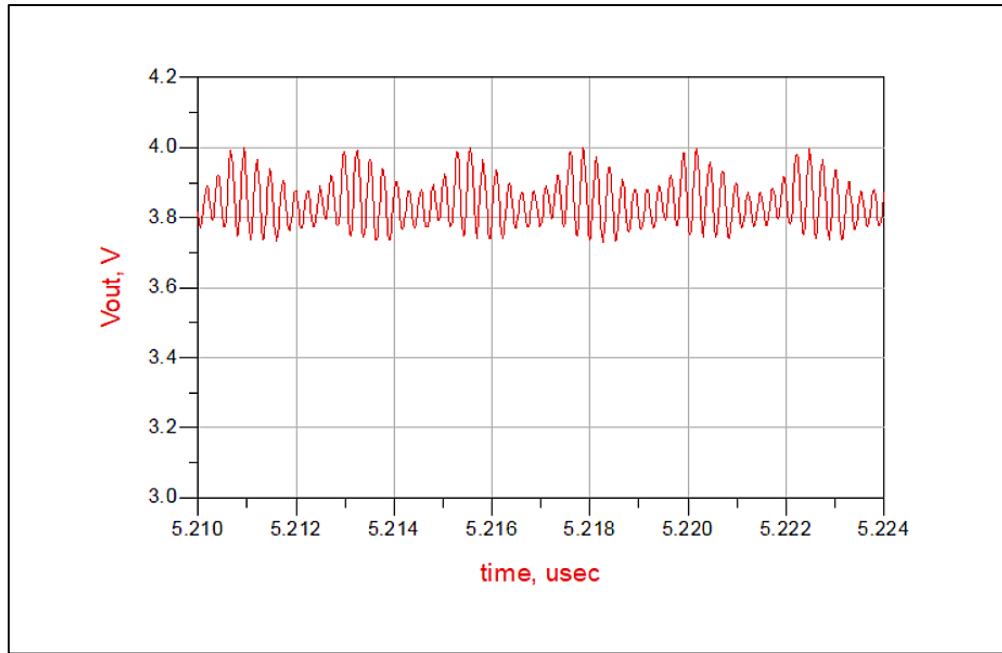
35

Fig. 3.3. Output voltage of the single stage rectifier operating at 433 MHz.

Figure 3.4 displays the waveforms of the output current at single stage rectifier that was designed for 433MHz. The output current is close to 1.8 mA. Changing the load value will change the output current though.
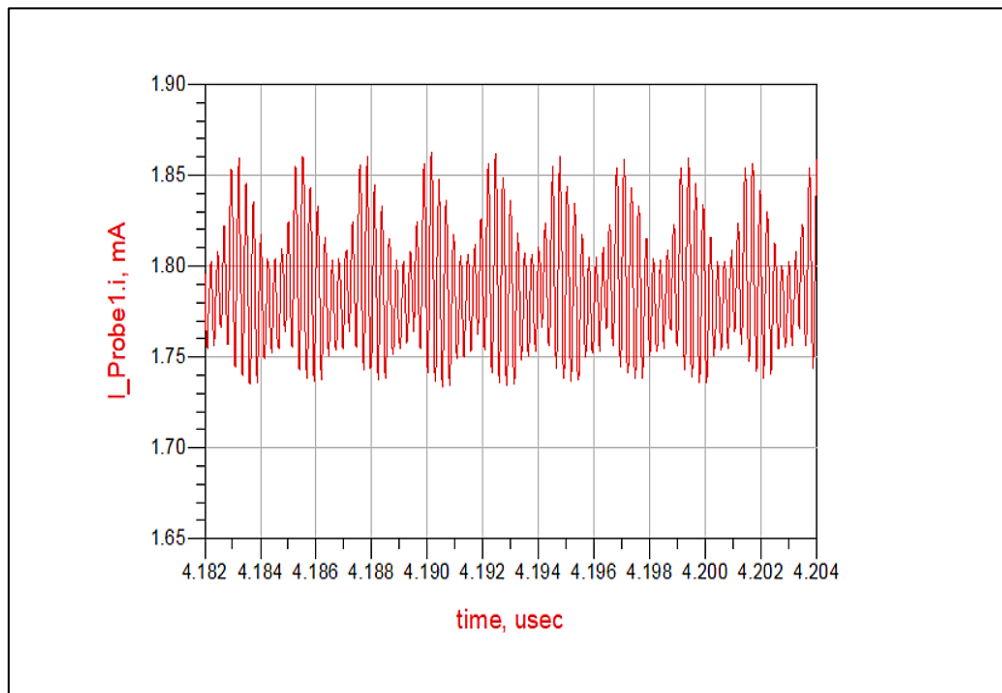

Fig. 3.4. Output current of single stage rectifier at 433 MHz

.

The conversion efficiency is used to measure the rectifier's performance in addition to Vout's value and quality. It has been investigated how the input power (Pin) affects the output voltage and efficiency. The relationship between the output voltage (Vout) and Pin (dBm) of a single stage at 433MHz is shown in Figure 3.5. It can be clearly seen that the output voltage increases exponentially with increasing the input power. A maximum output voltage of 4 V is achieved at input power of 10 dBm, which is equivalent to 10 mW.
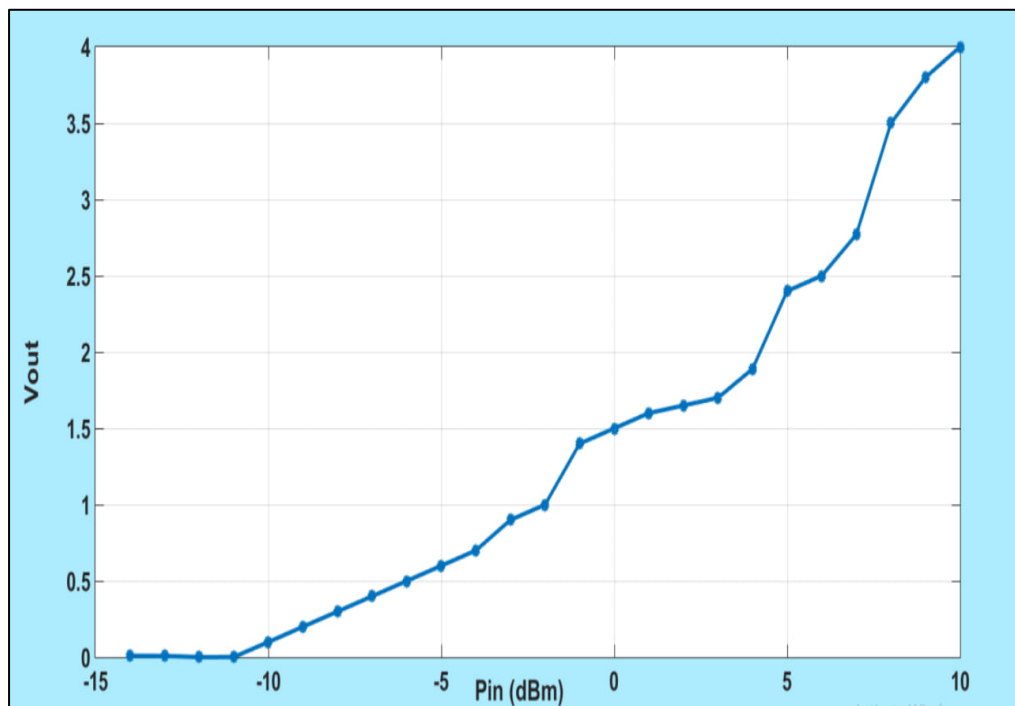

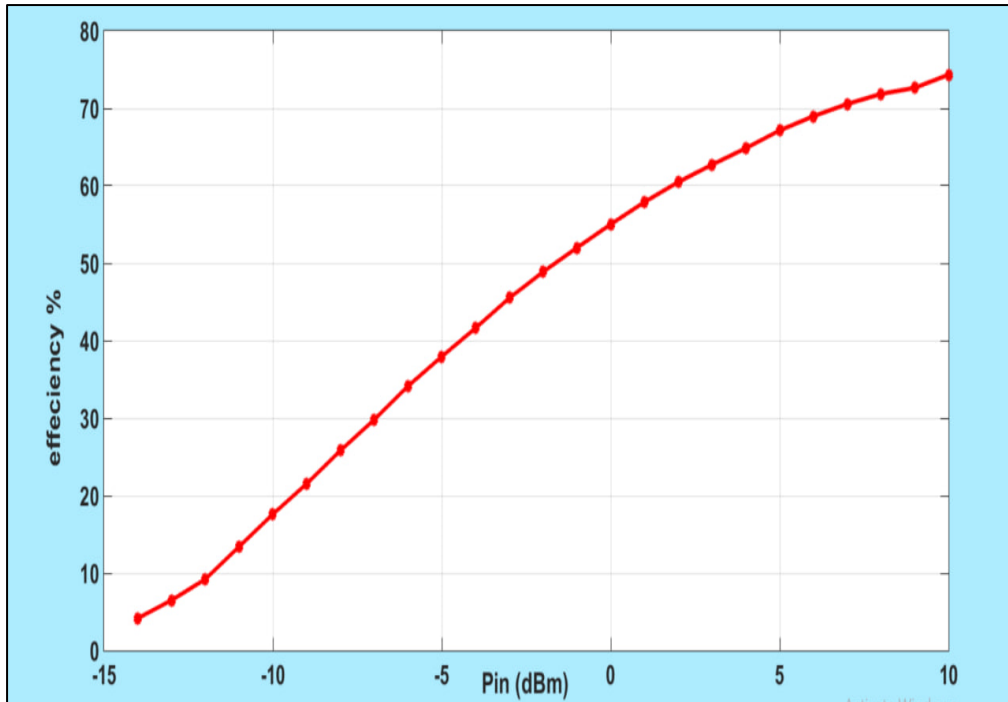**Fig. 3.5.Pin (dBm) and Vout (V) of single stage rectifier at 433MHz**

Fig.3.6. Efficiency versus input power of single stage rectifier at 433MHz.

Figure 3.6 shows that when the input power increases, the efficiency rises rapidly. Thus, it suggests that a slight increase in input power might result in a significant improvement in system performance. In other words, increasing the input power from 0 dBm to 10 dBm can result in an output voltage rise from 1.5 V to 4 V. Additionally, Fig. 3.6 shows how the input power affects the rectifier's conversion efficiency. The findings demonstrated that improving input power increases conversion efficiency. It has been found that the increase in efficiency was from 18% to 73 % when the input power is changed from -10 dBm to 10 dBm.

Rectangular microstrip lines were added to the circuit, as seen in Figure 3.1, to connect the components on the printed circuit board (PCB). In order to give the simulations the necessary dose of reality and produce more precise findings, the substrate details were

38

added. As a result, the source's impedance (50 Ω) on this substrate and at this particular frequency must be taken into account when choosing the suitable width of the strip lines (at 433 MHz). The achievement of the study to ascertain how the strip line width affects overall performance is shown in Figure 3.7. In figure 3.7, it can observed that 3 mm is the best width for maximizing efficiency, which is exactly in line with the result of theoretical calculations.
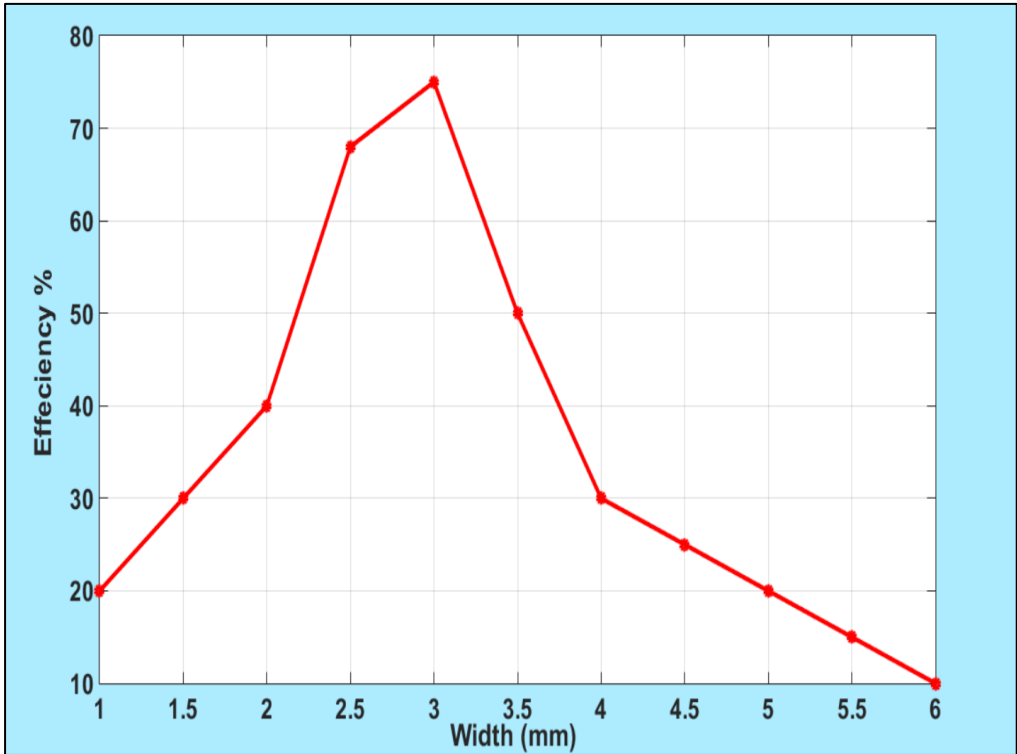

Fig.3.7.The width (mm) of microstrip line versus efficiency at 433MHz

3.2 DOUBLE STAGE RECTIFIER AT 433 MHZ

A double stage rectifier circuit can be formed by simulating two of the single stage rectifier from earlier and connecting both circuits to the same source and load, but with reversed diodes, as illustrated in

Figure 3.8. The input voltage variation with time is shown in figure 3.9. Figure 3.10 depicts the output voltage with a focused zoom in time where it is clearly visible to illustrate the voltage ripple, which is measured to be around 0.07 V with a maximum obtained voltage of 4.8 V. Figure 3.11 below shows the output current of double stage rectifier for 433 MHz, which reached around 2.43 mA .
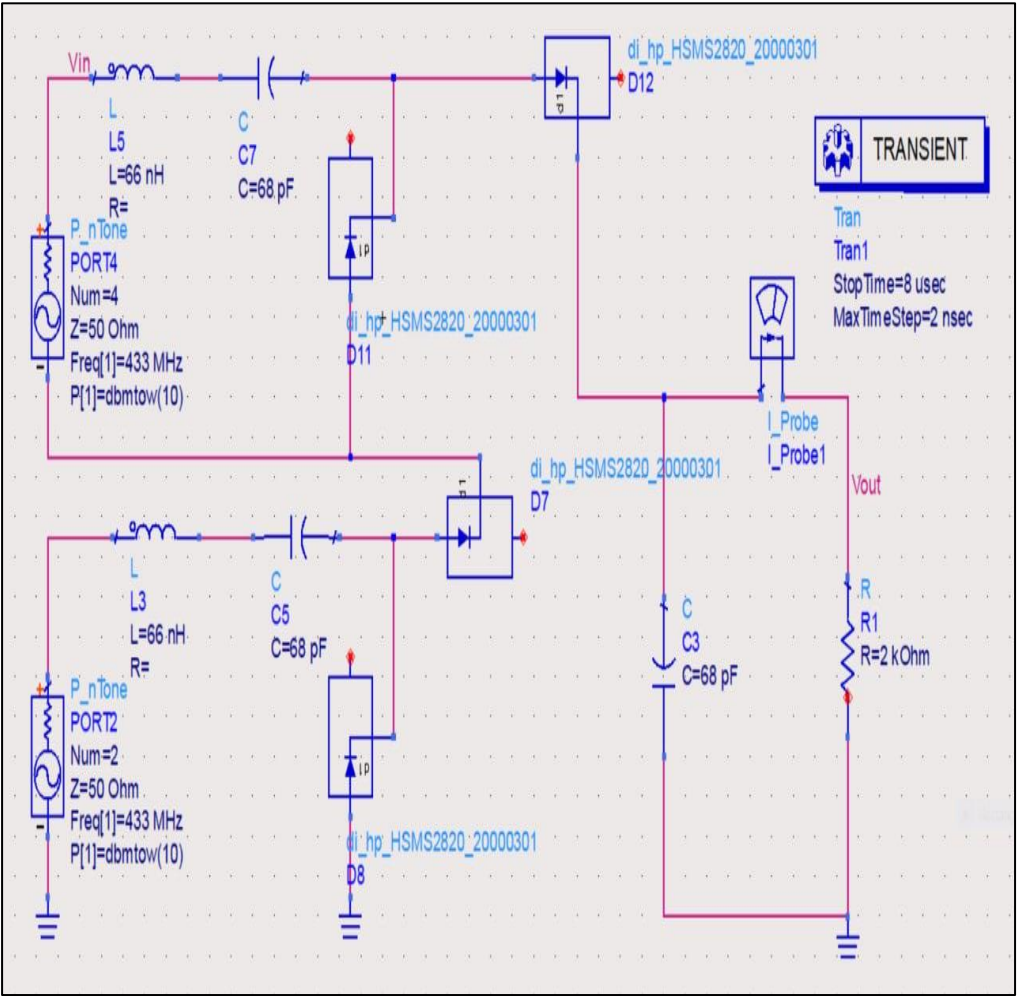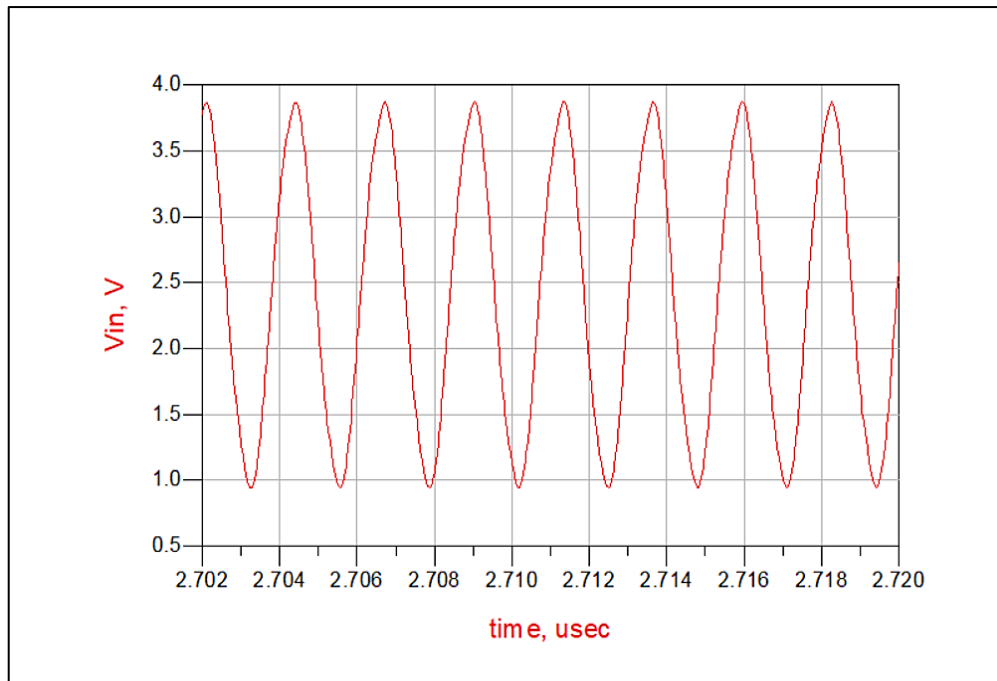

Fig.3.8.Double stage rectifier at 433 MHz.

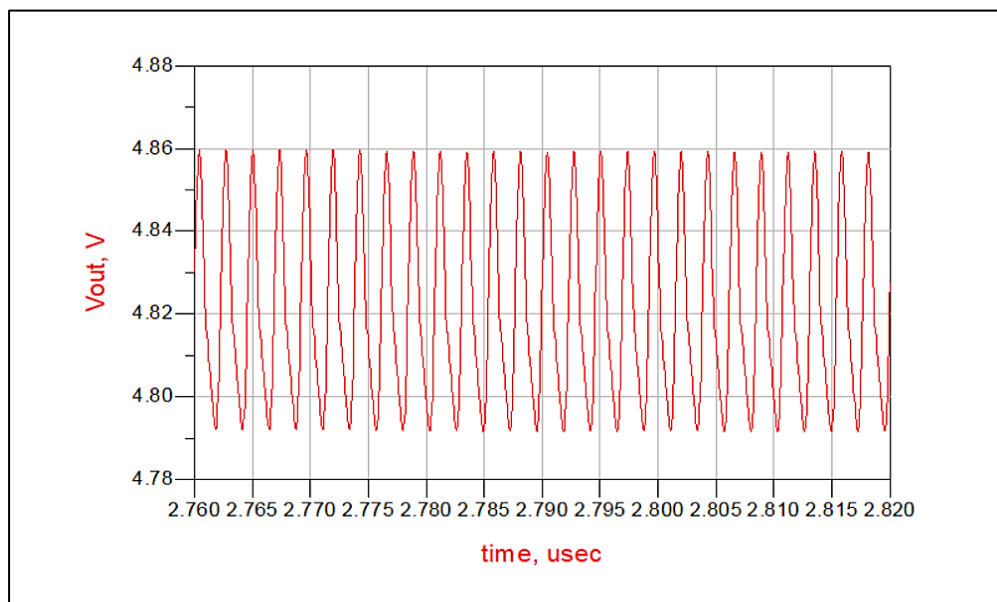**Fig. 3.9. Vin (V) of double stage rectifier at 433 MHz.**

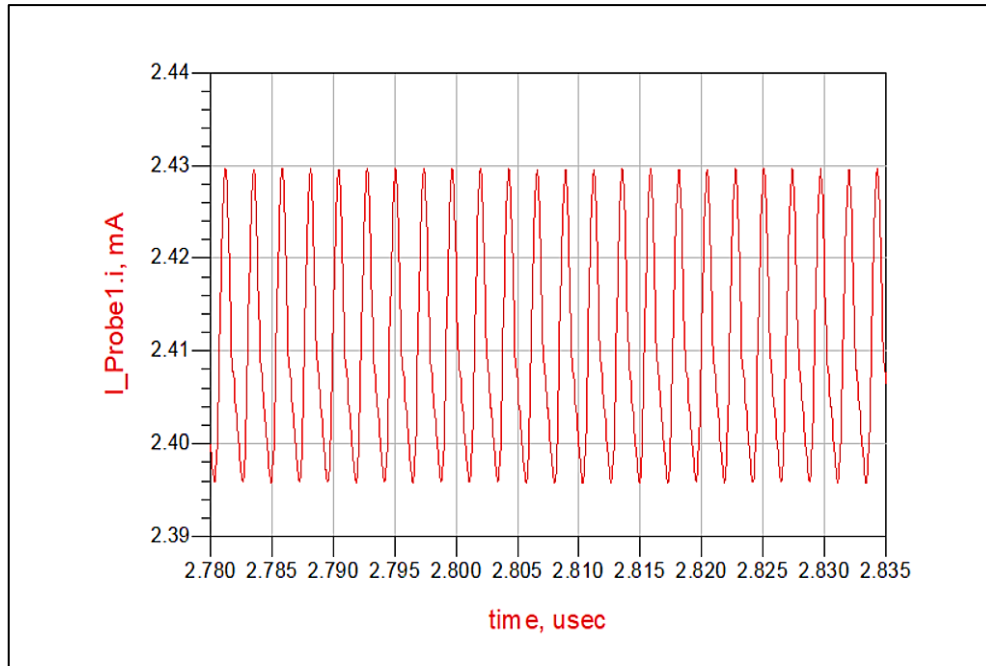**Fig. 3.10. Vout (V) of double stage rectifier at 433 MHz.**

41

Fig. 3.11. Output current (mA) of double stage rectifier at 433 MHz.

Figure 3.12 shows the relationship between the input power and the output voltage for the double stage rectifier operating at 433MHz. The outcome of this graph demonstrated how, similarly to a single stage rectifier, increasing the input power leads to increasing the output voltage that reached 3.8 V. The relationship between input power and output voltage bears the same observation. The figure 3.13 shows the relationship between input power in dBm with efficiency where it is obvious that the efficiency has increased to more 57.121% when the input power was around 10 dBm.
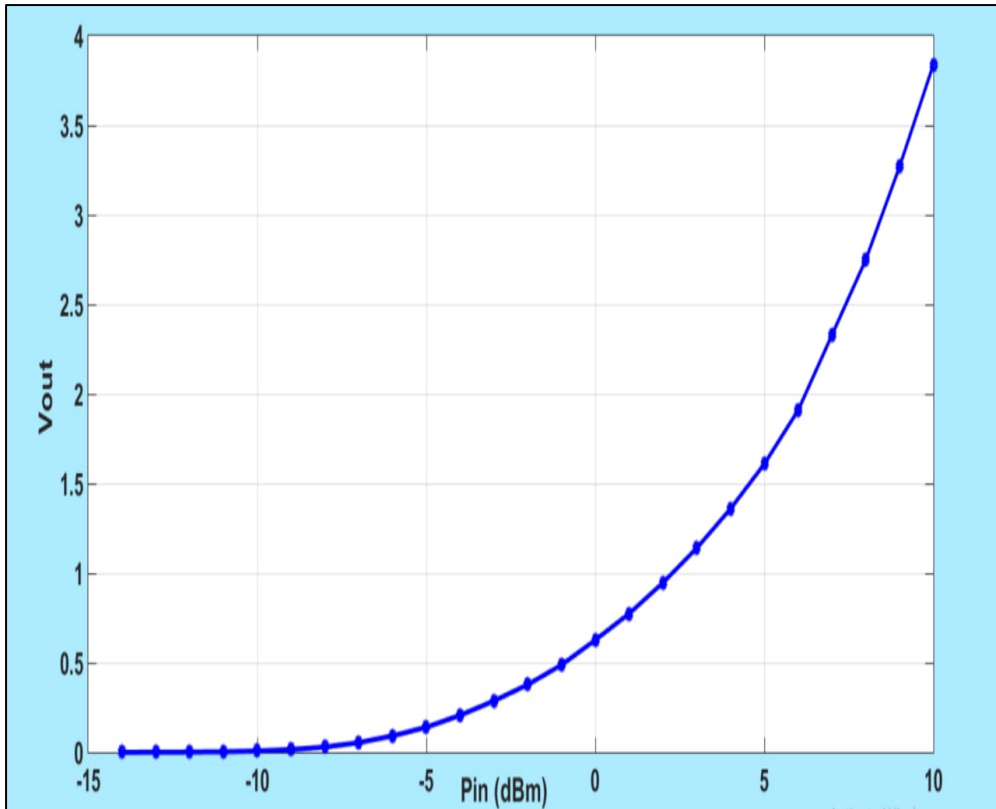
Fig. 3.12. Pin (dBm) and Vout (V) of double stage rectifier at 433MHz.
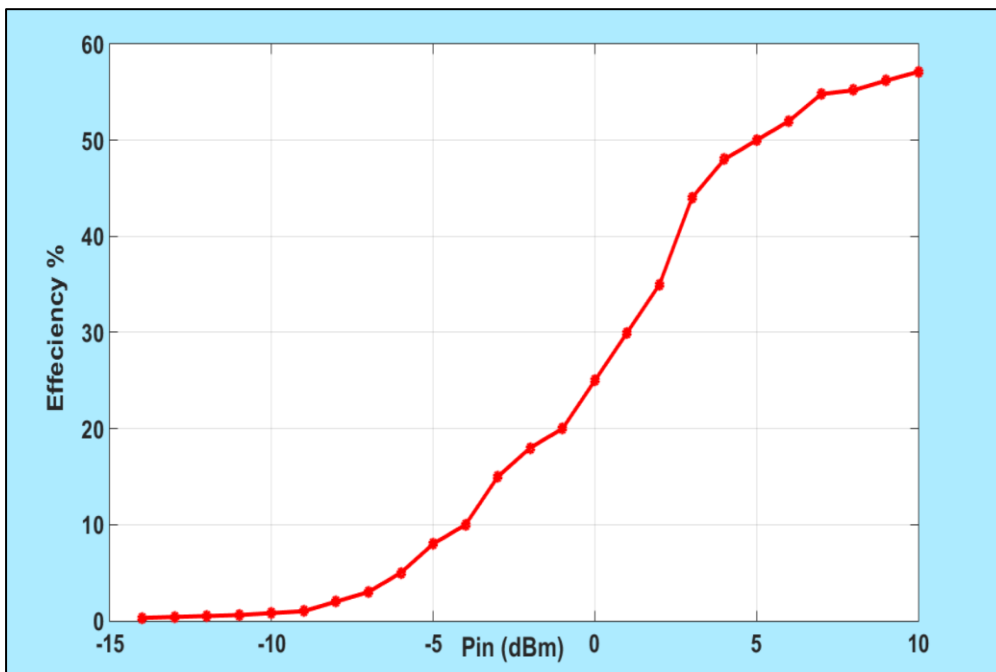
Fig. 3.13. Pin (dBm) and efficiency of double stage rectifier at 433MHz.

3.3 TRIPLE STAGE AT 433 MHZ

A triple stage rectifier is also produced and simulated as shown in Figure 3.14. The waveform of the triple stage rectifier with an input voltage (Vin) of around 4.8 V is shown in Figure 3.15. The output voltage and output current of the triple stage rectifier at 433 MHz is depicted in figures 3.16 and 3.17, respectively.

Fig.3.14. Triple stage rectifier at 433 MHz.
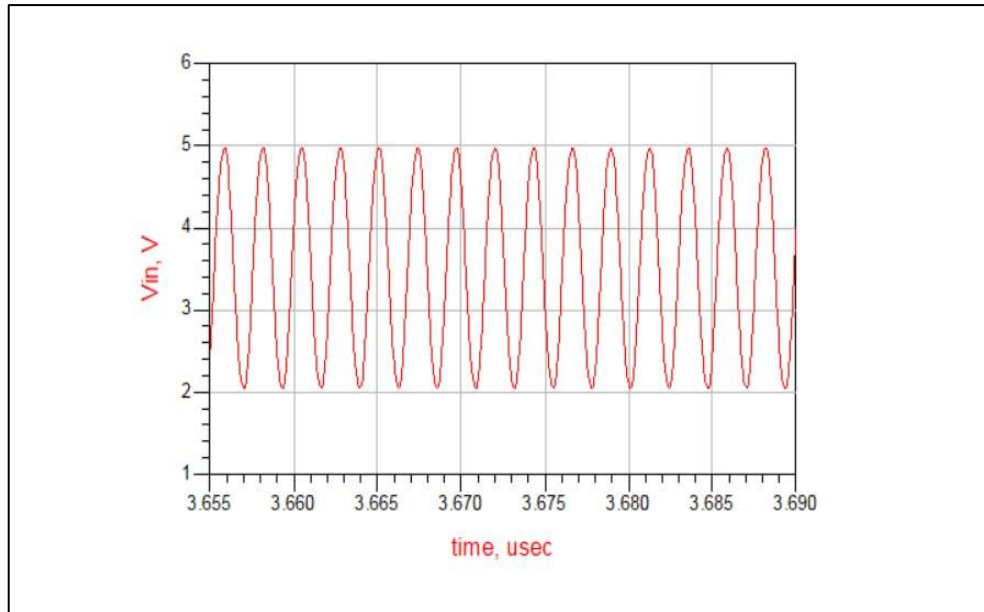
Fig. 3.15. Vin (V) of double stage rectifier at 433 MHz.

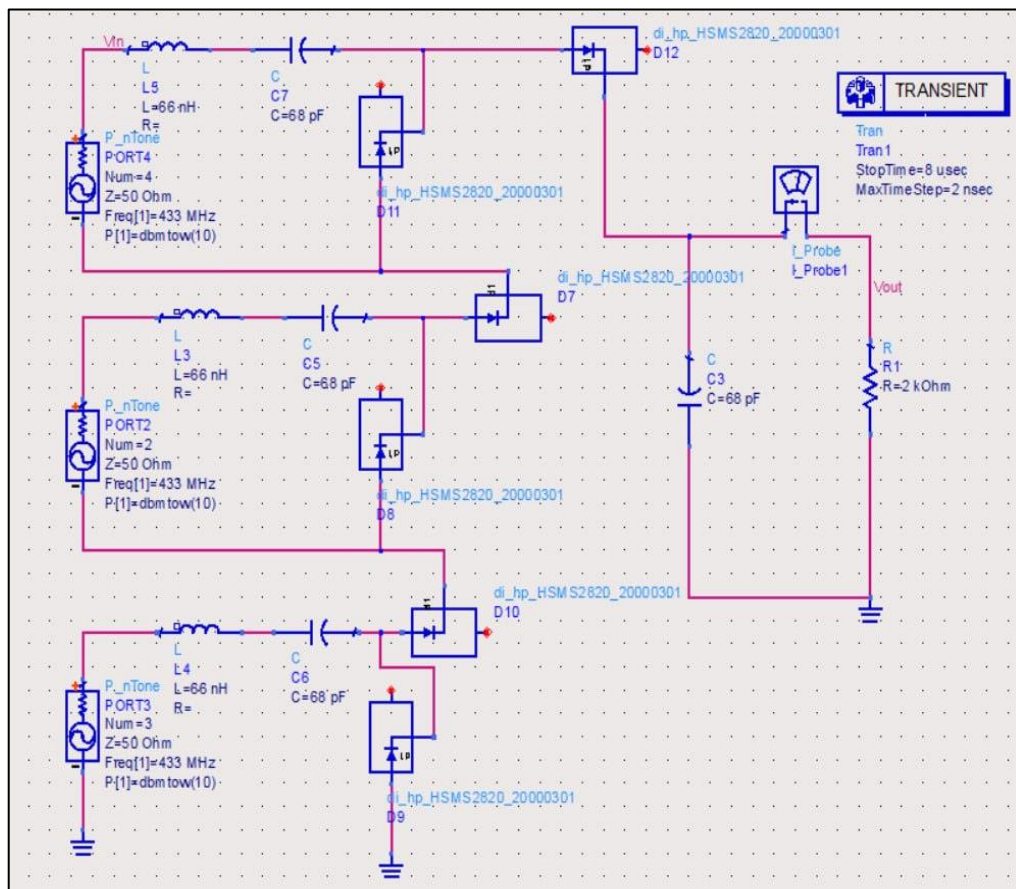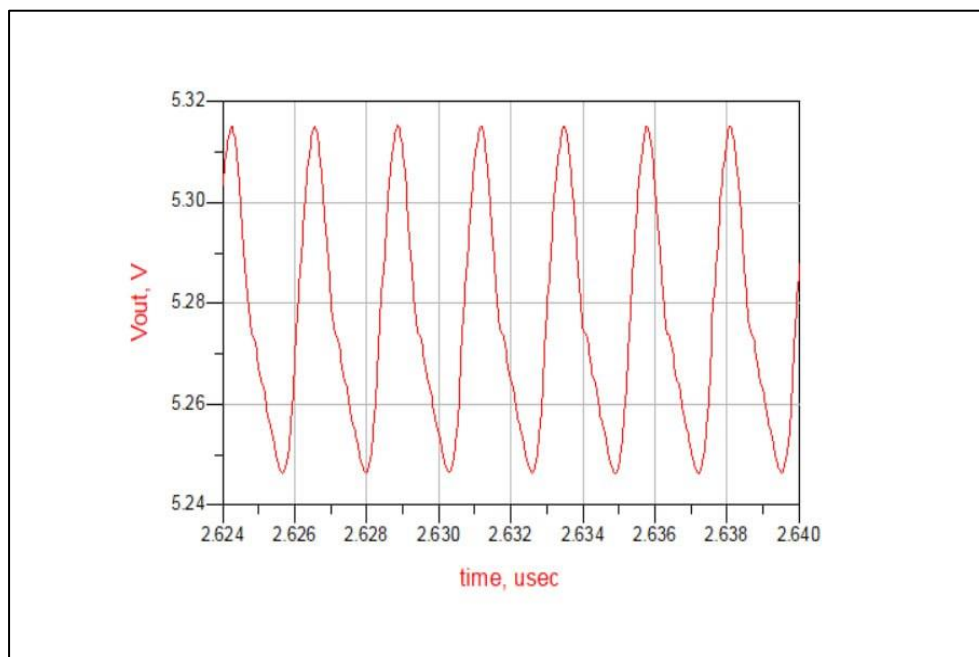**Fig. 3.16. Vout (V) of double stage rectifier at 433 MHz.**

45
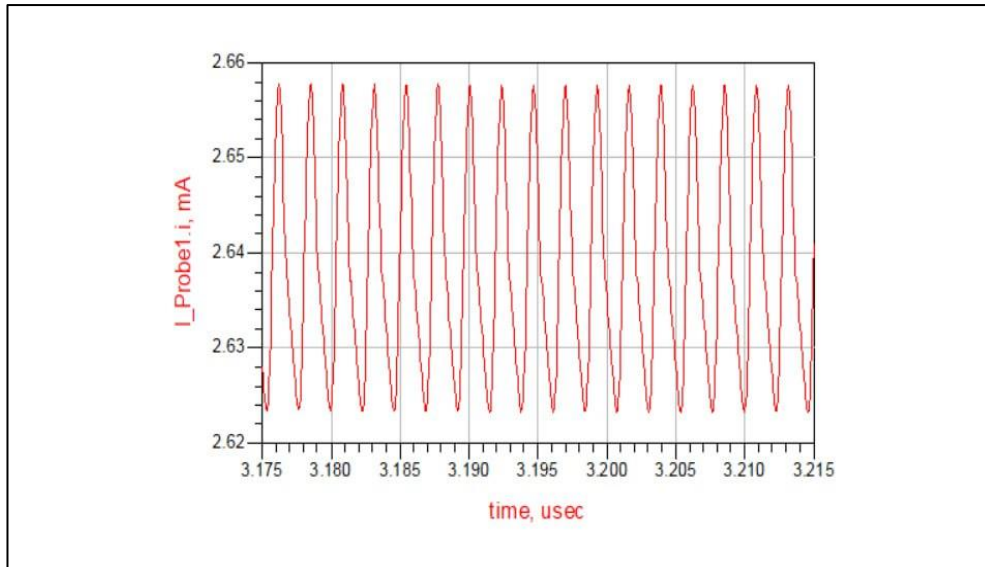
Fig. 3.17. Output current (mA) of triple stage rectifier at 433 MHz.

Figures 3.18 and 3.19 illustrate the relationship between the input power and the efficiency and output voltage for a three stage rectifier operating at 433MHz, respectively. It can be seen from the aforementioned figures that the achieved output voltage is 5.3 V with a total conversion efficiency of 47% at input power 10 dBm .
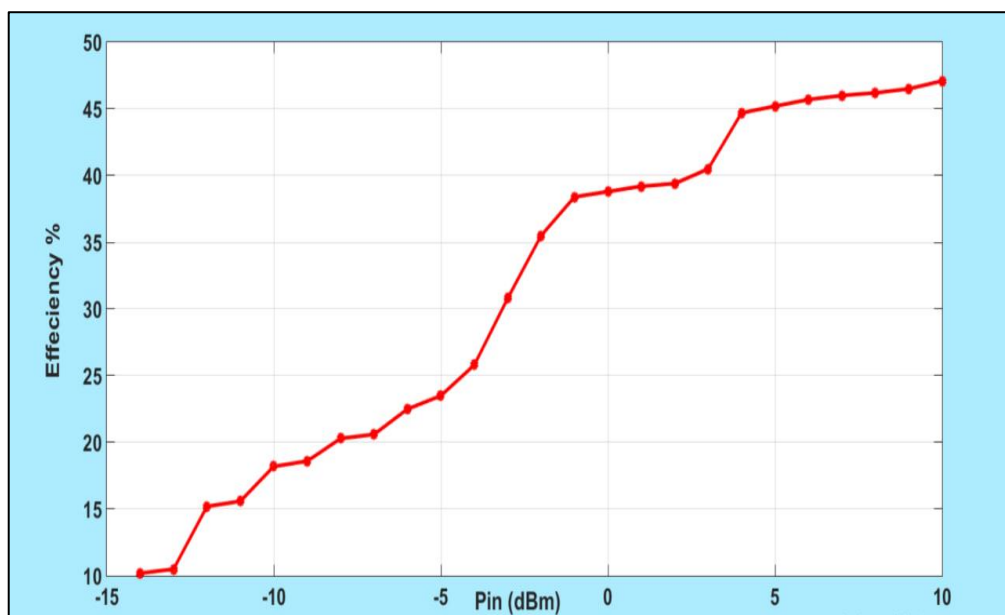
Fig. 3.18. Pin (dBm) and efficiency of triple stage rectifier at 433MHz.

46
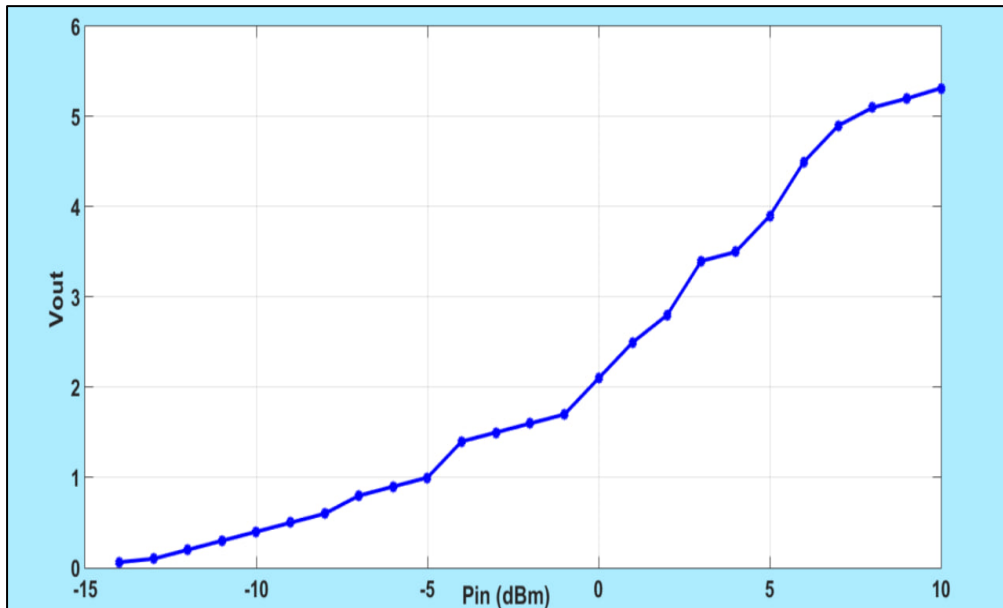
Fig. 3.19. Pin (dBm) and Vout (V) of triple stage rectifier at 433MHz.

3.4 SINGLE STAGE RECTIFIER AT 915 MHZ

As shown in Figure 3.20, a single stage rectifier operating at 915 MHz is constructed and simulated. The circuit is fed by an AC power source operating at 915 MHz, simulating a microstrip antenna made to operate at that frequency. Figures 3.21, 3.22 and 3.23 display the waveforms of the input voltage, output voltage and output current for the single stage rectifier at 915 MHz, respectively. The findings indicated that the increased frequency and the accompanying losses lead to a poorer efficiency and a lower output voltage for the single stage rectifier. Additionally, increasing the frequency could change the circuit's impedance matching condition and increase mismatching losses.
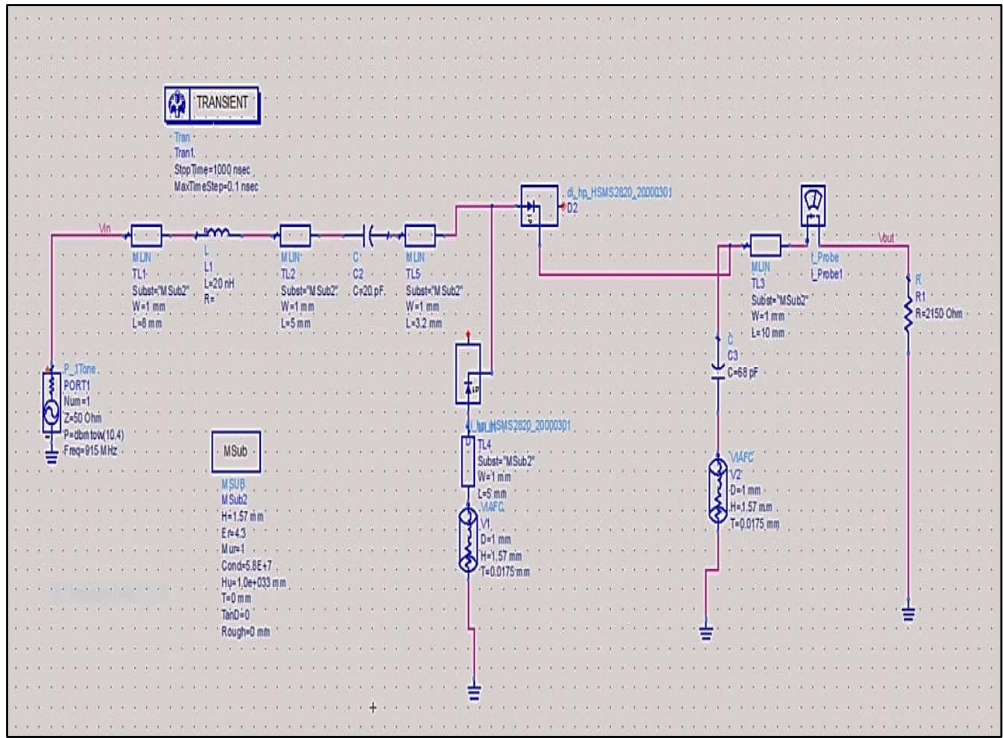
Fig.3.20. Single stage rectifier at 915 MHz.
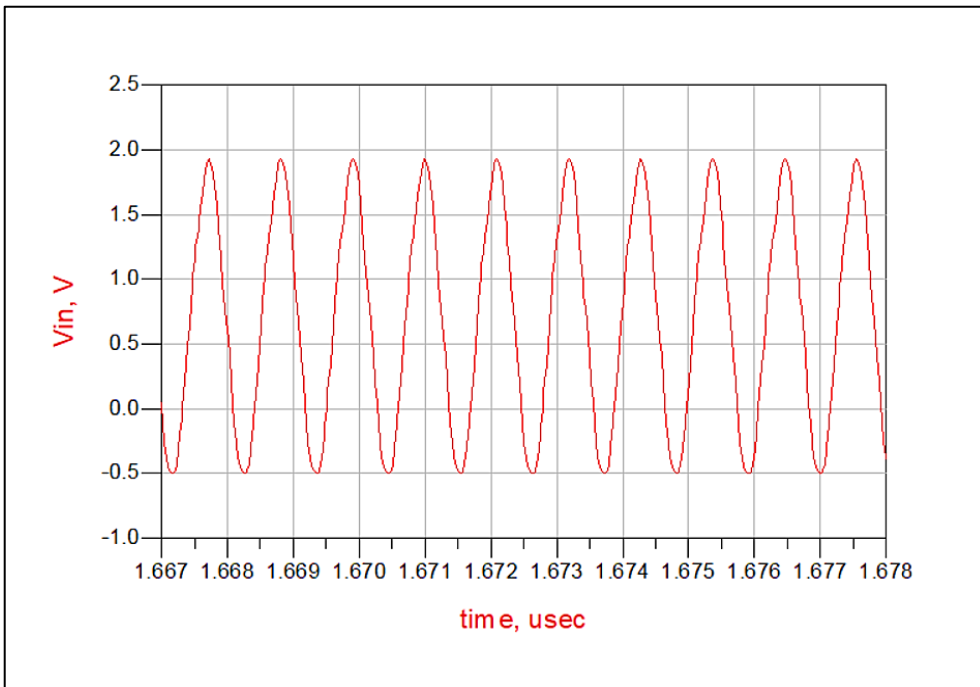
Fig.3.21. Input voltage for the single stage rectifier at 915 MHz.
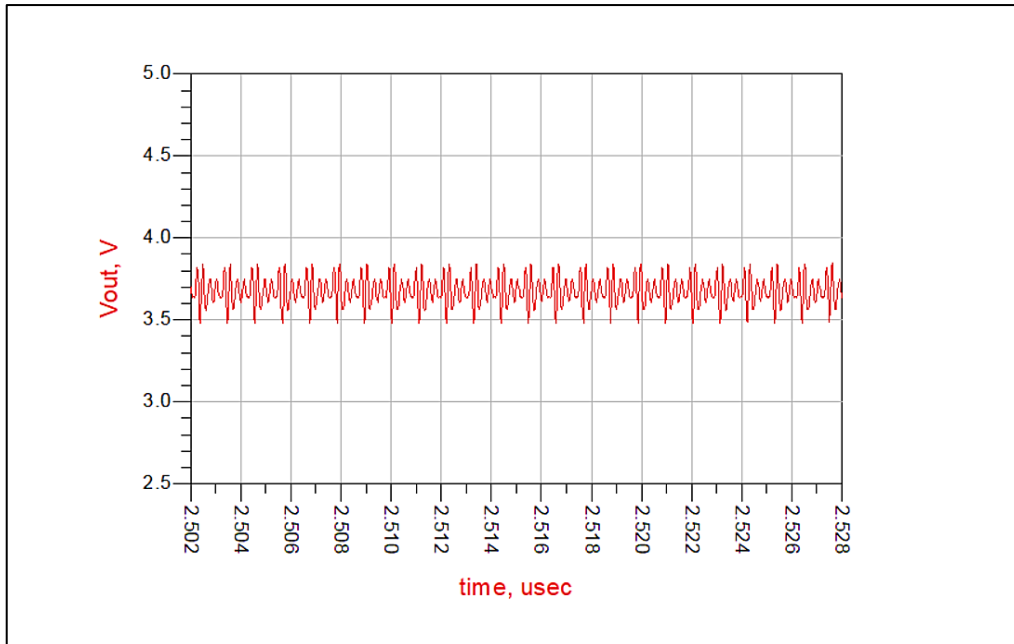
Fig .3.22. Output voltage for the single stage rectifier at 915 MHz.
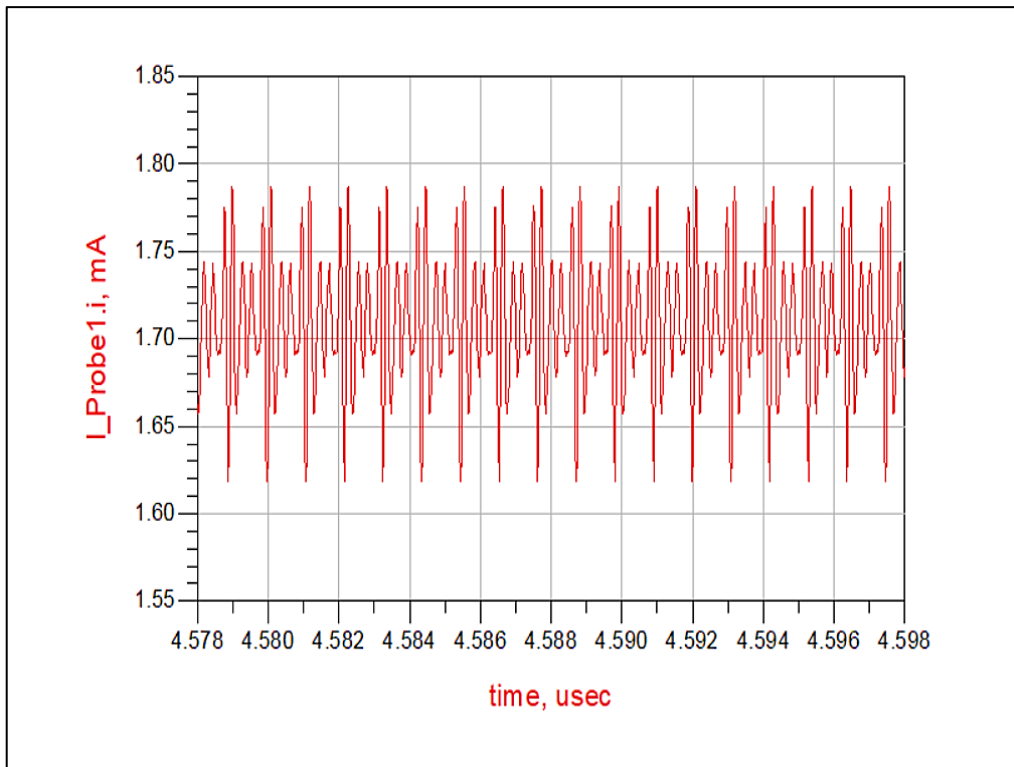
Fig .3.23. Output current for the single stage rectifier at 915 MHz.

By looking at the relation between the input power and the output voltage as well as the relation of the efficiency with the input power for the single stage rectifier at 915 MHz, it can be seen that the obtained output voltage was around 3.9 V only leading to a conversion efficiency of more than 82% as illustrated in Figs. 3.24 and 3.25. It is thus concluded that the single stage rectifier is promising to operate at 915 MHz and can provide a good output voltage and efficiency. This gives a motivation to try out the double stage rectifier in order to increase the output voltage and improve the system performance.
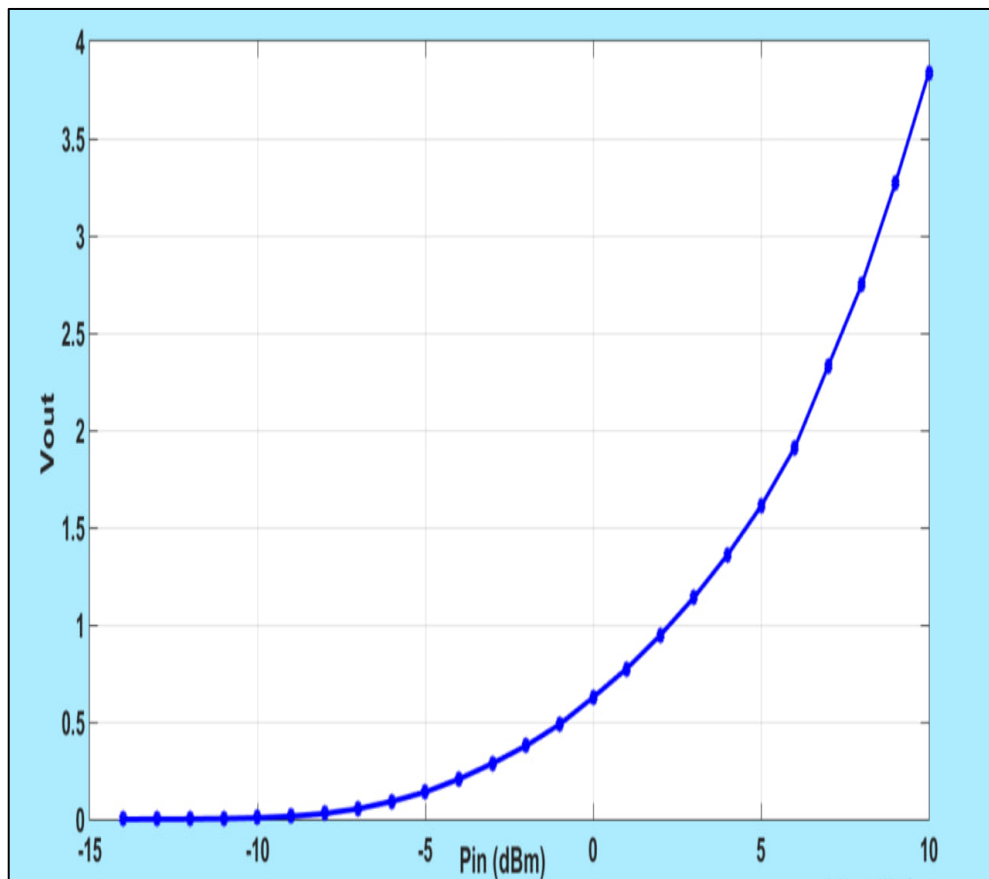
Fig.3.24. Vout versus input power of single stage rectifier at 915 MHz.
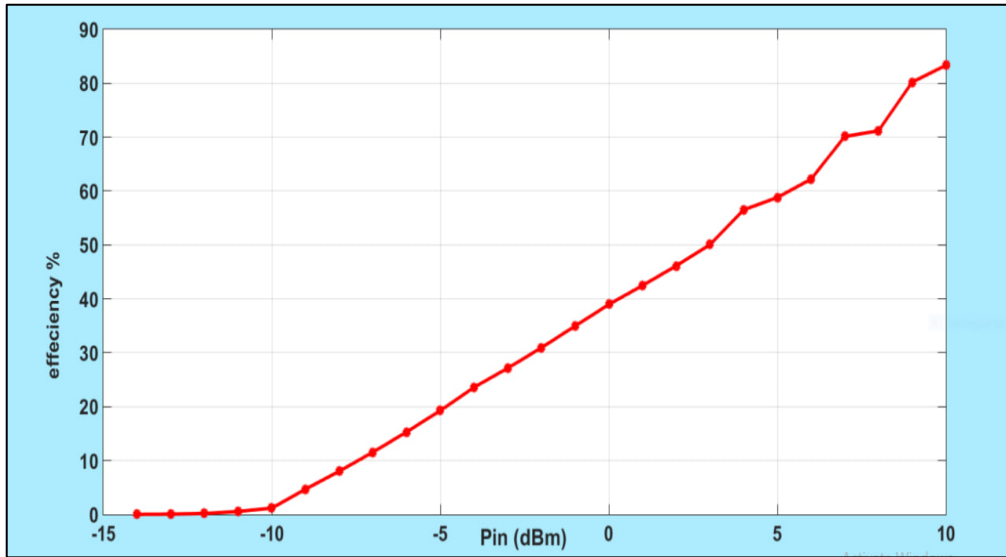
Fig .3.25. Efficiency versus input power of single stage rectifier at 915 MHz.

Figure 3.26 displays the results of a study to determine how the strip line width impacts overall performance. The ideal width for optimizing the efficiency was 3 mm at 433 MHz, whereas at 915 MHz it is found that the strip line must not exceed 1 mm as it is shown in figure 3.26, which is completely in line with the outcome of theoretical calculations.
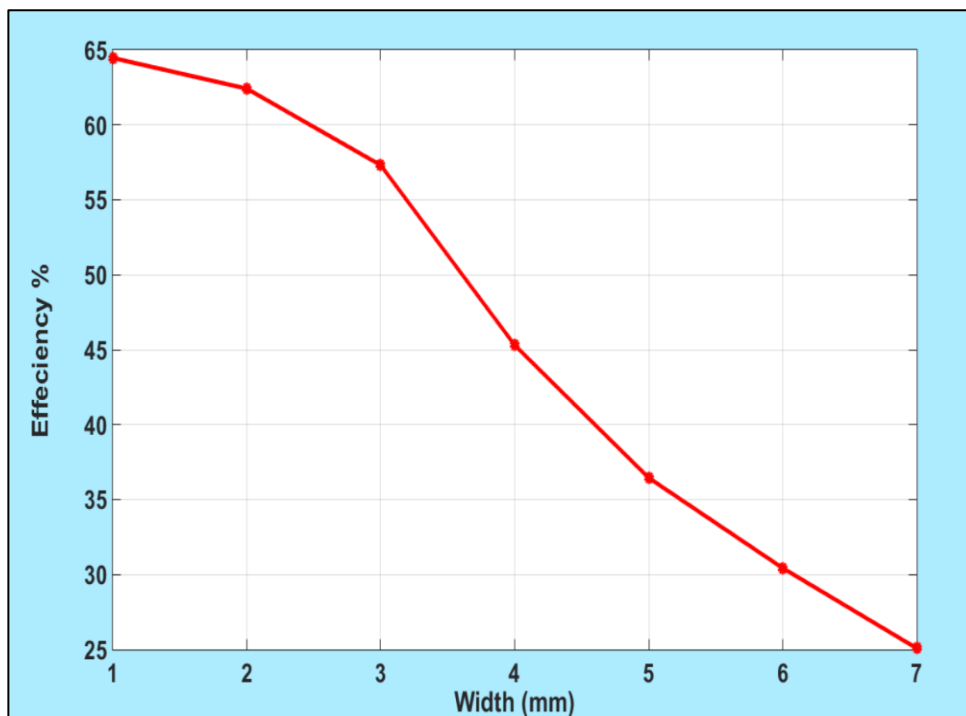
Fig.3.26. Efficiency versus strip line width at 915 MHz.

3.5 DOUBLE STAGE RECTIFIER AT 915 MHZ

For the sake of further improving of the system performance in terms of output voltage and conversion efficiency, a double stage rectifier at 915 MHz is designed and simulated as shown in Figure 3.27 . Similarly, the single stage rectifier circuit it is replicated but with reversed diodes and the two parts are connected to one source and one load. The double stage rectifier is expected to achieve higher output voltage.

Fig.3.27. Double stage rectifier at 915 MHz.

The waveforms of the double stage rectifier at 915MHz are shown in Figures 3.28, 3.29, and 3.30 It is noted that the input voltage (Vin) is around 3.7 and DC output voltage (Vout) is more than 5.23 V and the recorded load current is around 2.635 mA.

Fig .3.28. Input voltage (Vin) for the double stage rectifier at 915 MHz.
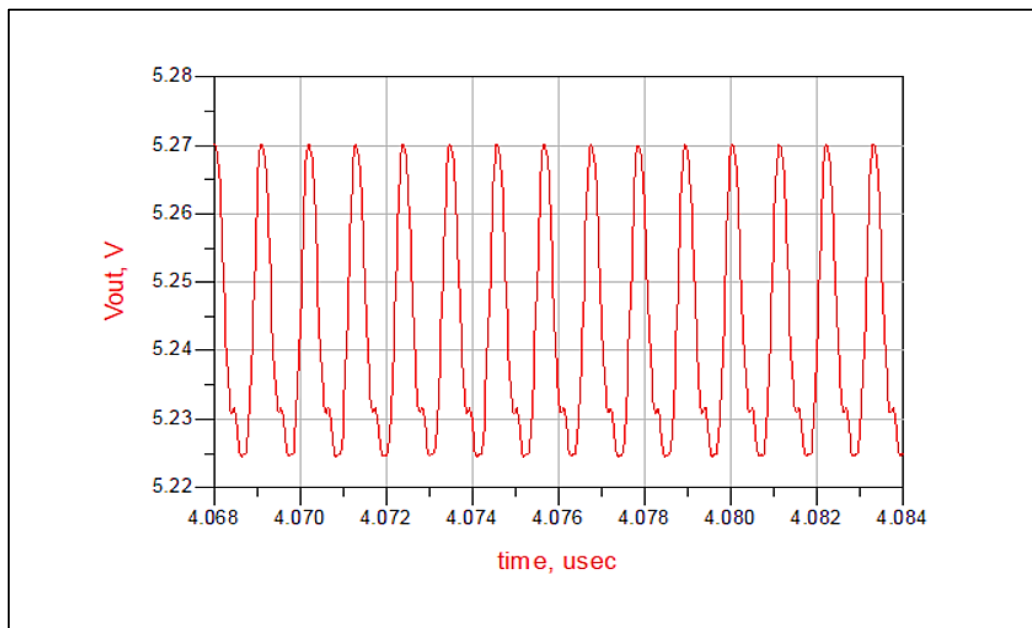
Fig .3.29. Output voltage (Vout) for the double stage rectifier at 915 MHz.

53
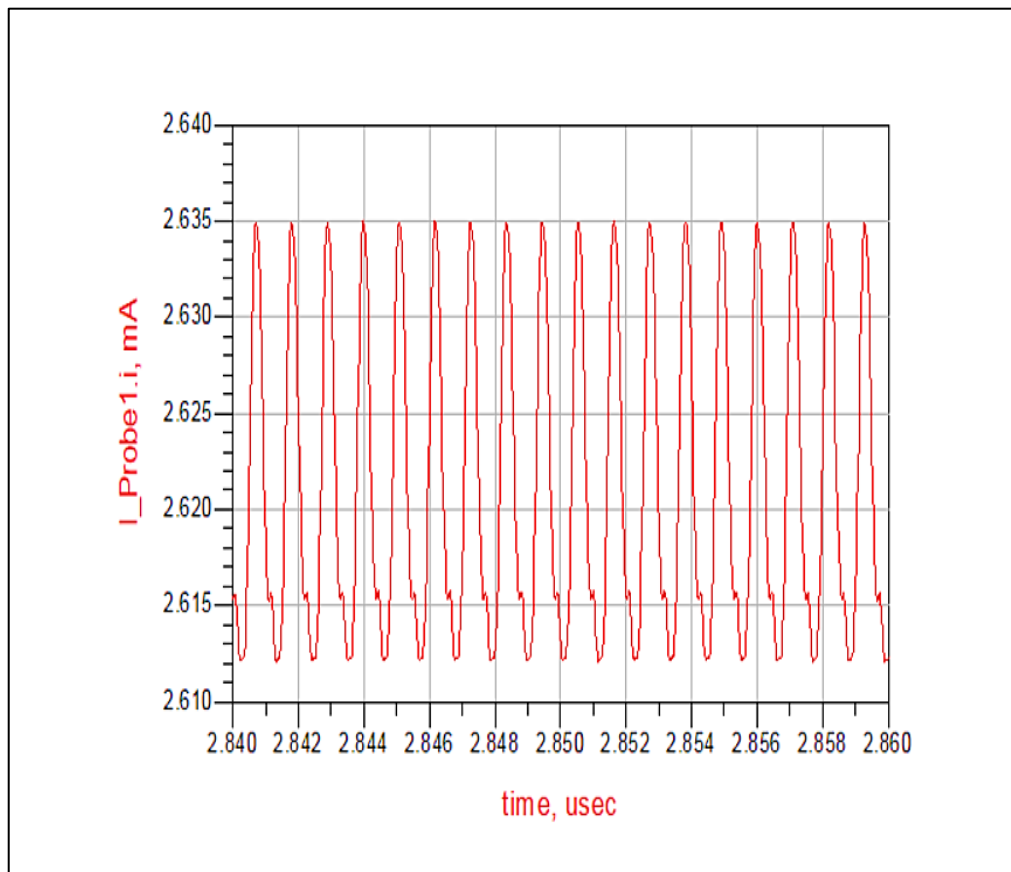
Fig.3.30. OUTPUT current (Iout) for the double stage rectifier at 915 MHz.

By looking at the relation between the input power and the output voltage as well as the relation of the efficiency with the input power for the double stage rectifier at 915 MHz as depicted in figures 3.31 and 3.32, it can be seen that the obtained output voltage was around 5.7 V when the input power was 14 dBm leading to a total conversion efficiency around 63%.
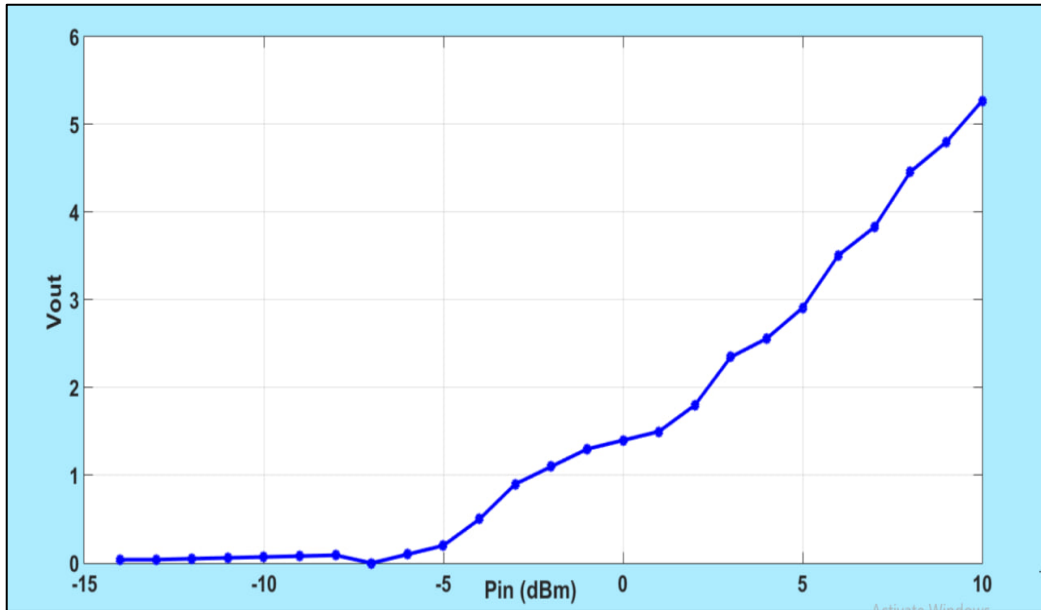
Fig. 3.31. Pin (dBm) and Vout (V) of double stage rectifier at 915 MHz.
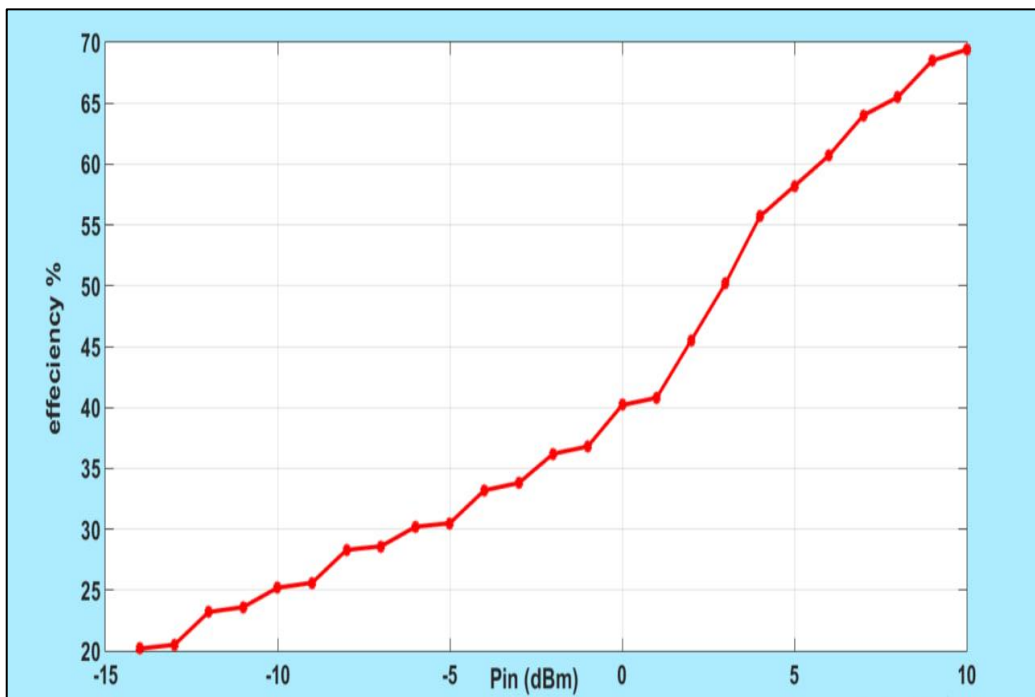
Fig .3.32. Pin (dBm) and efficiency of double stage rectifier at 915 MHz.

55

3.6 TRIPLE STAGE 915MHZ

A third stage rectifier at 915 MHz is constructed and simulated to further enhance the system's performance in terms of output voltage and conversion efficiency, as illustrated in Figure 3.33. The single stage rectifier circuit is then duplicated, but with the diodes in the other direction, and the three components are linked to the same load but with different sources.
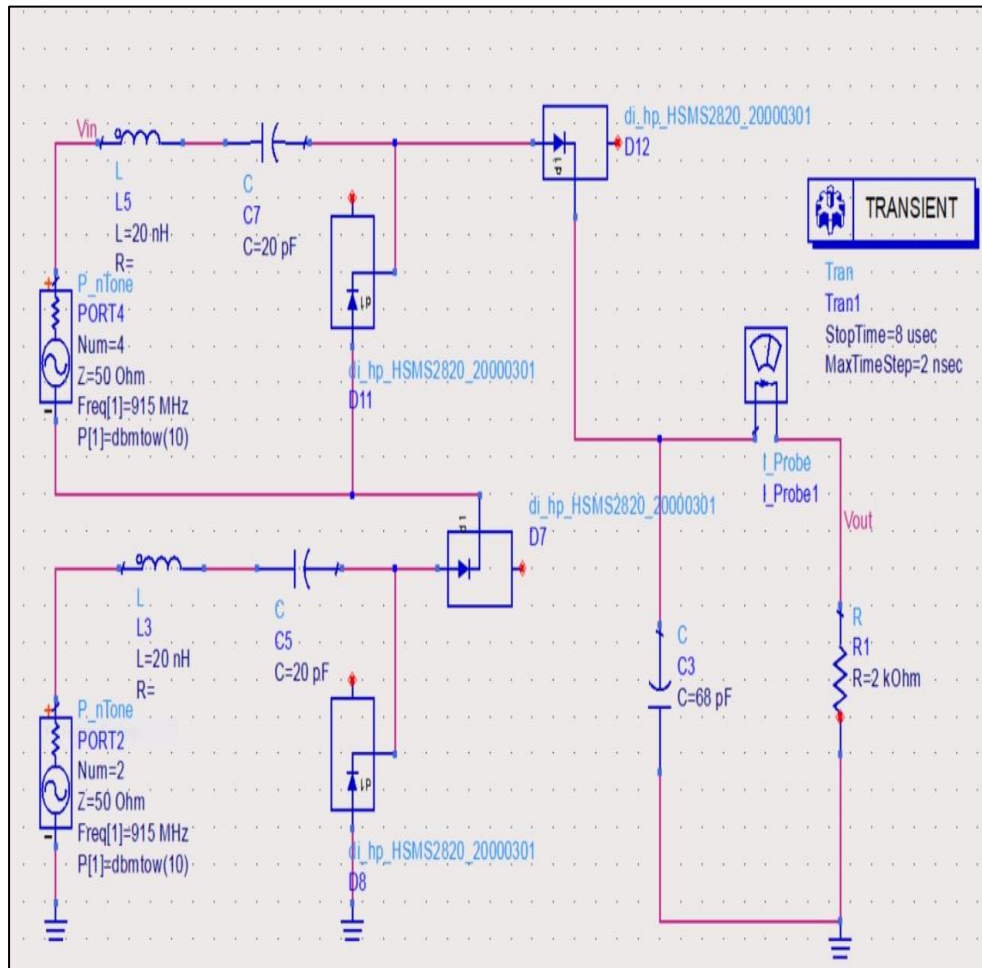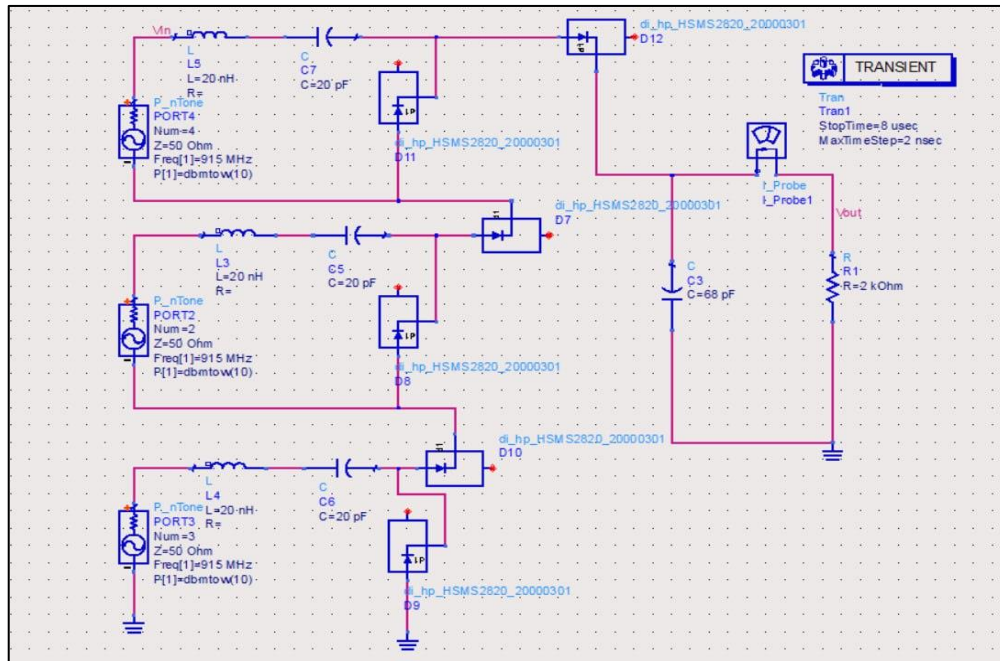

Fig.3.33. triple stage rectifier at 915 MHz.

The waveforms of the triple stage rectifier at 915MHz are shown in figures 3.34, 3.35, and 3.36. It is noted that the DC output voltage (Vout) is approximately 5.96 V and the recorded load current is around 2.9 mA.
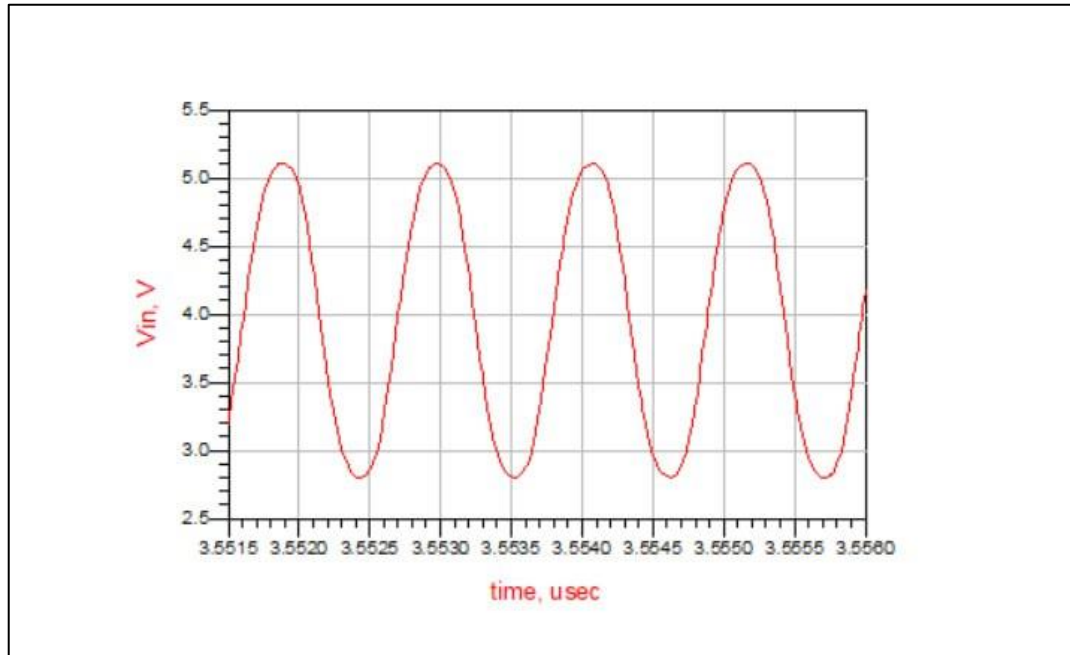
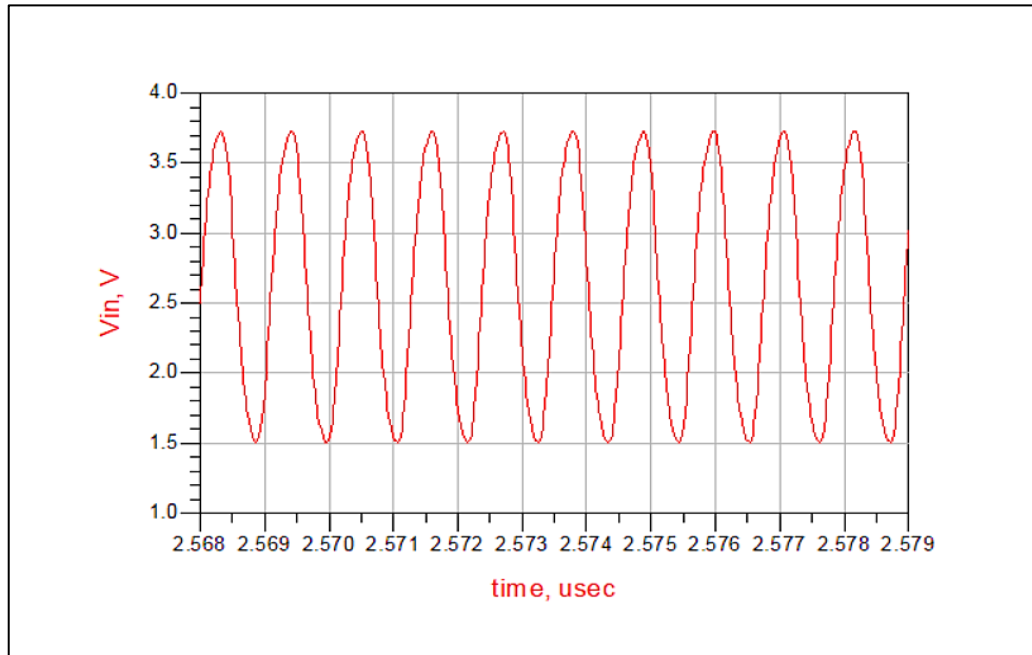**Fig .3.34. Input voltage (Vin) for the triple stage rectifier at 915 MHz**.
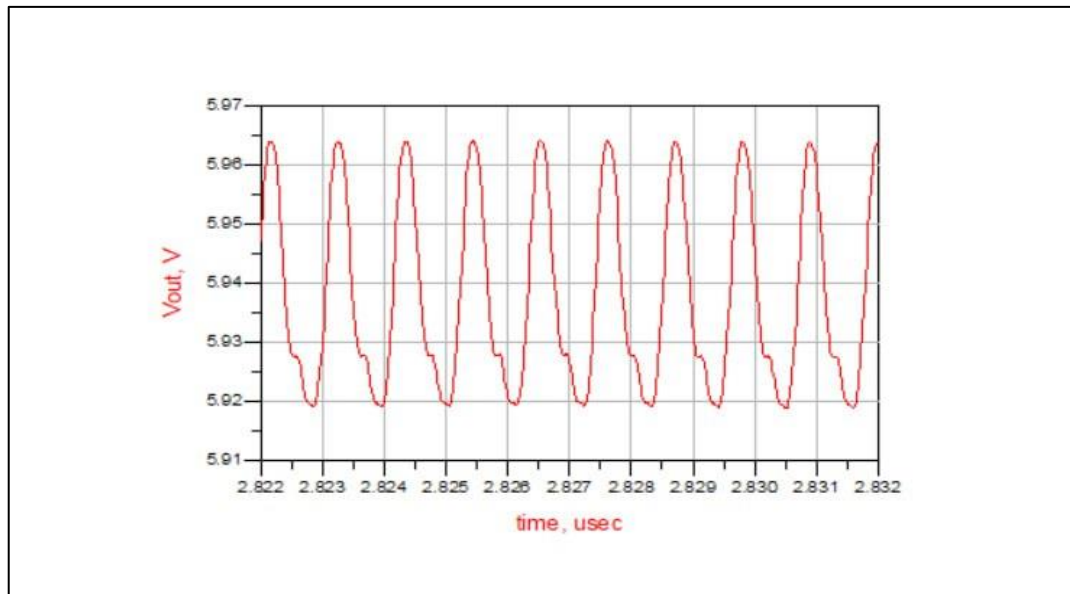
Fig .3.35.Output voltage (Vout) for the triple stage rectifier at 915 MHz.
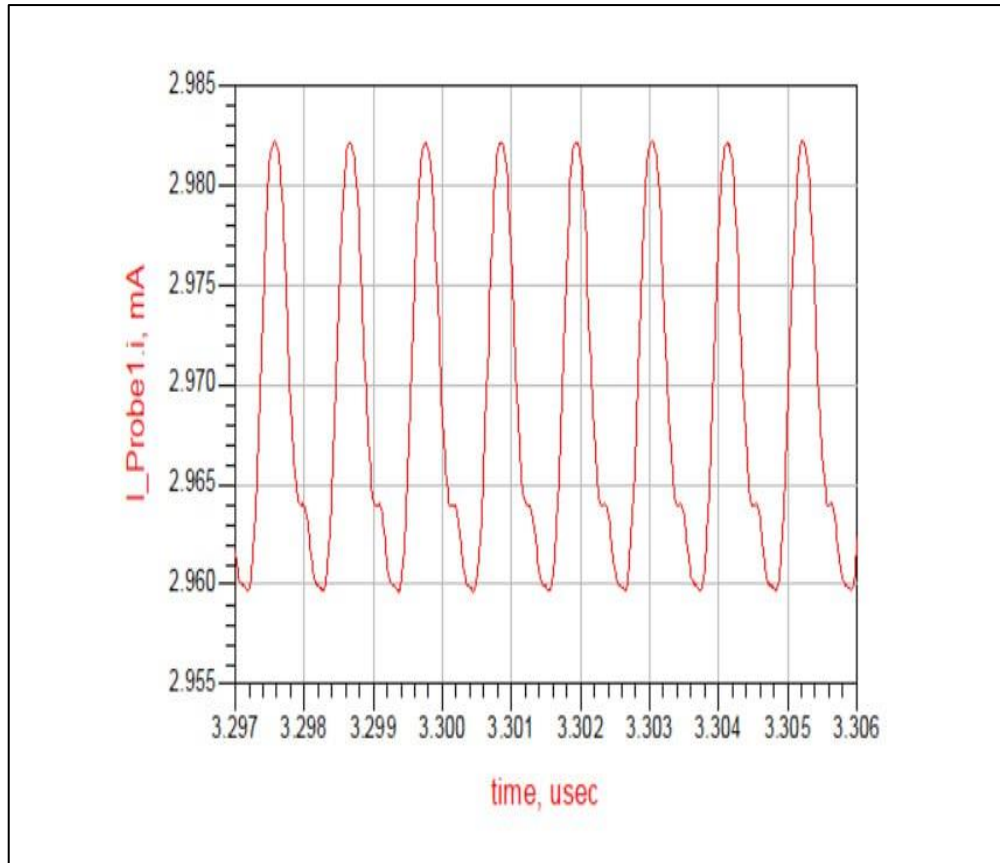
Fig.3.36. OUTPUT current (Iout) for the triple stage rectifier at 915 MHz.

By looking at the relation between the input power and the output voltage as well as the relation of the efficiency with the input power for the triple stage rectifier at 915 MHz as depicted in figures 3.36 and 3.37, it can be seen that the maximum obtained output voltage was around 6 V when the input power was 10 mW leading to a conversion efficiency around 60%.
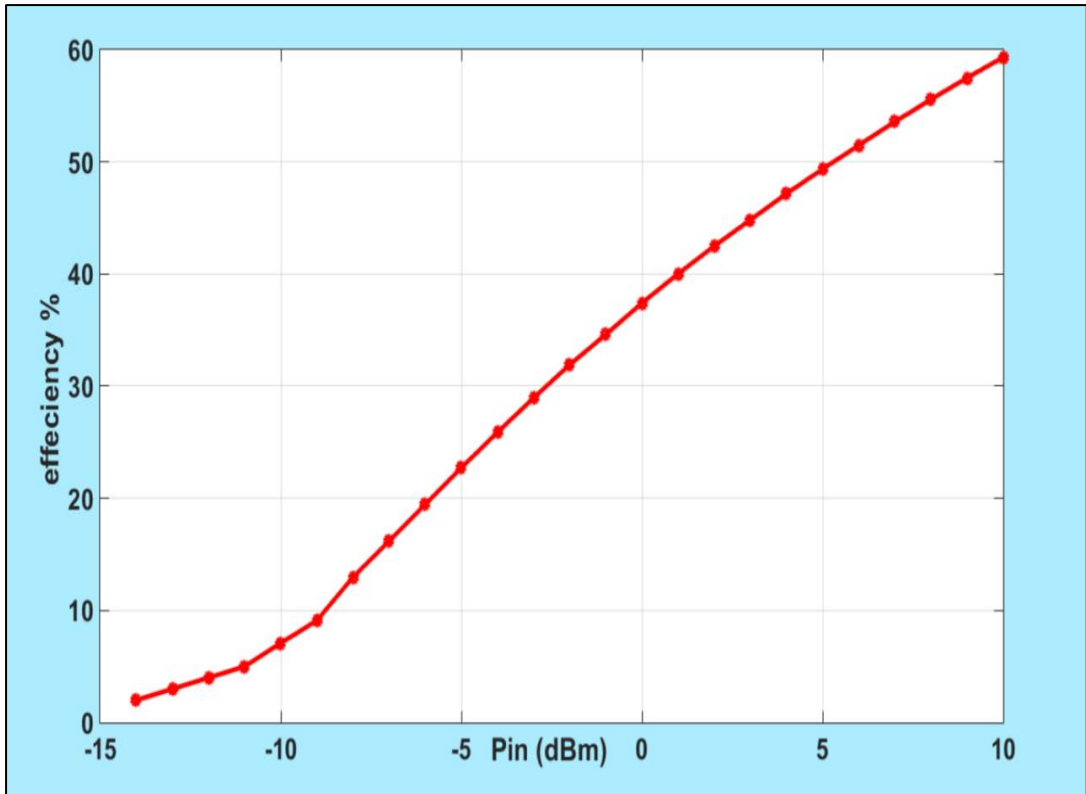
Fig .3.37. Pin (dBm) and efficiency of triple stage rectifier at 915 MHz.
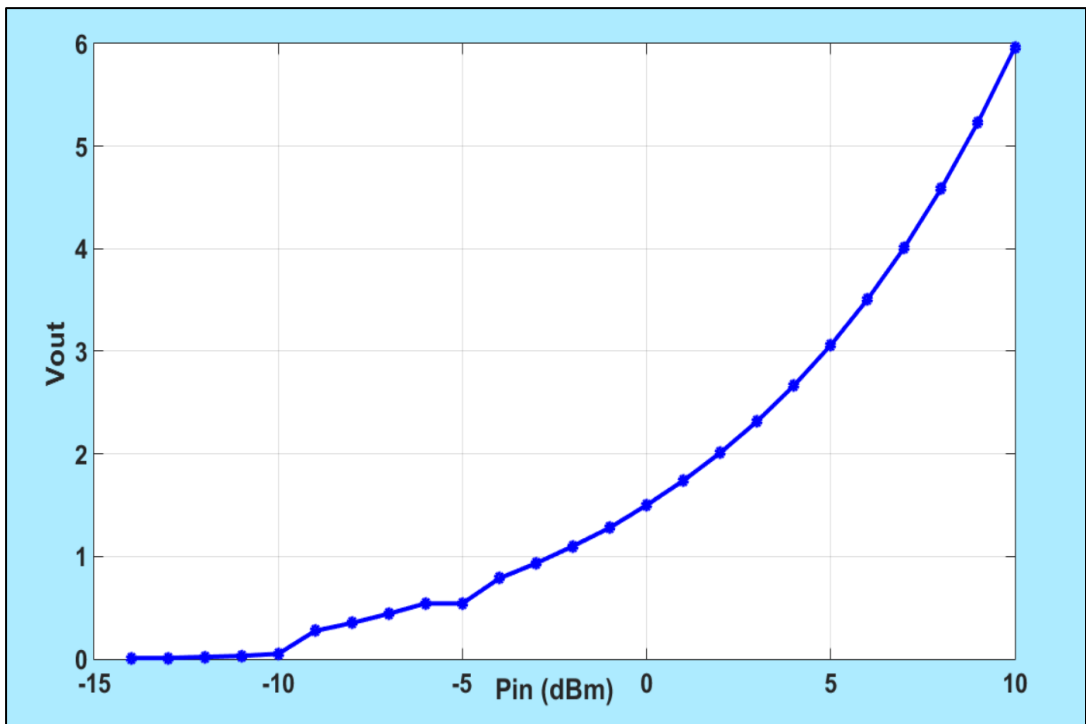
Fig .3.38. Pin (dBm) and Vout of triple stage rectifier at 915 MHz.

59

3.7 FABRICATION AND EXPERIMENTAL VALIDATION

To prove the concept and for the sake of experimental validation, the single stage rectifier circuit operating at 433 MHz was fabricated using PCB technology. FR4 substrate with dielectric constant of 4.3 and thickness of 1.6 mm is employed. Figure 3.38 shows the PCB schematic diagram of the fabricated circuit where it is a double layer circuit with a full groundplane at the back of the substrate. All the circuit components were available in the market except the 56 nH inductor. It took the researcher long time to afford this specific inductor but all the attempts were unsuccessful unfortunately. Thus, due to the time constraints of the thesis submission, it was decided to use 16 inductors (1 μH) connected in parallel to obtain a 62.5 nH equivalent inductor.
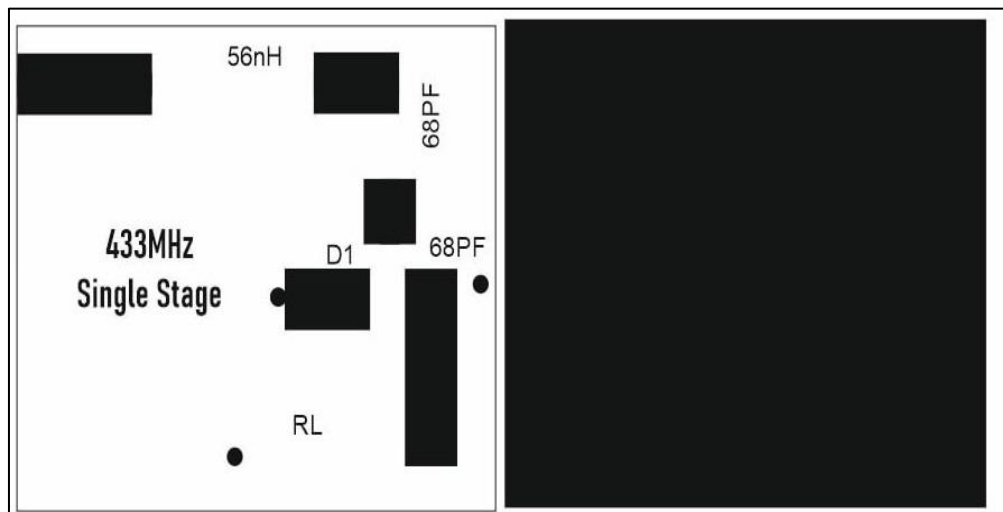
Fig .3.39. PCB schematic of the fabricated rectifier circuit (font and back views).

The fabricated rectifier circuit was fed by TGR 1040 1GHz .
Synthesised RF Signal Generator with a variable input power level
(in dBm) through a rigid microwave coaxial cable. SMA
connector is attached to the input port of the fabricated circuit and
the output voltage is measured by using multipurpose digital AVO
meter as shown in Figure 3.39.
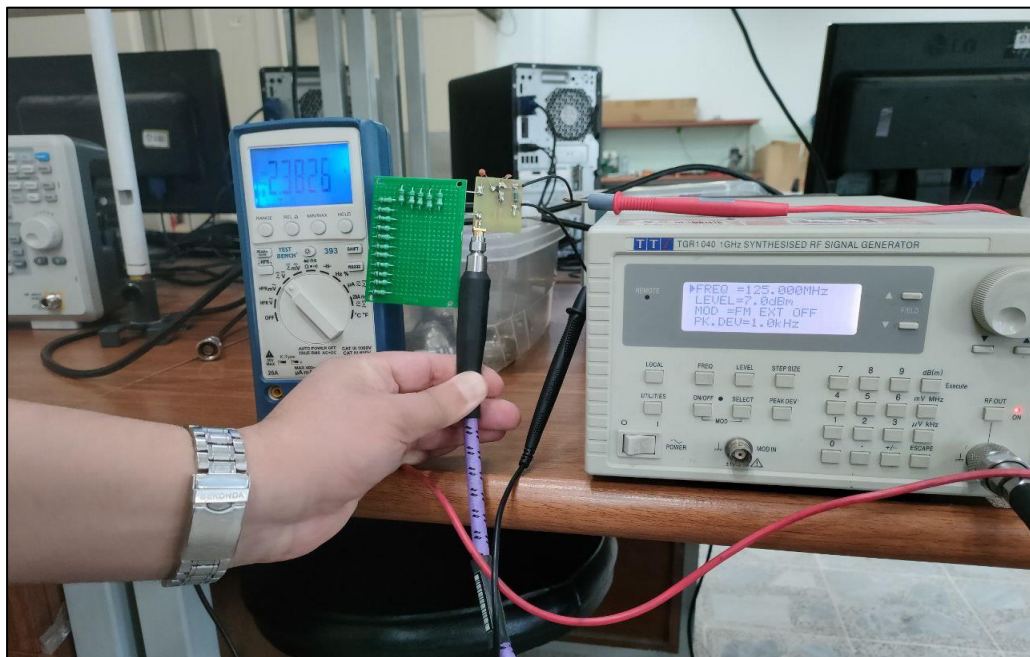
Fig .3.40. Experimental setup of the 433 MHz rectifier circuit.
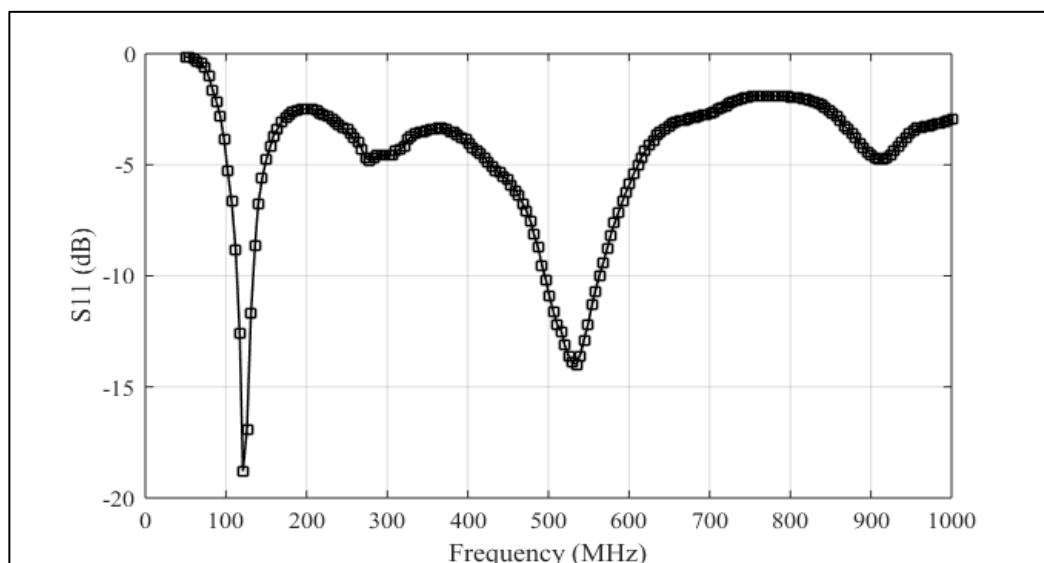
Fig .3.41. Measured reflection characteristics of the fabricated rectifier circuit.

The first step in the measurement procedure was to measure the S-parameters of the fabricated circuit to determine the matching at each operating frequency within the range 50-1000 MHz. A vector network analyzer was utilized to measure S11 for the circuit. The variation of S11 (dB) with frequency is illustrated in Figure 3.40. It is shown that the fabricated circuit can operate at two frequencies only 125 MHz and 516 MHz with better reflection characteristics (matching) was recorded at 125 MHz with return loss near -20 dB. Although the circuit was designed to operate at 433 MHz, however the lack of proper circuit component such as the inductor and the large number of soldering points in the 16 parallel inductors may lead to changing the circuit input impedance and hence shift the resonant frequency from 433 MHz to 125 MHz. Since the aim is to prove the concept and to get a DC power at the output of the circuit, it was decided to adopt the fabricated circuit and go ahead with the measurements at 125 MHz instead of 433 MHz. The variation of the output voltage and efficiency with input power is depicted in Figures 3.41 and 3.42, respectively.
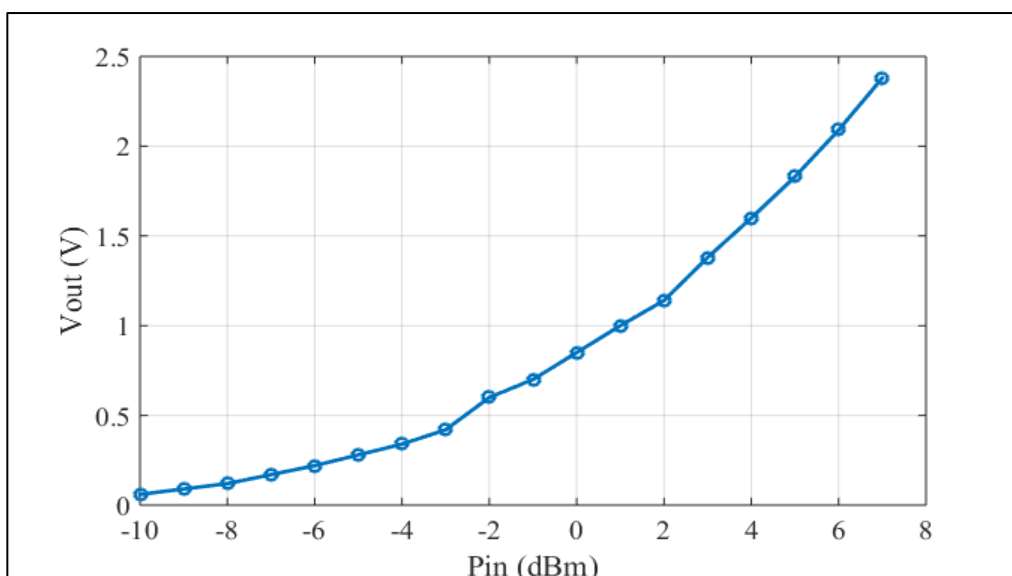
Fig .3.42. Measured output voltage versus input power for the fabricated rectifier circuit.

62
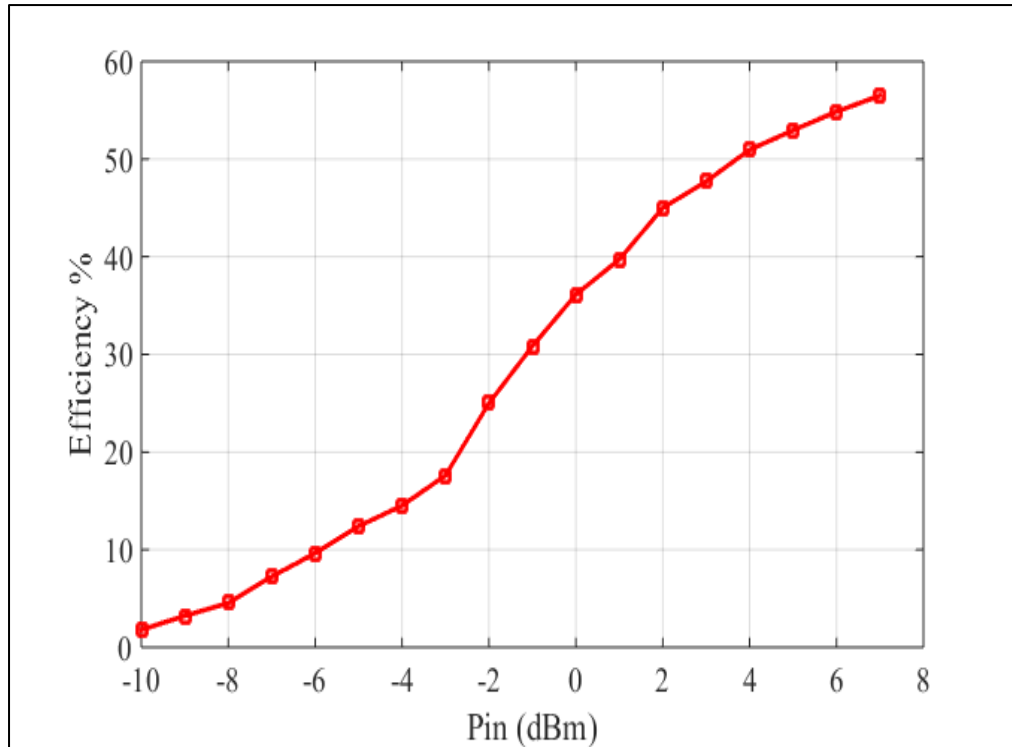
Fig .3.43. Measured efficiency versus input power for the fabricated rectifier circuit.

It is shown the fabricated circuit responded well to the input RF power and was successfully able to convert it into DC power. Due to the limitation of the available RF signal generator in the lab, the RF input power was varied from -10 dBm to 7 dBm and the DC output voltage was recorded to vary from 60 mV to 2.38 V for the aforementioned input power range. On the other hand, the recorded conversion efficiency showed that value of the efficiency started from 1.8 % for the -10 dBm input power to 56.5% for 7 dBm input power. The obtained measurement results agree well with the simulation results as it is shown in Figures 3.43 and 3.44, respectively.
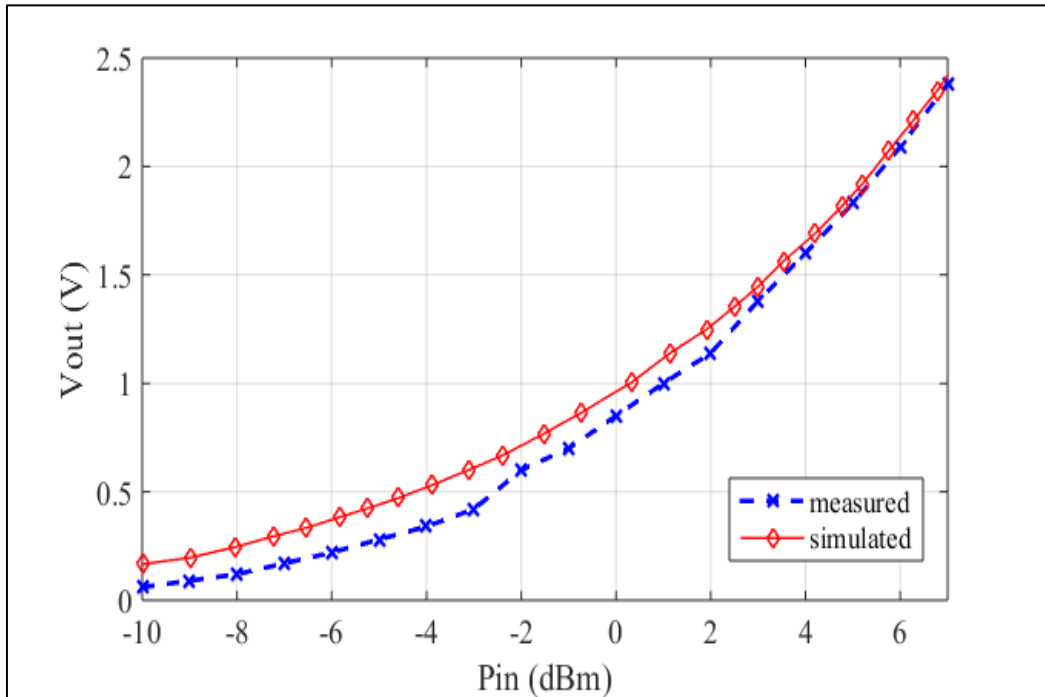
Fig .3.44. Comparison between measured and simulated output voltage for the fabricated circuit.
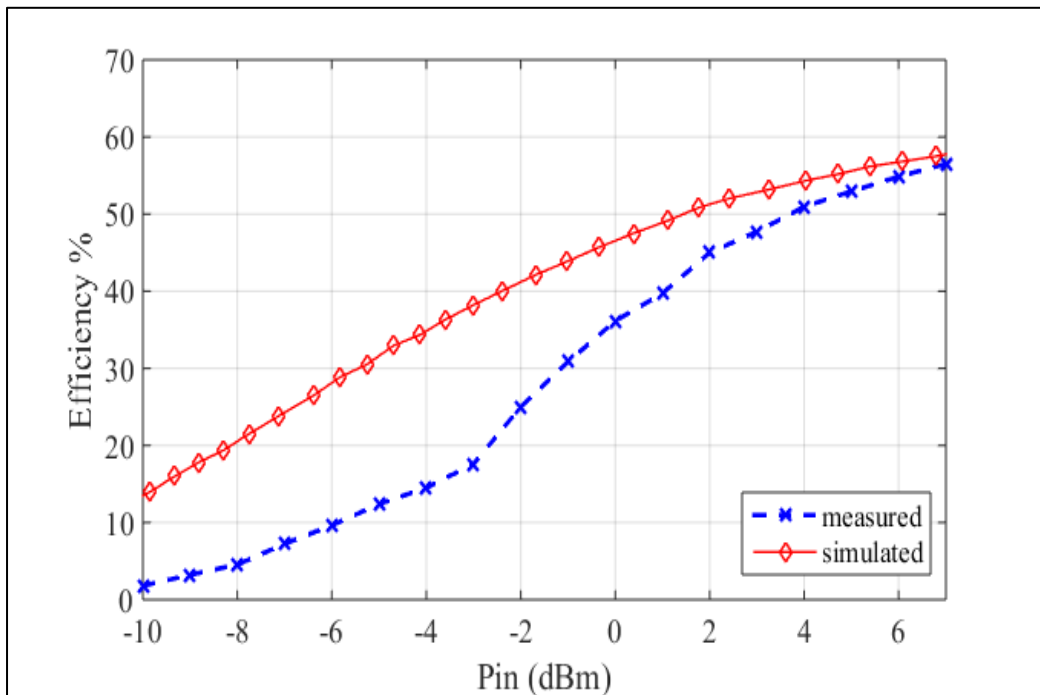
Fig .3.45. Comparison between measured and simulated efficiency for the fabricated circuit.

It is clearly shown from the comparisons above that both simulation and measurement results agree very well for the output voltage relation with increasing input power with nearly exact performance. In contrast, the measured efficiency is slightly less than the simulated one for many reasons including that the simulation procedure neglect many sources of loss inside the circuit and assume almost perfect component, substrate and copper traces. In addition, there is always a power loss between 1-2 dB in the coaxial cable. Finally, in the simulation it is assumed to have one 56 nH inductor while in the measurement 16 parallel inductors were used, which means a considerable amount of power will be lost in the internal resistance of these inductors as well as in the connecting board traces and soldering points. The aforementioned points justify why the measured efficiency is less than the simulated one albeit it is still practically accepted.

CHAPTER FOUR

Antenna Design for Wireless Implantable Devices

4.1 Introduction

Antennas are employed in IMDs for communication and powering those implanted devices. This include both wearable and implanted antennas at different frequencies and for various medical and health applications. There are two frequency bands exploited in this work for implanted antennas 433 MHz and the second type utilizes 915 MHz. These antennas are basic and are intended to be a component of a communication and WPT system. Since implantable antennae are intended to function inside the human body, designing them is a difficult task. The body is a non-homogenous medium. Based on the following factors, the performance of antenna will change:

- ➢ The location on the body where the antenna is inserted.
- ➢ The difference in tissue layer thickness surrounding the antenna.
- ➢ The depth antenna at interior body.

Several implantable antennas will be employed in this work since our goal is to look into the feasibility of using antennas for WPT systems in one small rectenna circuit. The MICS band for communications and the ISM band between 433 MHz and 915 MHz for WPT are the research's target bands. The first antenna is a meandered line antenna that is utilized in the designed rectifiers for the far-field energy harvesting. The designed antennas in this work all are chosen to be meander line antennas operating at 433 MHz and 915 MHz. This type of antennas is chosen due to its

small size and compact nature compared with other types of antennas such as dipoles, monopoles and printed F antennas and also because they are compatible with integrated circuits since it contains a full ground plane at the back side of the substrate.

4.2 ANTENNAS DESIGN AND SIMULATION

4.2.1 Antenna 1 at 915 MHz

CST software was used to design and simulate the meander line antennas. The antenna is constructed on a 1.6mm thick double-sided copper FR4- printed circuit board (PCB) with a dielectric constant of 4.3 . The antenna is designed to operate at a resonant frequency of 915 MHz. The substrate dimensions including the antenna structure is (100 × 100) mm in total. An omni-directional radiation pattern is altered by the presence of groundplane on the PCB's opposite side from where the antenna construction is located. Figure 4.1 below illustrates the structure and dimensions of the meander line antenna (Antenna 1) at 915 MHz.

Table 4.1 displays the dimension values for Antenna 1. These values represent the length and width of the antenna in millimeters (mm) with substrate size   (100 × 100) mm at 915 MHz. Furthermore, Table 4.2 below displays all dimensions and geometrical details of Antenna 1. It is worth mentioning here that a resonant $\lambda/2$ antenna would have a total length of 17 cm at 915 MHz, whereas the designed antenna has much small dimensions at the same frequency.
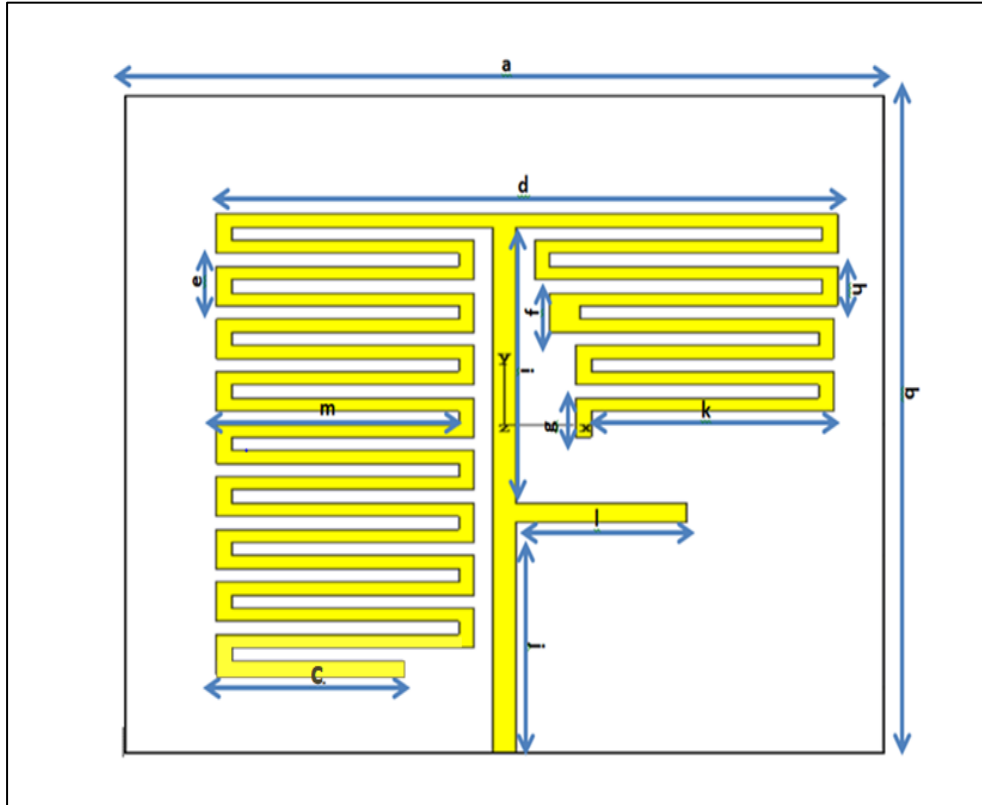
Fig.4.1. Antenna 1 at selected frequency band 915MHz with dimensions.

Table 4.1: Substrate geometrical details.

Name	Value (mm)
Width of substrate	100
Length of substrate	100
Width of patch	50
Length of patch	50
Feeding line width	3
Thickness of substrate	1.645 mm
Dielectric constant of the substrate ε_r	4.3

Table 4.2: Detailed dimensions of Antenna 1.

Name	Value (mm)
a	100
b	100
c	24.50
d	82.00
e	6.00
f	6.00
g	6.00
h	6.00
i	42.00
j	35.00
k	32.00
l	22.50

Figure 4.2 below shows the S-parameters (S11), which typically gives a clear indication on the reflection and matching characteristics of the designed antenna. The S11 curve implies that this antenna radiates best at 915 MHz, which is so called resonant frequency, where the recorded S11 was around -25.51 dB at resonance. Furthermore, at 1000 MHz the antenna will radiate virtually nothing, as S11 is close to 0 dB (so all the power is reflected). If the bandwidth is defined as the frequency range where S11 is to be less than -10 dB, with 901.52 MHz the high end and 928.50 MHz the low end of the frequency band. It is also noticed that the designed antenna exhibits a multiband performance with three bands between 700 MHz to 1000 MHz.
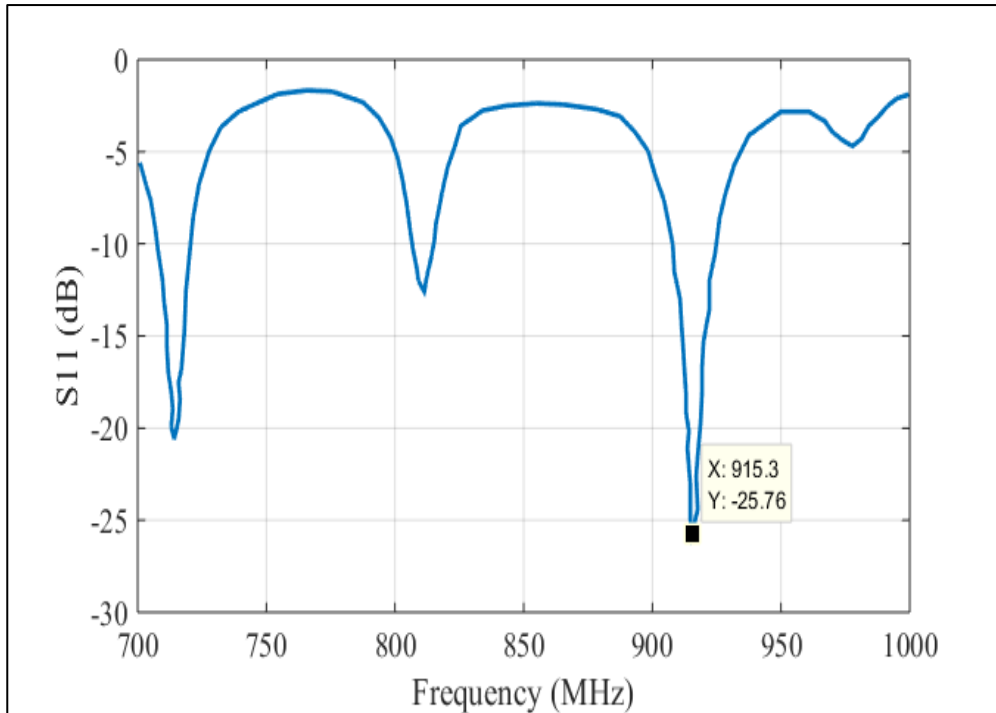
Fig.4.2. Simulated S11 for Antenna 1.

Figure 4.3 shows the antenna's 3D radiation pattern at 915.7 MHz. When an antenna is placed inside bodily tissues, its radiation pattern is altered. The antenna features a 4.89 dBi directivity. The ratio of the antenna's radiation intensity in a given direction to the radiation intensity that would be achieved if the power absorbed by the antenna were radiated isotropically is known as the antenna's IEEE gain.
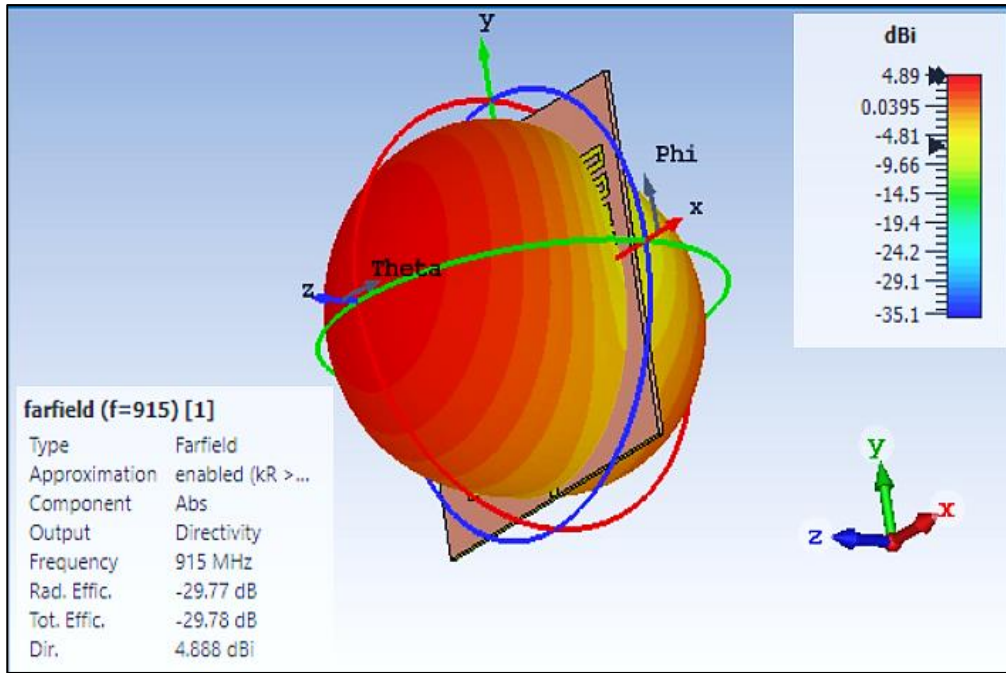
Fig.4.3. Simulated 3D radiation pattern for Antenna 1.

Figure 4.4 below depicts the 2D (Polar) radiation pattern of Antenna 1 at 915 MHz. The main lobe direction is 8.00 degrees, and the magnitude radiation from the main lobe has a magnitude of 4.89 dBi and a direction of 145 degrees. The side lobe level is -2.7 dB, and the angle's width is 103.5 degrees. A polar map of the radiation pattern of the compact size antenna at 915 MHz reveals the principal lobe's magnitude to be 4.89 dBi at this frequency.
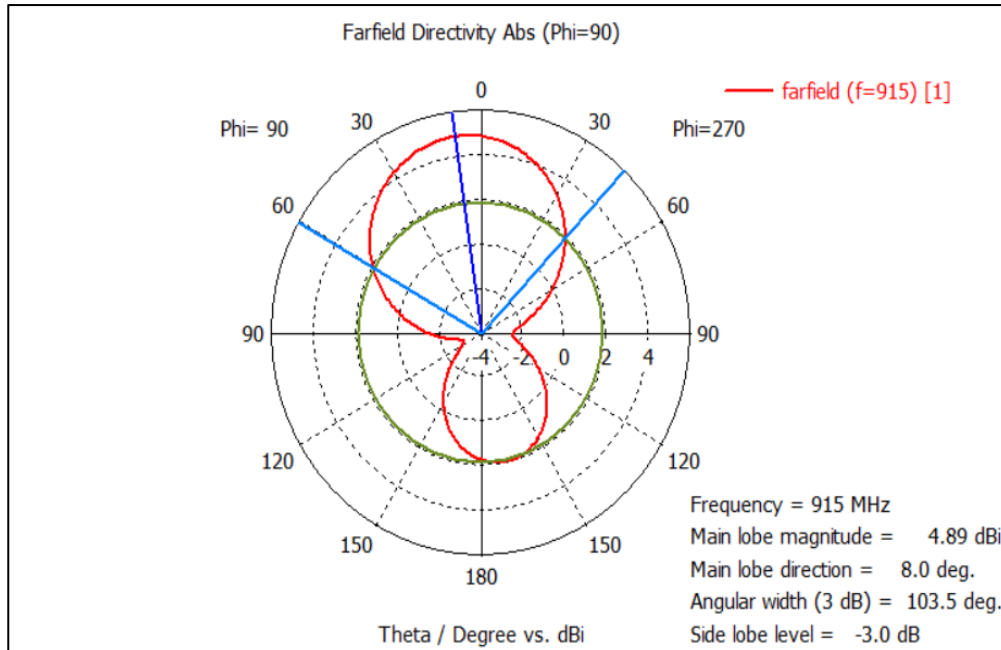
Fig. 4.4. Simulated 2D (Polar) radiation pattern for Antenna 1.

In order to show the possibility of fine tuning the resonant frequency, the length of the right branch of the antenna is changed slightly and the S11 is plotted. This will help the designer to shift the resonant frequency of the antenna slightly towards the lift or the right and hence improve the radiation and matching properties. Figure 4.5 below shows the S11 where the resonant frequency became 916.29 MHz S11= -18.79. The (**α**) represent the value of cutting of the shape of antenna as shown in the figure (α = **2.00 mm**). We noticed that when we cut a small part of the shape of antenna the frequency is increased and the S11 is decreased (the size of the antenna is inversely proportional to the frequency). To get a higher resonant frequency, the cut must be larger while maintaining other dimensions the same (The size of the antenna decrease with increasing frequency).
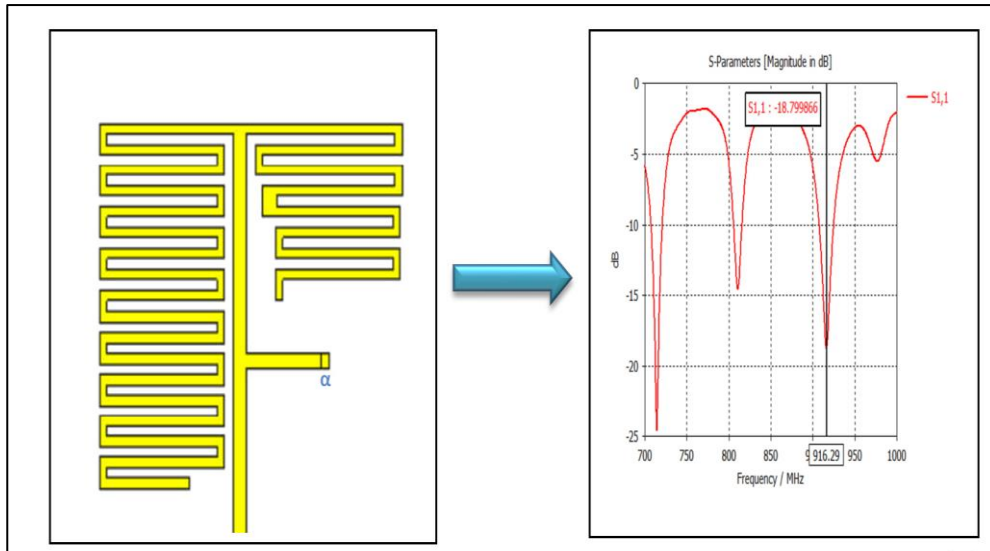
Fig.4.5. Simulated Antenna 1 after cutting a small portion by an amount of α.

The S parameter (S11) of (-26.331) at 916.29 MHz is seen in Figure 4.6 below. The (**α**) represents the value of adding extra length to the antenna's branch, with the value 6.00 mm as shown. The resonant frequency in now shifted and lowered to 914.5 MHz with S11 value around -30 dB.

Fig.4.6. Simulated Antenna 1 after adding a small portion by an amount of α.

4.2.2 Antenna 2 at 915 MHz

With the use of CST, the antenna model was created and simulated. The antenna is designed to operate at 915 MHz frequency. The antenna substrate size is 100 mm x 100 mm in overall dimension. Table 4.3 shows the substrate dimensions of Antenna 2. Figure 4.7 displays all dimensions and geometrical details of Antanna 2 at 915 MHz . All arrows here represent the width and height of Antenna 2 .

Figure 4.8 illustrate the simulated S11 parameters of Antenna 2. The antenna appears to radiate most effectively at 915.97 MHz with very strong resonance, where S11=-21.655797 dB.
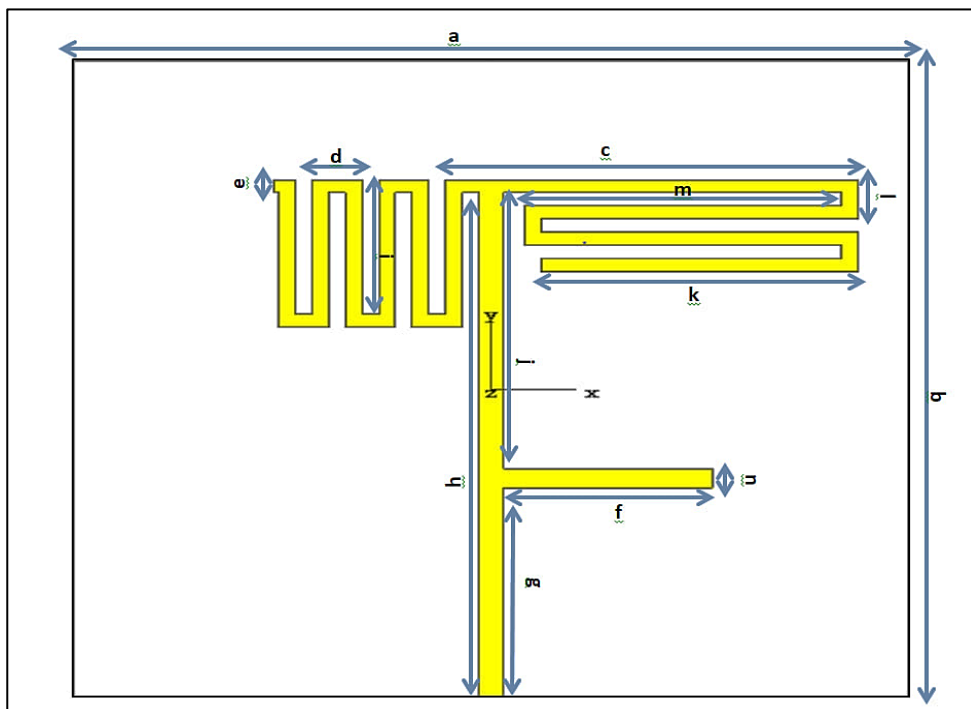
Fig.4.7. Antenna 2 at selected frequency band 915MHz with dimensions.

Table 4.3: antenna 2 design parameters.

Name	Measurement (mm)
Width of substrate	100
Length of substrate	100
Width of patch	50
Length of patch	50
Feeding point	3
Thickness of antenna	1.645 mm
Dielectric constant of the substrate ε_r	4.3

Table 4.4: The value of dimensions of Antenna 2.

Name	Value (mm)
a	100
b	100
c	49.50
d	6.00
e	2.00
f	25.10
g	35.00
h	80.00
i	20.50
j	42.00
k	37.99
l	6.00
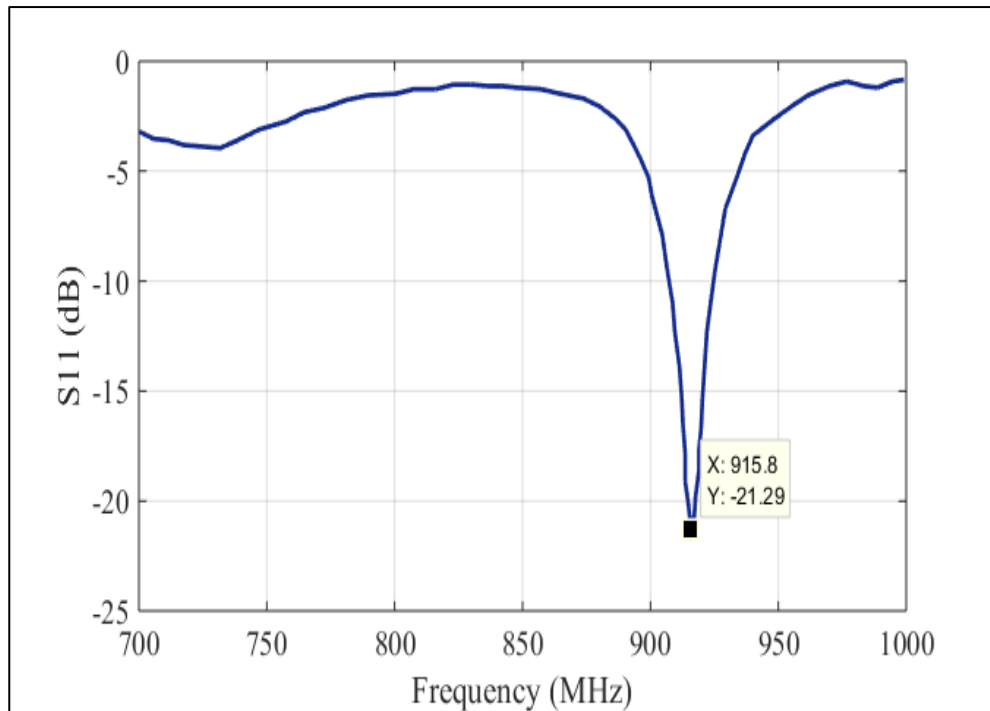
Fig.4.8. Simulated 1D (S parameter) for Antenna 2 at selected frequency band.

The 1D (polar) radiation pattern of an antenna at 915.97 MHz is depicted in Figure 4.9 below. The main lobe has a direction of 5.0 degrees, and its magnitude radiation has of 4.4 dBi. The angle's breadth is 105.2 degrees, and the side lobe level is - 4.1dB . The major lobe of the compact size antenna has a magnitude of 4.4 dBi at 915 MHz, according to a polar map of its radiation pattern.
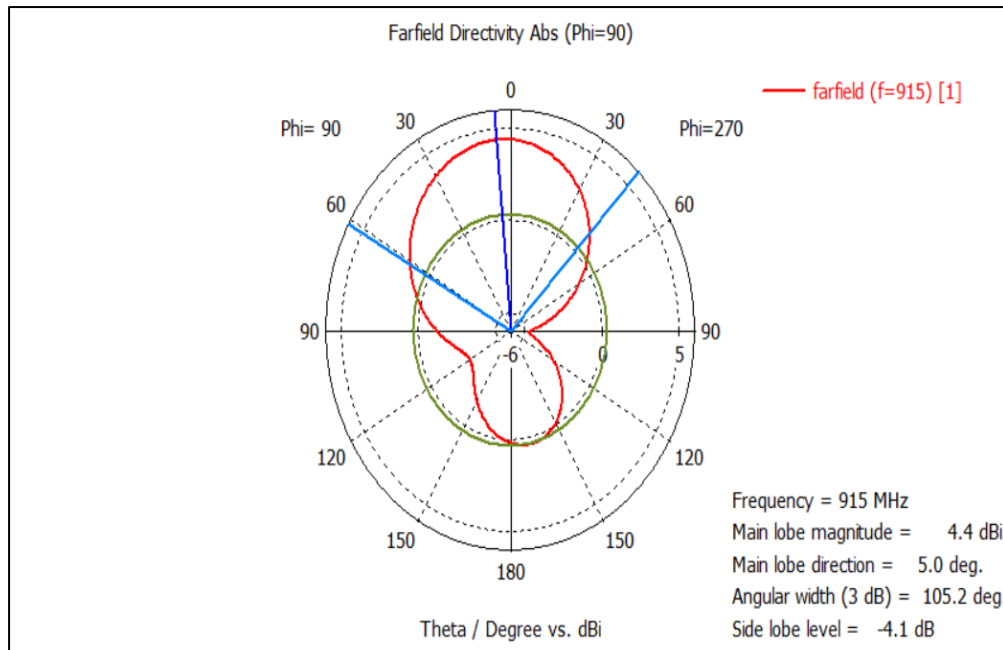
Fig. 4.9. Simulated 1D (Polar) radiation pattern for Antenna 2 at selected frequency band 915.7MHz

The antenna's 3D radiation pattern at 915.97 MHz is displayed in Figure 4.10 below. An antenna's radiation pattern transforms when it is placed into organic tissues. The antenna's IEEE gain is defined as the difference between the radiation intensity emitted in one direction by the antenna and the radiation intensity that would result from isotropic radiation of the antenna's power absorption.
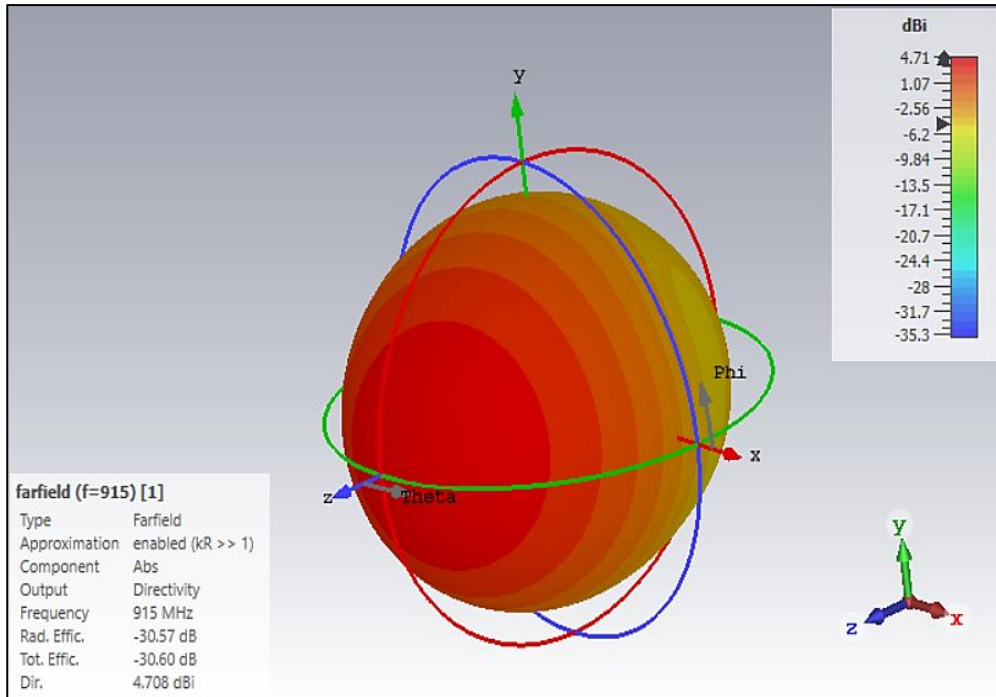
Fig.4.10. Simulated 3D radiation pattern for Antenna 2 at selected frequency band 915.7MHz

Figure 4.11 below shows the S11 where the resonant frequency became 917.29 MHz S11= -12.31. The (α) represent the value of cutting of the shape of antenna as shown in the figure (α = 3.00 mm). We noticed that when we cut a small part of the shape of antenna the frequency is increased and the S11 is decreased) the size of the antenna is inversely proportional to the frequency). To get a higher resonant frequency, the cut must be larger while maintaining other dimensions the same (The size of the antenna decrease with increasing frequency).
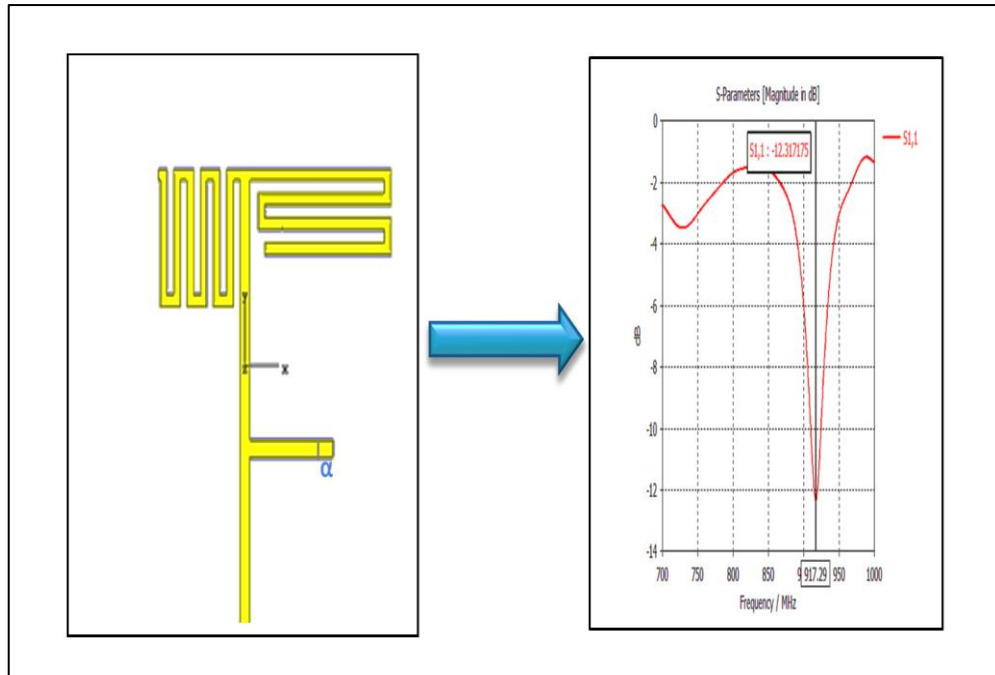
Fig.4.11. Simulated Antenna 2 after cutting a small portion by an amount of α.

The S parameter (S11) of (-29.17 dB) at 914.8 MHz is seen in Figure 4.12 below. The (α) represents the value of adding extra length to the antenna's branch, with the value 6.00 mm as shown. The resonant frequency in now shifted and lowered to 914.8 MHz with S11 value around -30 dB.
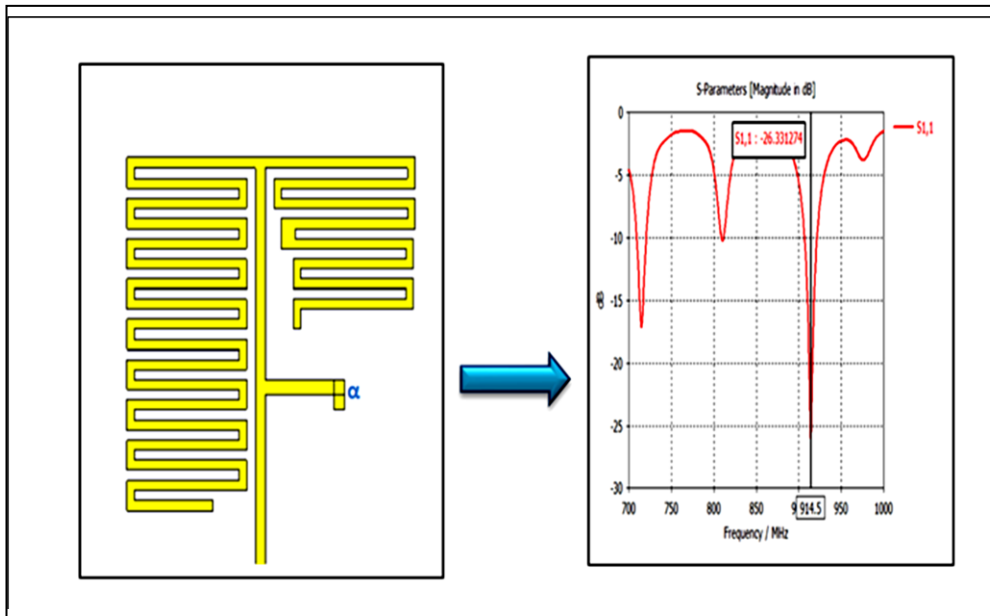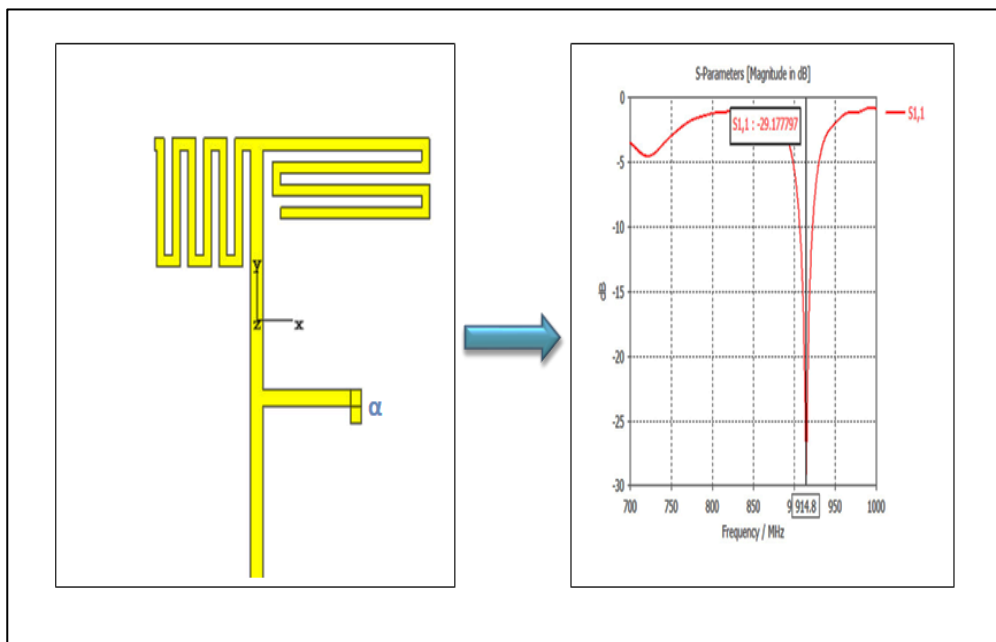

Fig.4.12. Simulated Antenna 2 after adding a small portion by an amount of α.

79

The performance comparison of the results is displayed for the two antennas at 915 MHz is listed in Table 4.5.

Table 4.5: Performance comparison between Antenna 1 and Antenna 2

1D Results / S-parameters	Substrates	
	Antenna 1	Antenna 2
Return Loss, S11(dB)	-25.519215	-21.655797
Directivity (dBi)	4.888	4.708
Bandwidth (MHz)	27	29
Side lobe level (dB)	3.0	-4.1

4.2.3 Antenna 3 at 433 MHz

With the help of CST, the antenna model was created and simulated. The antenna is designed to operate at 433 MHz frequency. The antenna substrate size is 100 mm x 100 mm in overall dimension. Table 4.6 shows the substrate dimensions of Antenna 3. Figure 4.13 displays all dimensions and geometrical details of Antanna 3 at 433 MHz . All arrows here represent the width and height of Antenna 3 .

Figure 4.14 illustrate the simulated S11 parameters of Antenna 3. The antenna appears to radiate most effectively at 433 MHz with very strong resonance, where S11=-20 dB.
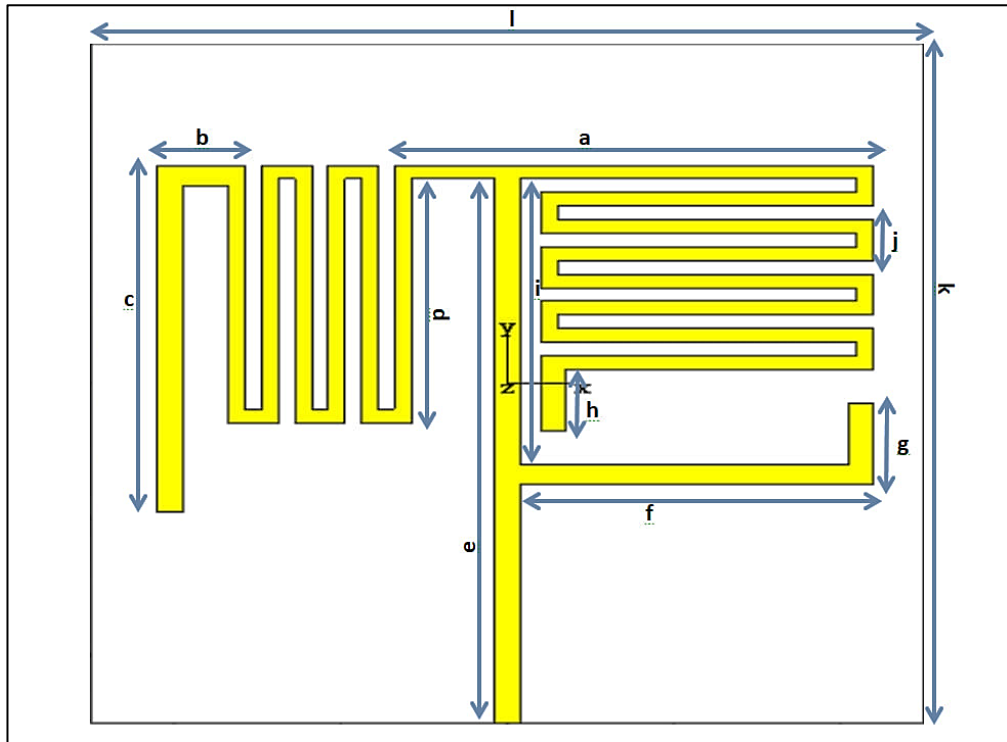
Fig. 4.13. Antenna 3 at selected frequency band 915MHz with dimensions.

Table 4.6: Antenna 3 design parameters

Name	Value (mm)
Width of substrate	100
Length of substrate	100
Width of patch	50 (Wp/2)
Length of patch	50 (Lp/2)
Feeding point	3
Thickness of antenna	1.645
Dielectric constant of the substrate ε_r	4.3

Table 4.7: The value of dimension at antenna 3.

Name	Value (mm)
a	57.50
b	10.50
c	51.00
d	36.00
e	80.00
f	42.50
g	12.00
h	9.00
i	42.00
j	6.00
k	100
l	100
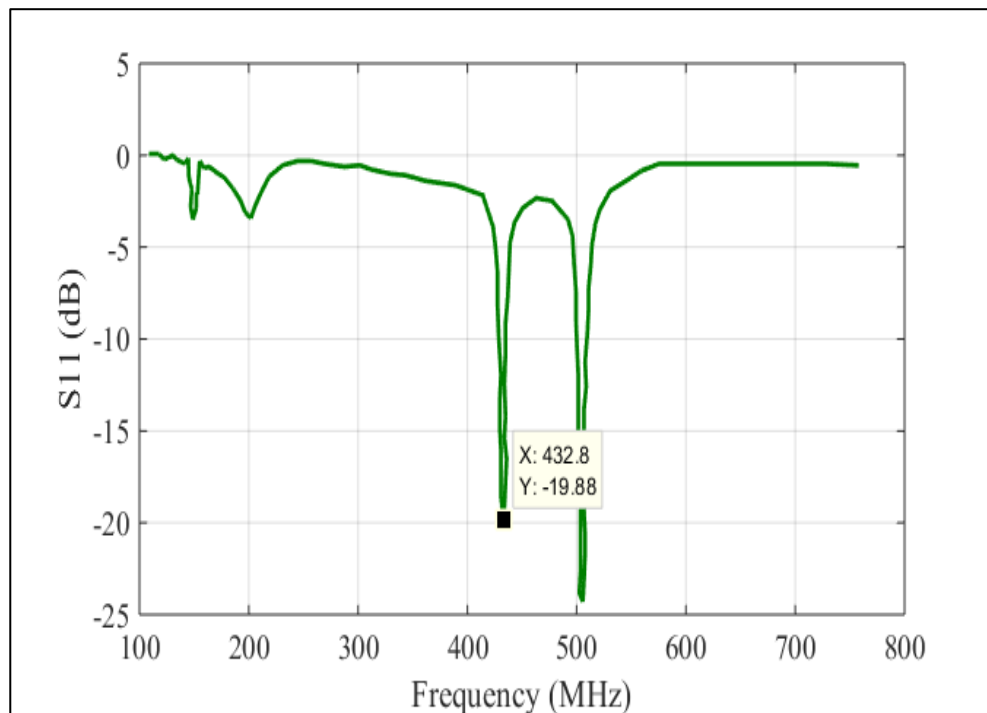
Fig. 4.14. Simulated 1D (S parameter) for Antenna 3 at selected frequency band.

The antenna's 3D radiation pattern at 433 MHz is depicted in Figure 4.15. An a ntenna's radiation pattern changes when it is inserted into biological tissues. The antenna's directivity is 3.41.The antenna's IEEE gain is defined as the ratio of the antenna's radiation intensity in a given direction to the radiation intensity that would be obtained if the antenna's power absorption were radiated isotropically.

Fig. 4.15. Simulated 3D radiation pattern for Antenna 3 at selected frequency band 433 MHz.

A 433 MHz, the antenna's 2D (polar) radiation pattern is depicted in figure 4.16. The main lobe direction is oriented at 170.00 degrees, and the main lobe has a magnitude of 2.98 dBi. The angle has a 111.2 degree breadth, and the side lobe level is -3.5 dB. The compact size antenna's principal lobe has a magnitude of 2.98 dBi at 433 MHz, as shown by a polar map of its radiation pattern.
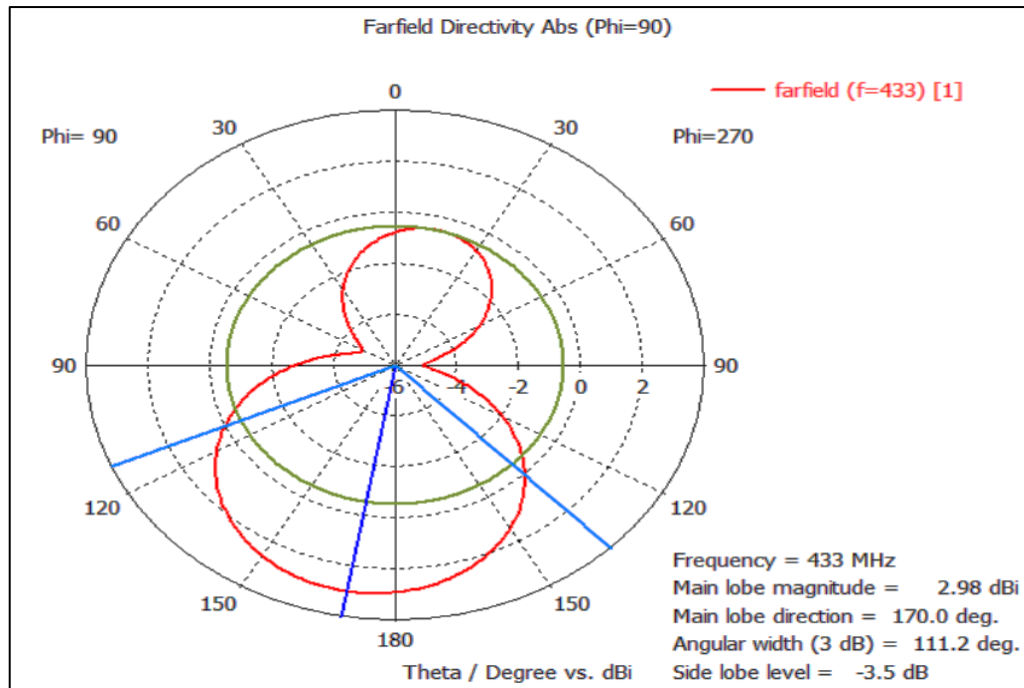
Fig. 4.16. Simulated 1D (Polar) radiation pattern for Antenna 3 at selected frequency band 433 MHz.

4.2.4 Antenna 4 at 433 MHz

The antenna is placed on a double-sided thick copper substrate with thickness of 1.6mm. The antenna is also designed to operate at 433 MHz frequency. The antenna size is 51 mm x 28 mm which is much smaller than previous antennas reported in this chapter. The antenna design is located on the opposite side of the PCB from the ground with a via is employed to connect both sides of the antenna which antennas providing a better matching at the ISM and the MICS band around 433 MHz as shown in figure 4.17. Table 4.8 shows the design parameters of Antenna 4. Table 4.9 display the geometrical details of Antenna 4.

Figure 4.18 implies that the antenna radiates best at 433 MHz, where S11=-27.16 dB. In addition, figure 4.29 shows the antenna's 3D radiation pattern at 433 MHz.

Table 4.8: Antenna 4 design parameters.

Name	Value (mm)
Width of substrate	51
Length of substrate	28
Width of patch	Ws/2
Length of patch	Ls/2
Feeding point	1.5
Thickness of antenna	1.645
Dielectric constant of the substrate ε_r	4.3

Table 4.9 : The value of dimension of Antenna 4.

Name	Value (mm)
a	51.00
b	28.00
c	25.10
d	25.50
e	15.13
f	8.00
g	12.00
h	17.50
i	23.50
j	24.10
k	18.13
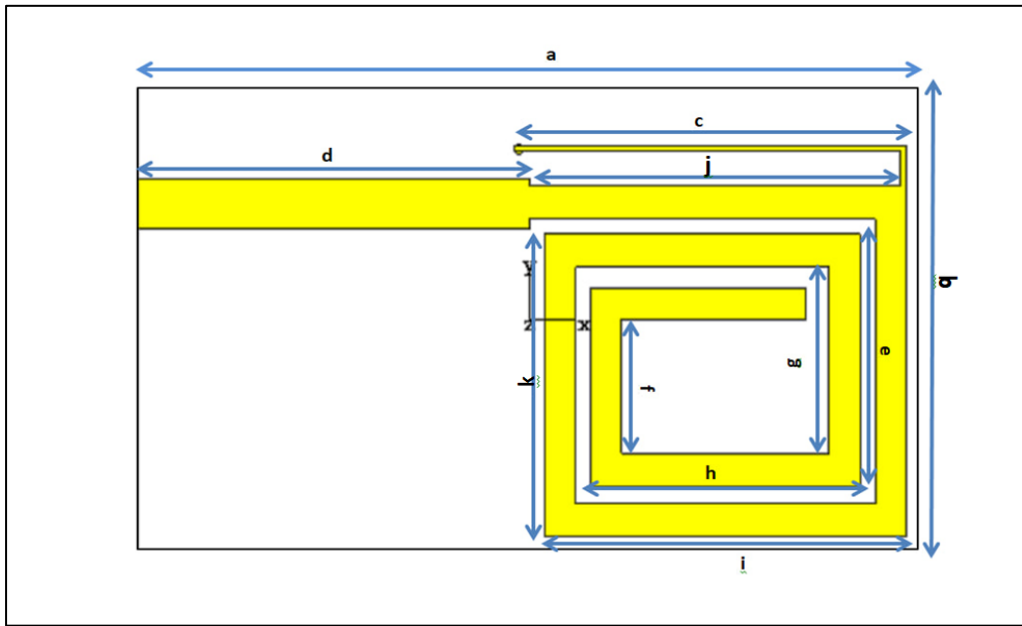
Fig. 4.17. Antenna 4 designed at frequency band 433MHz.

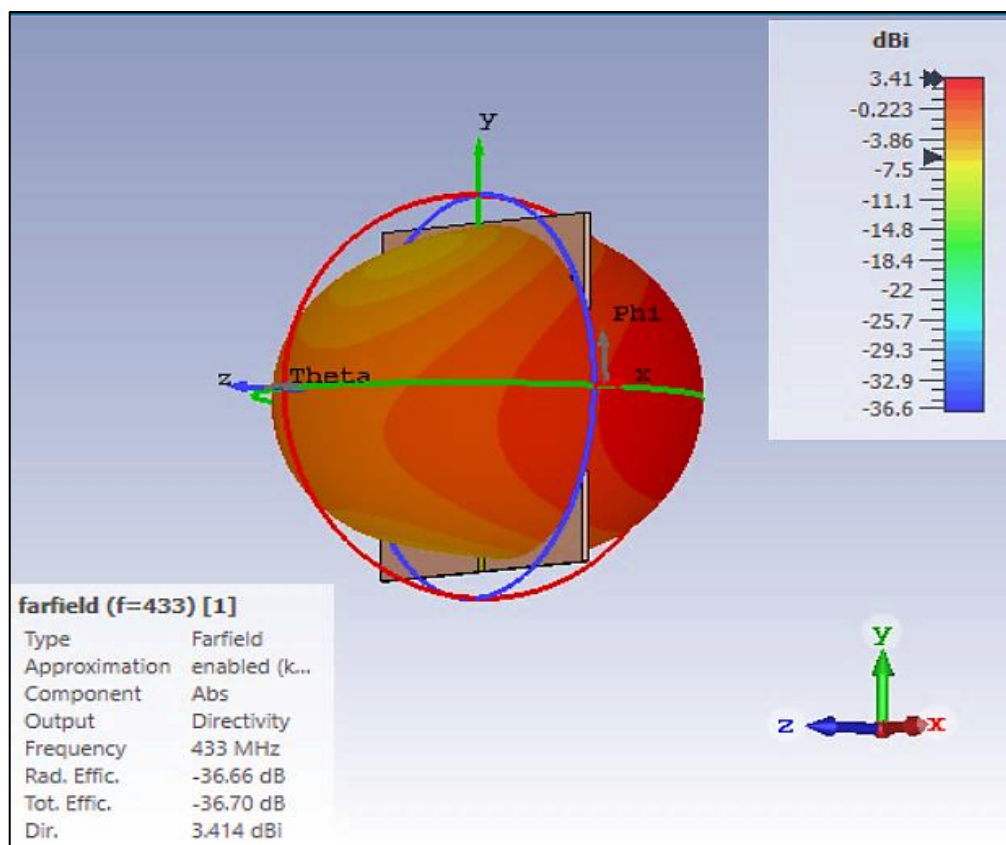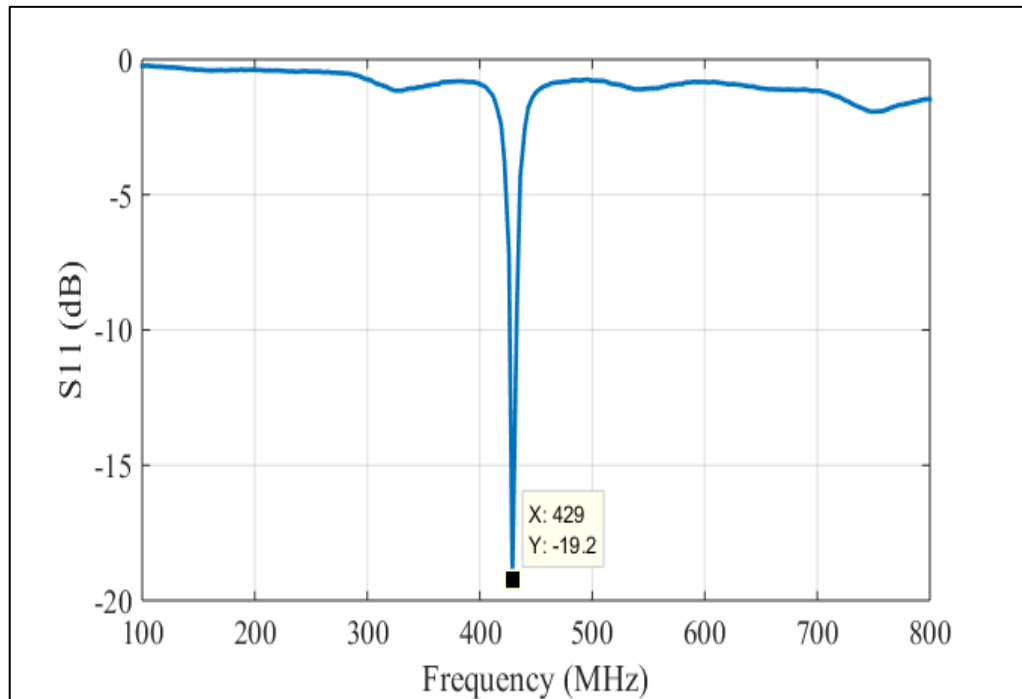**Fig.4.18. Simulated 1D (S parameter) for Antenna 4 at selected frequency band.**
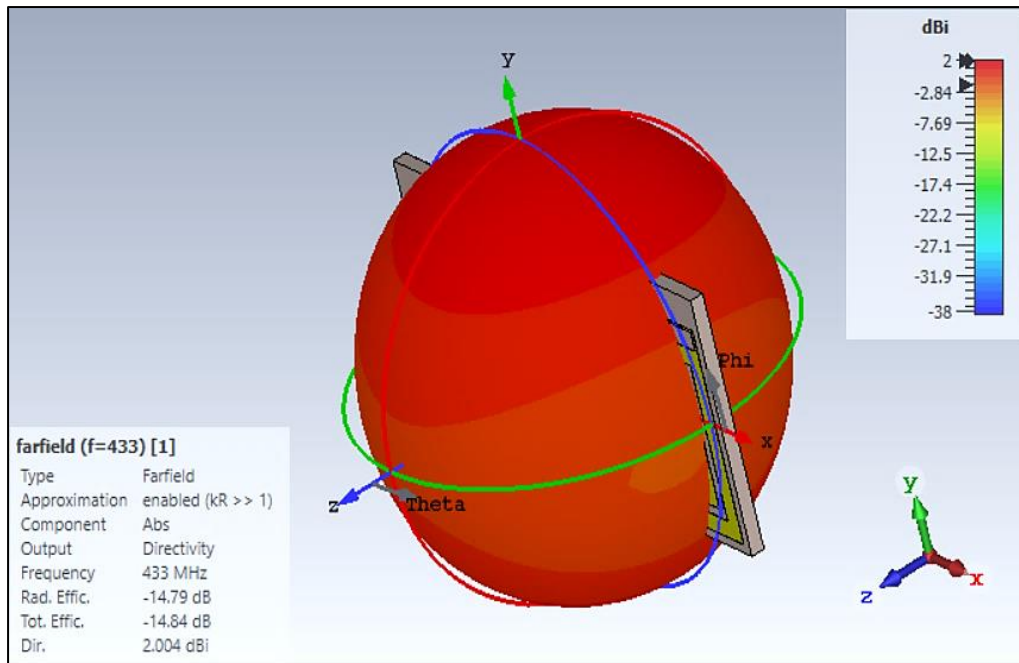
Fig.4.19. Simulated 3D radiation pattern for Antenna 4 at selected frequency band 433 MHz.

The 2D (polar) radiation pattern of an antenna at 433 MHz is depicted figure 4.20. The main lobe direction is 92 degrees, while the main lobe magnitude radiation has a magnitude of 1.96 dBi. The primary lobe's magnitude at 433 MHz is shown by a polar plot of the radiation pattern of the compact size antenna to be 1.96 dBi at this frequency.
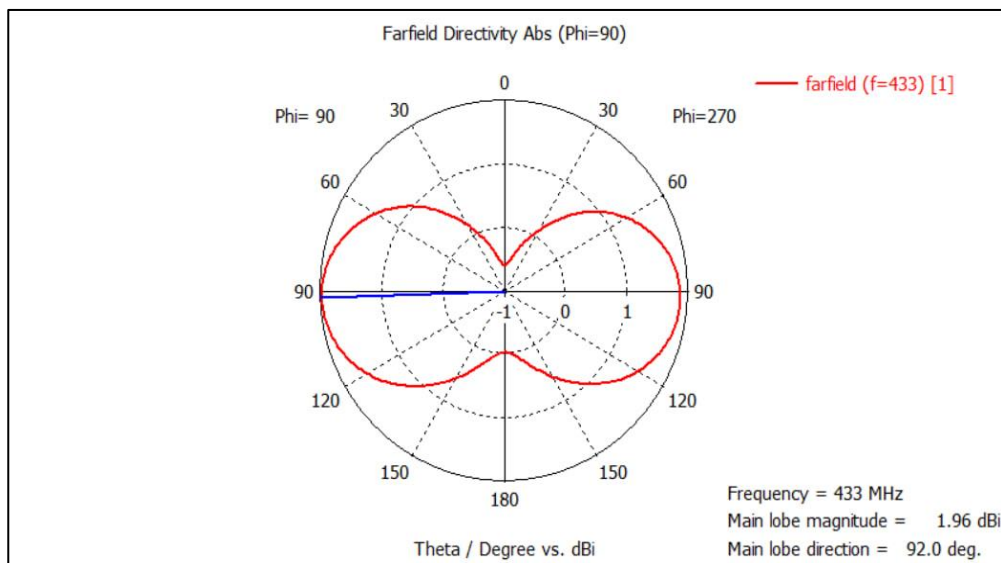
Fig. 4.20. Simulated 2D (Polar) radiation pattern for Antenna 4 at selected frequency band 433 MHz.

Figure 4.21 below shows the S11 where the resonant frequency became 435.2 MHz S11= -21.0528 . The (**α**) represent the value of cutting of the shape of antenna as shown in the figure (α = **2.00 mm**)**.** We noticed that when we cut a small part of the shape of antenna the frequency is increased and the S11 is decreased (the size of the antenna is inversely proportional to the frequency). To get a higher resonant frequency, the cut must be larger while maintaining other dimensions the same (The size of the antenna decrease with increasing frequency).
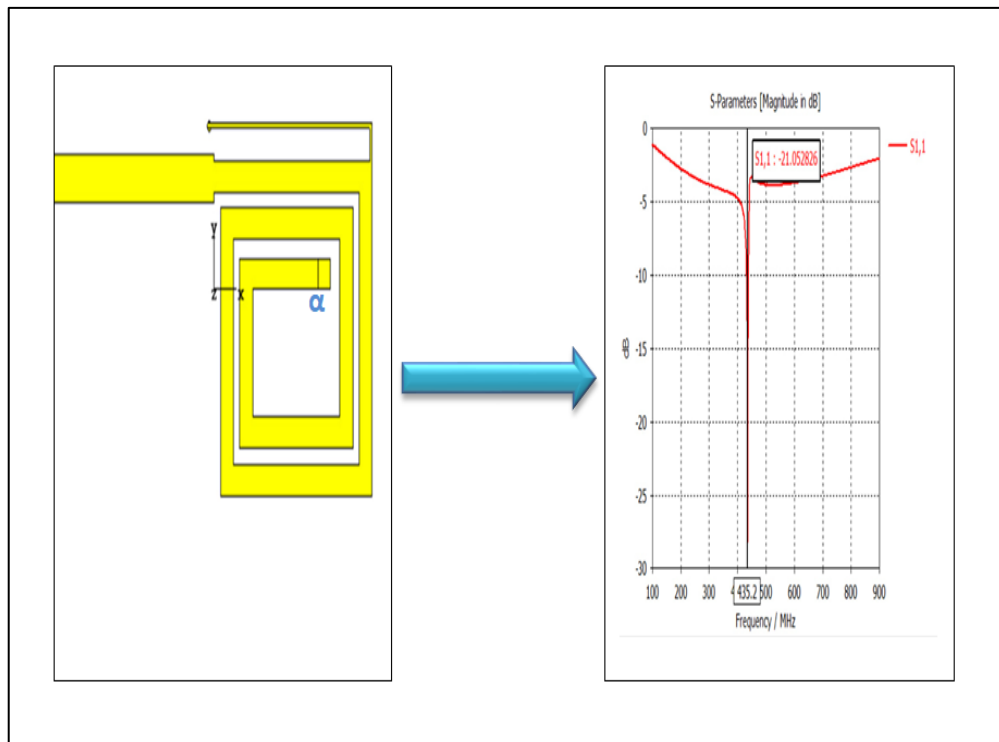
Fig.4.21. Simulated Antenna 4 after cutting a small portion by an amount of α.

The S parameter (S11) of (-25.5209 dB) at 432 MHz is seen in Figure 4.22 below. The (**α**) represents the value of adding extra length to the antenna's branch, with the value 5.00 mm as shown. The resonant frequency in now shifted and lowered to 914.8 MHz with S11 value around -30 dB.
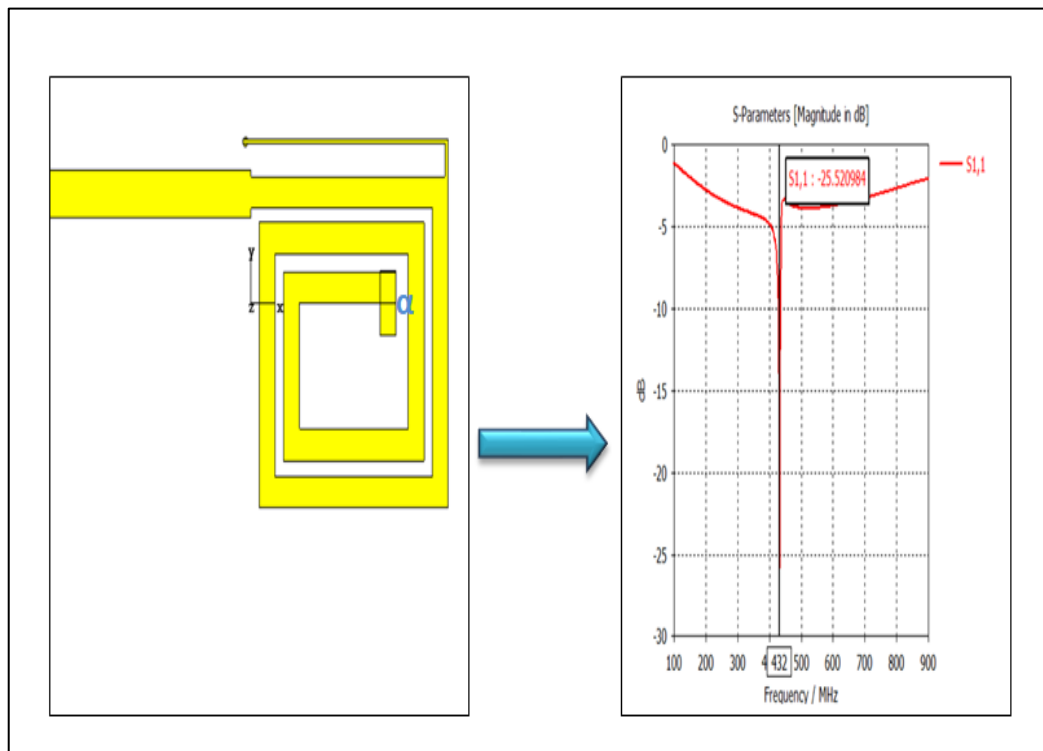
Fig.4.22. Simulated Antenna 4 after adding a small portion by an amount of α.

Table 4.10 compares the performance of Antenna 3 and Antenna 4 at 433 MHz.

Table 4.10: Comparison of performance for Antenna 3 and Antenna 4.

1D Results / S-parameters	Substrates	
	Antenna 3	Antenna 4
Return Loss, S11(dB)	-20.0	-27.1
Directivity (dBi)	3.41	2
Bandwidth (MHz)	20	10
Side lobe level (dB)	-3.5	-4.1

4.3 Fabrication and Experimental Validation

In section 4.2, two antennas were designed and simulated at 915 MHz and other two antenna were designed and simulated at 433 MHz for implantable medical devices. The four antennas were fabricated using PCB technology on a FR-4 substrate with dielectric constant of 4.3 and a thickness of 1.6 mm. Figure 4.23 shows photographs of manufactured antennas at 915 MHz, whereas Figure 4.24 shows photographs of manufactured antennas at 433 MHz. SMA connector was attached to each antenna for measurement purposes.

Vector Network Analyzer is utilized to measure the S11 of antennas at the designed frequency of each antenna. figure 4.25 shows the experimental setup used to measure the S-parameters.
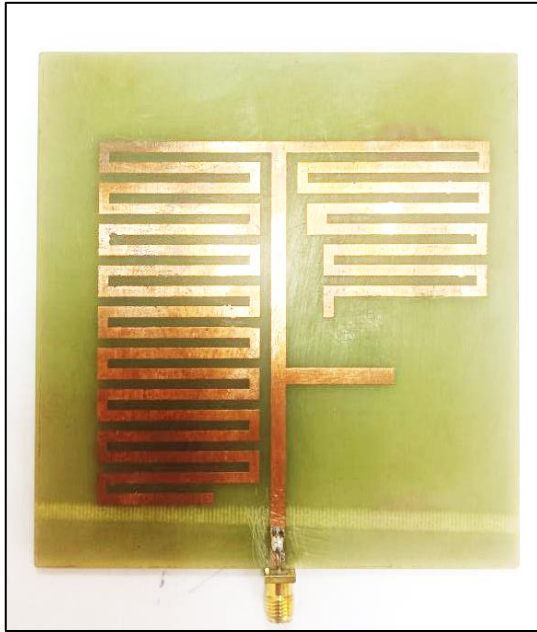
Antenna 1
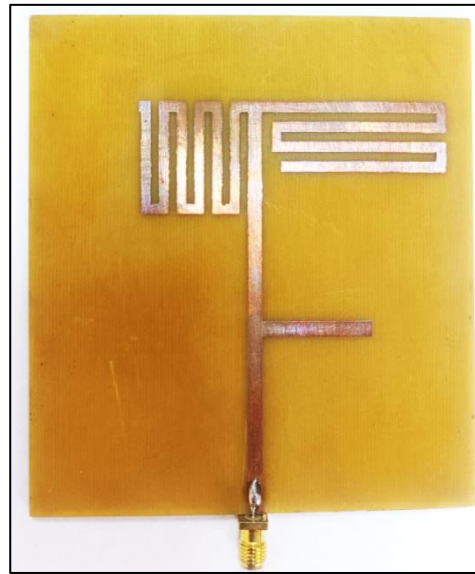
Antenna 2

Fig. 4.23. Photographs of manufactured antennas at 915 MHz.

Antenna 3

Antenna 4

Fig. 4.24. Photographs of manufactured antennas at 433 MHz.

Fig. 4.25. Experimental set up for measuring the antenna S-parameters.

Figures 4.26 to 4.29 compares the simulated and measured S11 for each fabricated antenna.
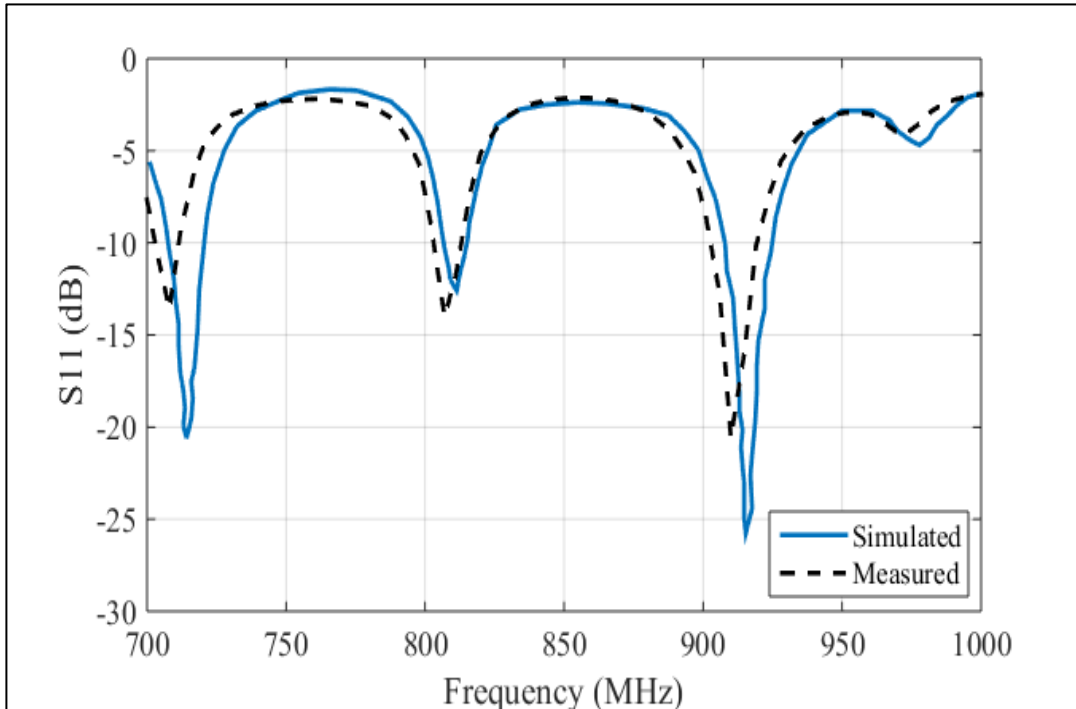
Fig. 4.26. Measured and simulated S11 for Antenna1.
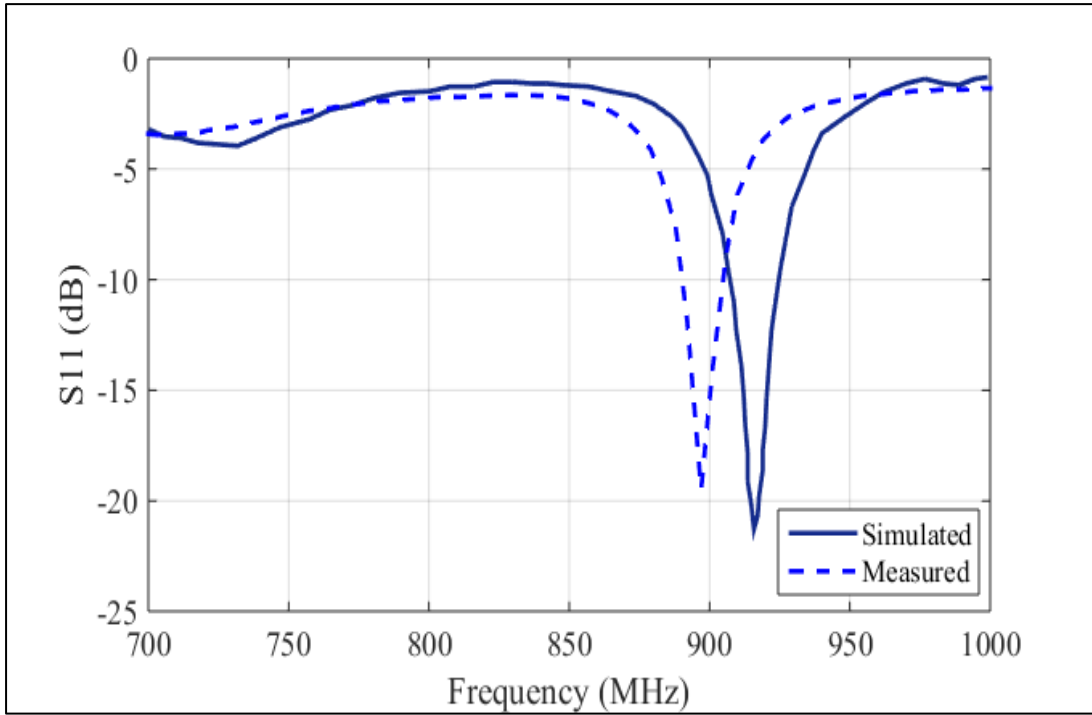
Fig. 4.27. Measured and simulated S11 for Antenna 2.
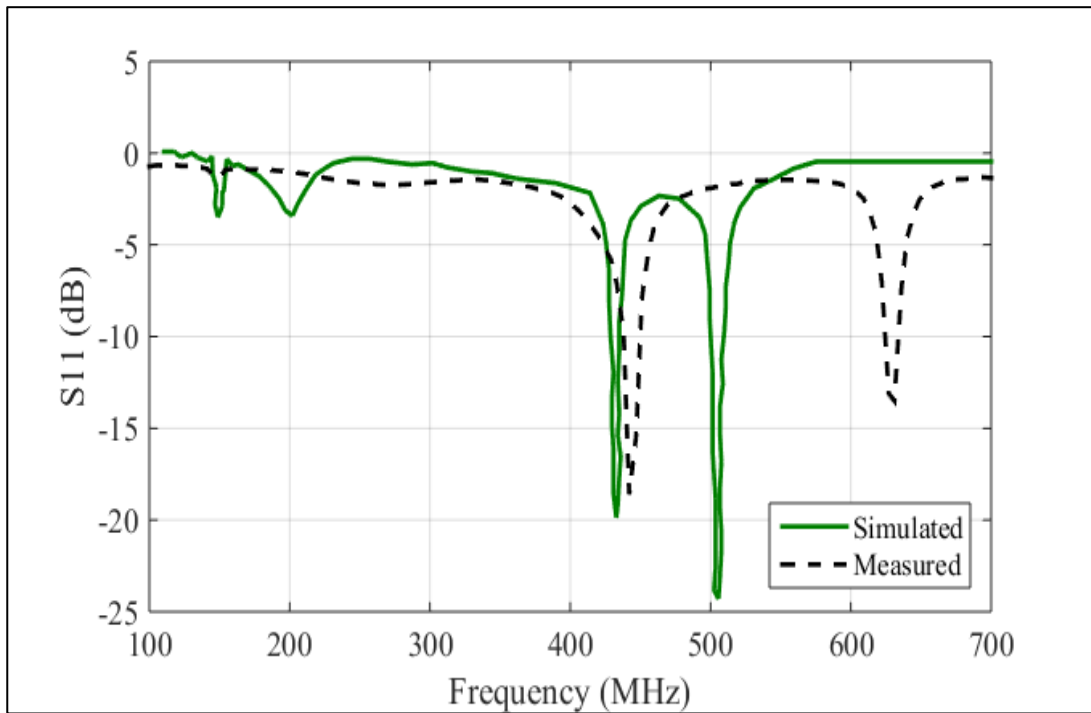
Fig. 4.28. Measured and simulated S11 for Antenna3.
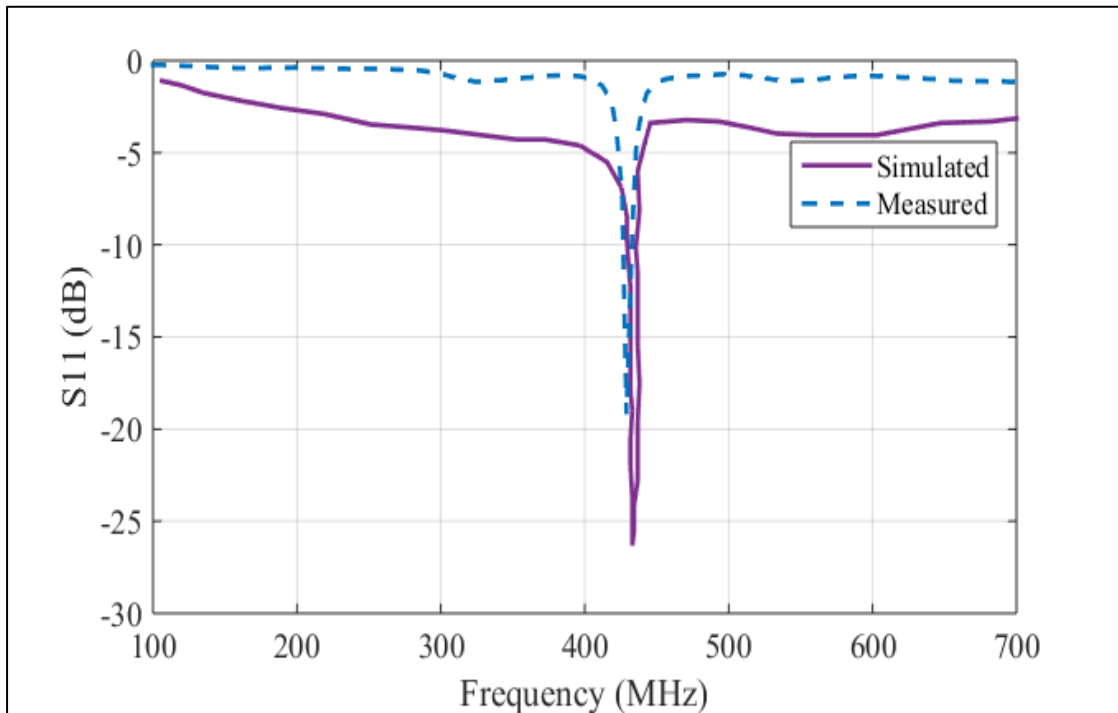
Fig. 4.29. Measured and simulated S11 for Antenna 4.

It can be clearly seen from the above figures that there is an excellent agreement between the measured and simulated results especially for Antenna 1 and Antenna4. This gives a clear indication about the accuracy of the simulation procedure adopted in this work. This procedure can be employed again and again to design and develop more antennas for IMDs without the need to fabricate and realize as it is already validated.

CHAPTER FIVE

CONCLUSIONS AND FUTURE WORK

5.1 Conclusions

In the current study, a voltage doubler rectifier circuit design was examined and simulated using the ADS software at the frequency bands of 433 MHz and 915 MHz. Multi-stage rectifiers were designed and simulated by using the FR4 substrate. With the help of this rectifier, a made-up implanted battery can be easily wirelessly charged. The rectifier's circuit were combined with microstrip transmission lines to achieve better matching. The results showed that a total conversion efficiency of around 60% was achieved with an output DC voltage of 6V. To be employed in a far-field WPT system, this rectifier was attahced to a meandered line implantable antenna. In order to reduce the size of the microstrip transmission lines, the overall components have been modified. The aim is to achieve a compact design with the highest conversion efficiency. The proposed rectifiers in this work were designed to function with antennas and was optimized for a reference impedance of 50 Ω. It is concluded that:

1- Achieving high AC to DC conversion efficiency of up to 60% using a voltage doubler rectifier is feasible.

2- Input power levels less than -15 dBm and frequency range below 1 GHz are handled by Schottky diodes of the series HSMS- 2820. For energy harvesting applications at 433 MHz and 915 MHz, this series is quite helpful.

3- By combining all of the components, including the transmission lines, optimally, the rectifier circuit was reduced to a relatively small size. The developed rectifier circuits may

be used successfully to charge batteries of IMDs with a capacity below 10 mA•h, where these batteries are beneficial for ultra low-power medical applications.

4- Since there was a good agreement between the simulated and measured results, the design procedure for both the rectifier and antenna using ADS and CST, respectively is valid and applicable to other designs.

Six rectifier circuits were designed and simulated using ADS. Three circuits (single-, double- and triple-stage) were designed to operate at 433 MHz and another three were designed at 915 MHz. The variation of output voltage and efficiency with changing the input power is recorded and used as a measure of the rectifier performance. Wide range of input power (-15 dBm to 10 dBm) was used in this study to measure the real impact of input power on the system performance. It was found that the output voltage and efficiency increase exponentially with increasing the input power due to the non-linear characteristics of Schottky diodes.

Practically, we obtained an efficiency of about 60% out of the single stage at 433MHz with an output voltage of approximately 3.5V, while the obtained output voltage by the double stage rectifier at 433 MHz was more than 5V with almost similar efficiency and so on for the other circuits at 915 MHz. This clearly shows the feasibility of employing the double stage rectifiers taking into account the resultant increased system complexity.

On the other hand, antennas were designed to be used in the ISM band and was constructed and tested by utilizing CST. In this work, four meandered line antennas were designed, simulated and

tested at 433MHz and 915 MHz. A very good radiation and reflection coefficient was achieved at 433 MHz and 915 MHz. The obtained S11 for all cases was less than -20 dB, which indicates an excellent matching and this is preferable in this application.

5. 2 **Future works**

- The designed voltage doubler rectifiers have shown promising results. Thus, it may be a good idea to explore and investigate other types of rectifiers and compare their performance.

- Microwave frequency band can also be explored and compared to rectenna systems at 433 MHz and 915 MHz.

- The impact of changing the load type and value on the system perforamce can be suggested as future work.

- Various substrate materials will be taken into consideration when designing rectifiers and antennas to obtain compact size rectenna system.

- Using variable topologies as rectifier circuit or different types of diodes and studying the impact on the efficiency

References

[1] H. Raillard, "Development of an implantable cardiac pacemaker," Solid-State Circuits Conference. Digest of Technical Papers, IEEE International, Philadelphia, PA, USA, pp. 88- 89, 1962.

[2] A Brief Chronology of Medical Device Security. https://cacm.acm.org/magazines/2016/10/207766-a-brief-chronology-of-medical-device-security/fulltext, 2017.

[3] Parkinson Association. http://www.parkinsonassociation.org/facts- about-parkinsons-disease/.

[4] Global Report on Diabetes. http://apps.who.int/iris/bitstream/10665/204871/1/9789241565257_eng.pdf, 2014.

[5] Pacemakers Fail More Often Than Manufacturers Acknowledge.http://www.pbs.org/wgbh/nova/next/body/pacemakers-fail-more- often-than-manufacturers-acknowledge/, 2017.

[6] E. T. S. Institute, "Ultra Low Power Active Medical Implants (ULP-AMI) and Peripherals (ULP-AMI-P) operating in the frequency range 402 MHz to 405 MHz," 2009.

[7] J. A. Von Arx, W. R. Mass, S. T. Mazar, and M. D. Amundson, "Antenna for an implantable medical device," ed: US patent 7,483,752 B2, Jan. 27, 2009.

[8] S. Vajha, K. R. Maile, D. E. Larson, D. A. Chizek, and J. M. Edgell, "Folded antennas for implantable medical devices," ed: US patent 2012/0130451 A1, May 24, 2012.

[9] Ben Amar A, Kouki AB, Cao H. Power Approaches for Implantable Medical Devices. Sensors (Basel). 2015 Nov 13;15(11):28889-914. doi: 10.3390/s151128889. PMID: 26580626; PMCID: PMC4701313.

[10] A. Kiourti, J. R. Costa, C. A. Fernandes, A. G. Santiago and K. S. Nikita, "Miniature Implantable Antennas for Biomedical Telemetry: From Simulation to Realization," in IEEE Transactions

on Biomedical Engineering, vol. 59, no. 11, pp. 3140-3147, Nov. 2012, doi: 10.1109/TBME.2012.2202659.

[11] Reem Shadid, Sima Noghanian, "A Literature Survey on Wireless Power Transfer for Biomedical Devices", International Journal of Antennas and Propagation, vol. 2018, Article ID 4382841, 11 pages, 2018. https://doi.org/10.1155/2018/4382841

[12] S. R. Khan, S. K. Pavuluri, G. Cummins, and M. P. Y. Desmulliez, "Wireless Power Transfer Techniques for Implantable Medical Devices: A Review," Sensors, vol. 20, no. 12, p. 3487, Jun. 2020, doi: 10.3390/s20123487. [Online]. Available:

http://dx.doi.org/10.3390/s20123487

[13] Kazanskiy NL, Butt MA, Khonina SN. Recent Advances in Wearable Optical Sensor Automation Powered by Battery versus Skin-like Battery-Free Devices for Personal Healthcare-A Review. Nanomaterials (Basel). 2022 Jan 21;12(3):334. doi: 10.3390/nano12030334. PMID: 35159679; PMCID: PMC8838083.

[14] O' Dwyer S, Riordain RN. The patient experience of dental implant surgery: a literature review of pertinent qualitative studies. Ir J Med Sci. 2021 May;190(2):835-842. doi: 10.1007/s11845-020-02327-y. Epub 2020 Jul 27. PMID: 32720197.

[15] Kod, Muayad. "Wireless Powering and Communication of Implantable Medical Devices." PhD Thesis, University of Liverpool, (2016).

[16] H. Raillard, "Development of an implantable cardiac pacemaker," Solid-State Circuits Conference. Digest of Technical Papers, IEEE International, Philadelphia, PA, USA, pp. 88- 89, 1962.

[17] Massachusetts Institute of Technology, "http://groups.csail.mit.edu/netmit/IMDShield/," 2011.

[18] K. S. Nikita, Handbook of biomedical telemetry: John Wiley & Sons, 2014.

[19] H. S. Savci, A. Sula, Z. Wang, N. S. Dogan, and E. Arvas, "MICS transceivers: Regulatory standards and applications," Proceedings of the IEEE SoutheastCon 2004, pp. 179-182, 2005.

[20] R. Das and H. Yoo, "Biotelemetry and Wireless Powering for Leadless Pacemaker Systems," IEEE Microwave and Wireless Components Letters, vol. 25, pp. 262-264, Apr 2015.

[21] J. Miller, "Wireless power for tiny medical implants," Physics Today, vol. 67, pp. 12-14, Aug 2014.

[22] C. S. Niu, H. W. Hao, L. M. Li, B. Z. Ma, and M. S. Wu, "The transcutaneous charger for implanted nerve stimulation device," 2006 28th Annual International Conference of the IEEE Engineering in Medicine and Biology Society, Vols 1-15, pp. 3237-3240, 2006.

[23] K. Bazaka and M. V. Jacob, "Implantable devices: issues and challenges," Electronics, vol. 2, pp. 1-34, 2012.

[24] J. M. Rabaey, M. Mark, D. Chen, C. Sutardja, C. Tang, S. Gowda, et al., "Powering and communicating with mm-size implants," in 2011 Design, Automation & Test in Europe, 2011, pp. 1-6.

[25] N. Mano, "A 280 μW cm− 2 biofuel cell operating at low glucose concentration," Chemical Communications, pp. 2221-2223, 2008.

 [26] R. Venkatasubramanian, C. Watkins, D. Stokes, J. Posthill, and C. Caylor, "Energy harvesting for electronics with thermoelectric devices using nanoscale," 2007 IEEE International Electron Devices Meeting, Vols 1 and 2, pp. 367-370, 2007.

[27] R. Sidhu, D. Sanders, A. Morris, and M. McAlindon, "Guidelines on small bowel enteroscopy and capsule endoscopy in adults," Gut, vol. 57, pp. 125- 136, 2008.

[28] Small Bowel Capsule Endoscopy – A Backgrounder. Available: http://www.olympusamerica.com/presspass/press_pass_cut/docum ents/End oCapsuleBackgrounder.pdf

[29] Costanzo, A.; Dionigi, M.; Masotti, D.; Mongiardo, M.; Monti, G.; Tarricone, L.; Sorrentino, R. Electromagnetic Energy Harvesting and Wireless Power Transmission: A Unified Approach. Proc. IEEE 2014, 102, 1692–1711.

[30]Garnica, J.; Chinga, R.A.; Lin, J. Wireless Power Transmission: From Far Field to Near Field. Proc. IEEE 2013, 101, 1321–1331.

[31]Wang, G.; Liu, W.; Sivaprakasam, M.; Kendir, G.A. Design and analysis of an adaptive transcutaneous power telemetry for biomedical implants. IEEE Trans. Circuits Syst. Regul. Pap. 2005, 52, 2109–2117.

[32] Sauer, C.; Stanacevic, M.; Cauwenberghs, G.; Thakor, N.V. Power harvesting and telemetry in CMOS for implanted devices. IEEE Trans. Circuits Syst. Regul. Pap. 2005, 52, 2605–2613.

[33] Inanlou, F.; Ghovanloo, M. Wideband Near-Field Data Transmission Using Pulse Harmonic Modulation. IEEE Trans. Circuits Syst. I Regul. Pap. 2010, 58, 186–195.

[34]Ghovanloo, M.; Najafi, K. A Modular 32-site wireless neural stimulation microsystem. IEEE J. Solid State Circuits 2004, 39, 2457–2466.

[35] Sallan, J.; Villa, J.; Llombart, A.; Sanz, J. Optimal Design of ICPT Systems Applied to Electric Vehicle Battery Charge. IEEE Trans. Ind. Electron. 2009, 56, 2140–2149.

[36] Villa, J.L.; Sallán, J.; Llombart, A.; Sanz-Osorio, J. Design of a high frequency Inductively Coupled Power Transfer system for electric vehicle battery charge. Appl. Energy 2009, 86, 355–363.

[37] Wang, C.-S.; Covic, G.; Stielau, O. Power Transfer Capability and Bifurcation Phenomena of Loosely Coupled Inductive Power Transfer Systems. IEEE Trans. Ind. Electron. 2004, 51, 148–157.

[38] Wang, C.-S.; Stielau, O.; Covic, G. Design Considerations for a Contactless Electric Vehicle Battery Charger. IEEE Trans. Ind. Electron. 2005, 52, 1308–1314.

[39] Xie, L.; Shi, Y.; Hou, Y.T.; Lou, A. Wireless power transfer and applications to sensor networks. IEEE Wirel. Commun. 2013, 20, 140–145.

[40] Kim, H.-J.; Hirayama, H.; Kim, S.; Han, K.J.; Zhang, R.; Choi, J.-W. Review of Near-Field Wireless Power and

Communication for Biomedical Applications. IEEE Access 2017, 5, 21264–21285.

[41] O'Driscoll, S.; Poon, A.; Meng, T.H. A mm-sized implantable power receiver with adaptive link compensation. In Proceedings of the 2009 IEEE International Solid-State Circuits Conference-Digest of Technical Papers, San Francisco, CA, USA, 8–12 Febuary 2009; IEEE: San Francisco, CA, USA; pp. 294–295.

[42] H. W. Cheng, T. C. Yu, and C. H. Luo, "Direct current driving impedance matching method for rectenna using medical implant communication service band for wireless battery charging," IET Microwaves Antennas & Propagation, vol. 7, pp. 277-282, Mar 19 2013.

[43] Avago Technologies, "Schottky Diode Voltage Doubler," Application Note 956-4, 2010.

[44] Avago Technologies, "HSMS-282x Surface Mount RF Schottky Barrier Diodes," Data Sheet, 2014.

[45] P. Lipinski, "On charging the battery of an Implantable device," Modern Problems of Radio Engineering, Telecommunications and Computer Science, Proceedings, pp. 365-366, 2002.

[46] C. R. Liu, Y. X. Guo, H. C. Sun, and S. Q. Xiao, "Design and Safety Considerations of an Implantable Rectenna for Far-Field Wireless Power Transfer," IEEE Transactions on Antennas and Propagation, vol. 62, pp. 5798-5806, Nov 2014.

[47] Z. Duan, Y. X. Guo, M. Y. Je, and D. L. Kwong, "Design and in Vitro Test of a Differentially Fed Dual-Band Implantable Antenna Operating at MICS and ISM Bands," IEEE Transactions on Antennas and Propagation, vol. 62, pp. 2430-2439, May 2014.

[48] R. Alrawashdeh, "Implantable antennas for biomedical applications," PhD thesis, University of Liverpool, 2015.

[49] S. A. Kumar and T. Shanmuganantham, "Implantable CPW-fed Z-monopole antennas at 2.45 GHz ISM band for biomedical applications," International Journal of Microwave and Wireless Technologies, vol. 7, pp. 529-533, Oct 2015.

[50] S. A. Kumar, J. N. Sankar, D. Dileepan, and T. Shanmuganantham, "Design and Performances of Implantable CPW Fed Apollian Shaped Antenna at 2.45 GHz ISM Band for Biomedical Applications," Transactions on Electrical and Electronic Materials, vol. 16, pp. 250-253, Oct 25 2015.

[51] H. Y. Lin, M. Takahashi, K. Saito, and K. Ito, "Design of Miniature Implantable Tag Antenna for Radio-Frequency Identification System at 2.45 GHz and Received Power Analysis," IEICE Transactions on Communications, vol. E97b, pp. 129-136, Jan 2014.

[52] C. R. Liu, Y. X. Guo, and S. Q. Xiao, "Capacitively Loaded Circularly Polarized Implantable Patch Antenna for ISM Band Biomedical Applications," IEEE Transactions on Antennas and Propagation, vol. 62, pp. 2407-2417, May 2014.

[53] H. Li, Y. X. Guo, and S. Q. Xiao, "Broadband circularly polarized implantable antenna for biomedical applications," Electronics Letters, vol. 52, pp. 504-505, April 2016.

[54] X. Qing, Z. Chen, T. See, C. Goh, T. Chiam, "Characterization of RF transmission in human body," 2010 IEEE Antennas and Propagation Society International Symposium, pp. 1-4, 2010.

[55] N. Kuster, Q. Balzano, "Energy absorption mechanism by biological bodies in the near field of dipole antennas above 300 MHz," IEEE Transactions on Vehicular Technology, vol. 41, no. 1, pp. 17-23, 1992.

[56] H. Lin, M. Takahashi, K. Saito, K. Ito, "Characteristics of electric field and radiation pattern on different locations of the human body for in-body wireless communication," IEEE Transactions on Antennas and Propagation, vol. 61, no. 10, pp. 5350-5354, 2013.

[57] M. Vallejo, J. Recas, P. Del Valle, J. Ayala, "Accurate human tissue characterization for energyefficient wireless on-body communications," Sensors, vol. 13, no. 6, pp. 7546-7569, 2013.

[58] A. Khan, Multi-antenna Systems for Wireless Capsule Endoscopy, MS thesis, Aalto University, 2016.

[59] R. Alrawashdeh, Implantable Antennas for Biomedical Applications, University of Liverpool, 2015.

[60] Merrill, D.R.; Bikson, M.; Jefferys, J.G.R. Electrical stimulation of excitable tissue: Design of efficacious and safe protocols. J. Neurosci. Methods 2005, 141, 171–198.

[61] Paralikar, K.; Cong, P.; Yizhar, O.; Fenno, L.E.; Santa, W.; Nielsen, C.; Dinsmoor, D.; Hocken, B.; Munns, G.O.; Giftakis, J.; et al. An implantable optical stimulation delivery system for actuating an excitable biosubstrate. IEEE J. Solid-State Circuits 2011, 46, 321–332.

[62] PATTNAYAK, Tapan; THANIKACHALAM, Guhapriyan; FAMILY, Associated Part. Antenna design and RF layout guidelines. Cypress Semiconductor AN91445, 2015, 17.

الملخص

في السنوات الأخيرة ، أصبحت الأجهزة الطبية القابلة للزرع شائعة واكتسبت اهتمامًا كبيرًا من قبل الباحثين ومقدمي الرعاية الصحية. يتم استخدامها الآن على نطاق واسع بسبب تقنيات الرعاية الصحية المتطورة والجودة العالية لعلاج المريض. التطور السريع في التكنولوجيا قد جعل تصنيع وتصغير هذه الأجهزة أمرًا سهلًا. يعد تشغيل الأجهزة المزروعة هو التحدي الرئيسي في تطوير مثل هذا النوع من الأجهزة الطبية. البطارية الأساسية هي مصدر الطاقة الأكثر استخدامًا. ومع ذلك ، تعد البطاريات من أكبر القيود المفروضة على عمر وحجم الأجهزة الطبية المزروعة. الحل الواعد للتغلب على هذا التحدي هو استخدام تقنية نقل الطاقة اللاسلكية (WPT). لذلك ، تركز هذه الأطروحة بشكل أساسي على تحليل وتطوير مقومات مضاعفة الجهد بالإضافة إلى الهوائيات التي يمكن استخدامها في انظمة WPT.

تعد دائرة المقوم من الأجزاء الأساسية في WPT. لذا تم تصميم المقومات في هذه الأطروحة بناءً على تقنية مضاعفة الجهد وتمت المحاكاة بواسطة برنامج نظام التصميم المتقدم (ADS). تتميز المقومات المصممة بكفاءة تحويل RF إلى DC قد تصل الى حوالي 60 ٪ مع فولتية اخراج للتيار مستمر تصل إلى 6 فولت ، وهو ما يكفي لتشغيل الجهاز الطبي و/ أو شحن البطارية المزروعة. بالإضافة إلى ذلك ، تم تصغير دائرة المقوم إلى أبعاد صغيرة وما زالت تتمتع بكفاءة تحويل RF إلى DC عالية نسبيًا. ومن الجدير بالذكر أنه تم استخدام نطاقي تردد في هذا العمل كما تمت مقارنة وتحليل أداء دائرة المقوم في كل نطاق تردد. نطاقات التردد هذه هي 433 ميجاهرتز و 915 ميجاهرتز.

الهوائيات هي الجزء الرئيسي من نظام WPT ونظام الاتصالات. تم تصميم ومحاكاة العديد من هوائيات الخطوط المتعرجة في هذا البحث باستخدام برنامج استوديو CST. تم تصميم هوائيين بتردد 433 ميجاهرتز وصمم هوائيان آخران للعمل عند 915 ميجاهرتز.

تم تصميم الهوائيات المتعرجة القابلة للزرع مع طبقة أرضي كاملة في الجانب الخلفي للهوائي وموصل SMA متصل بمنفذ إدخال الهوائي. يسهل هذا التصميم دمج الهوائيات المصممة مع المقومات لتشكيل نظام WPT صغير الحجم.

تم تصنيع دوائر ال Rectifier المصممة (المعدل + الهوائي) باستخدام تقنية PCB. تم اختبار أداء النماذج المصنعة في المختبر وتمت مقارنة النتائج المقاسة بالنتائج التي تم الحصول عليها عن طريق المحاكاة ووجد أنه تم تحقيق توافق ممتاز ، مما يجعل تصميمات المقوم والهوائي صحيحة. أكدت هذه التجارب قابلية استخدام التصاميم المقترحة لتوفير الطاقة الكافية للعديد من الأجهزة الطبية القابلة للزرع.

جامعـة نينوى

كلية هندسة الالكترونيات

قسم الالكترونيك

تجهيز القدرة لاسلكياً للأجهزة الطبية القابلة للزرع

ضحى حسن حسين محمد

رسالة في هندسة الالكترونيك

بإشراف

الاستاذ المساعد

احمد محمد احمد سلامة السبعاوي

1444 هـ

2023م

تجهيز القدرة لاسلكياً للأجهزة الطبية القابلة للزرع

رسالة تقدمت بها

ضحى حسن حسين محمد

إلى

بإشراف

الاستاذ المساعد

احمد محمد احمد سلامة السبعاوي

2023م   1444هـ